THESIS FOR THE DEGREE OF DOCTOR OF PHILOSOPHY

VSC-HVDC for Industrial Power Systems

CUIQING DU

Division of Electric Power Engineering
Department of Energy and Environment
CHALMERS UNIVERSITY OF TECHNOLOGY
Göteborg, Sweden 2007

VSC-HVDC for Industrial Power Systems
CUIQING DU
ISBN 978-91-7291-913-6

Doktorsavhandlingar vid Chalmers tekniska högskola
Ny serie nr. 2594
ISSN 0346-718X

Division of Electric Power Engineering
Department of Energy and Environment
Chalmers University of Technology
SE–412 96 Göteborg
Sweden
Telephone +46 (0)31–772 1000

Chalmers Bibliotek, Reproservice
Göteborg, Sweden 2007

To my parents

VSC-HVDC for Industrial Power Systems
CUIQING DU
Division of Electric Power Engineering
Department of Energy and Environment
Chalmers University of Technology

Abstract

The recent developments in semiconductors and control equipment have made the voltage source converter based high voltage direct current (VSC-HVDC) feasible. Due to the use of VSC technology and pulse width modulation (PWM) the VSC-HVDC has a number of potential advantages as compared with classic HVDC, such as short circuit current reduction, rapid and independent control of active and reactive power, etc. With those advantages VSC-HVDC will likely be widely used in future transmission and distribution systems. One such application is to supply industrial systems characterized by high load density, high requirements on reliability and quality together with high costs after production interruption.

In this thesis, the scenario of VSC-HVDC connecting two grids is studied as the starting point. Two different control strategies are implemented and their dynamic performances during disturbances are investigated in the PSCAD/EMTDC program. The simulation results show that the model can fulfill bi-directional power transfers, AC system voltage adjustment and fast response control.

The VSC-HVDC model is further investigated for its ability to supply industrial systems with and without on-site generation. The frequency controller is utilized in the inverter station to ride through voltage disturbances, where the frequency of the VSC output voltage is slightly decreased and thereby the inertia energy of rotating masses in the system is exploited. The motivation for choosing this strategy is that the processing industries are much more sensitive to voltage drops than to frequency deviations. Simulation results show that a VSC-HVDC applied to an industrial system significantly improves the power quality of the industrial plant during voltage disturbances. Furthermore, the use of the proposed frequency controller can increase the ride-through capability of the system. However, the current limit of the converter, the power production level of the on-site generation and the generator size significantly influence its ability to mitigate voltage dips.

Keywords: VSC-HVDC, vector controller, outer controller, current limit, voltage dips, industrial power systems.

Acknowledgements

The research work is carried out at the Division of Electric Power Engineering, Department of Energy and Environment at Chalmers University of Technology. The project was sponsored by Swedish Energy Agency, Elforsk, ABB, Areva and Banverket, Sweden. This is gratefully acknowledged.

First I would like to thank my supervisor Dr. Evert Agneholm for his help, guidance, patience and encouragement, without which this thesis would not be possible to finish. I would also like to thank my examiner Prof. Gustaf Olsson for many enlightening discussions and for his numerous contributions to the last stage of my Ph.D. study.

I want to express my gratitude to Prof. Math Bollen and Dr. Ambra Sannino, my former supervisors, for offering me the opportunity to explore the challenging and promising topic of the VSC-HVDC, for their support and inspiration during and after their supervision. A special thank to Prof. Jaap Daalder for his helpful contribution to my research project.

Many thanks go to the members of my steering group for their constructive suggestions and interesting discussions. The steering group consists of Roger Löfgren (Preem), Jan Svensson (ABB), Pehr Hjalmarson (P H Power Engineering) and Lars Liljestrand (ABB).

My gratitude also goes to Dr. Torbjörn Thiringer, Marcia Martins, Fainan Abdul-Magueed, Massimo Bongiorno, Roberto Chouhy Leborgne and all other colleagues at the Division of Electric Power Engineering for their help and cooperation. I always find my work environment to be pleasant and productive.

Last but not the least, I want to thank my husband Yongtao and my daughter Erica for their love and support.

Cuiqing Du
Göteborg, Sweden
April 2007

Contents

Chapter 1

Introduction

This chapter describes the background of the thesis and briefly reviews related research. The objective of the thesis, main contributions of the work and the outline of the thesis are also presented. Finally, the project publications are listed.

1.1 Background

Industrial power systems are characterized by high concentration of load. Many industrial loads are very sensitive to voltage dips and other disturbances originating from the grid [1, 2]. A paper machine could be affected by disturbances of only 10% voltage variation from nominal lasting as short as 100ms [3]. Voltage sags to 85 to 90% of nominal lasting as short as 16 ms have triggered immediate outages of critical industrial processes as mentioned in some reports [4]. Equipment mal-operation due to voltage dips and other disturbances can lead to high cost. An interrupted automotive assembly line costed one U.S. manufacturer $250000 a month until it was corrected. Interruptions to semiconductor hatch processing cost $30000-$l million per incident [5]. Therefore, electric power systems are faced with the challenge of providing high-quality power to industrial loads.

Power-electronic solutions have been suggested to solve specific power quality problems in industrial systems. An uninterruptible power supply (UPS) can provide ride-through capability against voltage interruptions and dips for small loads [6]. A dynamic voltage restorer (DVR) can alleviate a range of dynamic power quality problems such as voltage dips and swells [7]. A static synchronous compensator (STATCOM) has the ability to either generate or absorb reactive power at a faster rate than classical solutions. This allows for the mitigation of flicker and alleviation of stability problems [8, 9].

High voltage direct current (HVDC) transmission is a technology based on high power electronics and used in electric power systems for long distances power transmission, connection of non-synchronized grids and long submarine cable transmission [10, 11]. For many years, HVDC based on thyristor commutated converters was used [12, 13]. With the development of semiconductors and control equipment, HVDC transmission

with voltage source converters (VSC-HVDC) based on IGBTs is today possible and several commercial projects are already in operation [14–17]. The use of such DC links provides possible new solution to power-quality related problems in industrial power systems.

1.2 Review of related research

The topologies of two converters in the VSC-HVDC system have been studied in [17–21]. The two-level bridge is the simplest circuit configuration and there are several commissioned projects that use this topology [15, 16]. Recent practices have extended the principle to multilevel converters by the use of capacitors and diodes to increase the number of levels. The voltages can be clamped for different levels such as a three-level neutral point clamped voltage source converter [14, 18, 22] and a three-level flying capacitor voltage source converter [19, 21]. These multilevel converters provide improved waveform quality and reduced power losses. In [23] it is stated that the typical losses of the two-level and three-level VSC, operating at 1 pu power, are larger than 3% and between $1\% - 2\%$, respectively. However, due to the increased complexity in converter design with multilevel converters the two-level converter technology is still the most commonly used.

To fully exploit the capabilities of the VSC-HVDC proper control algorithms are needed. In a number of papers, such as [18, 22, 24, 25], different control systems of the VSC-HVDC have been analyzed. In [18] an inner current control loop for the use together with a carrier based PWM is presented. The inner current control loop is designed for a digital control implementation and for a dead-beat control of the converter current when the converter is connected to a very strong AC network. A grid-connected VSC using a discrete vector current controller is investigated in [24]. The influences of an incorrect controller tuning and grid voltage harmonics on current frequency responses at an operating point are also addressed. Moreover, some specific aspects of the VSC-HVDC are also studied in the literature. For instance, an analytical model of the power control terminal of a VSC-HVDC system is also analyzed and presented in [26–28]. The contribution of VSC-HVDC to short circuit currents is investigated in [29]. The inter-area decoupling and local area damping by the VSC-HVDC are studied in [30]. There are also some further possibilities for the improvement of VSC-HVDC. In [31] a static synchronous series compensation (SSSC) is embedded in the VSC-HVDC station to improve the dynamic characteristics of the VSC-HVDC link.

One of the attractive applications of the VSC-HVDC is that it can be used to connect a wind farm to an AC grid to solve some potential problems such as voltage flicker [32]. In [33] a technical and economical analysis is presented to evaluate the benefits and drawbacks of grid connected offshore wind farms through a DC link. In [34] the behavior of a VSC-HVDC system is studied, when feeding a weak AC network with power produced from an offshore wind farm (WF) of induction generators. The VSC-HVDC connect-

ing a wind farm to an AC system has also been implemented in some commissioned projects [15, 35, 36]. Two commercial VSC-HVDC transmission systems projects, Gotland and Tjæreborg, are feeding onshore wind power to the AC system. These projects have shown that VSC-HVDC is capable of handling wind power and reacting rapidly enough to counteract voltage variations in an excellent way. In February 2005 the world's first offshore VSC-HVDC transmission was successfully commissioned [36]. Overall, the theoretical investigations and experiences confirm that the VSC-HVDC is a promising concept for connecting large wind farms to AC systems.

A multiterminal VSC-HVDC can be an attractive alternative to the conventional AC system. The possible implementation of a multiterminal HVDC system and various aspects related to the multiterminal HVDC system have been studied [37–42]. The reliability of a hybrid multiterminal HVDC sub-transmission system is evaluated in [38]. The ability of the multiterminal VSC-HVDC system to improve power quality and how to deal with DC overvoltages during loss of a converter in the multiterminal VSC-HVDC system is investigated in [43] and [40]. The protection of multiterminal VSC-HVDCs against DC faults is also studied in [44].

In the literature there are some other applications of the VSC-HVDC technology. In [45] a study of SSTI (subsynchronous torsional interaction) related to VSC-HVDC is presented. One DC prototype system has been simulated to investigate the opportunities and challenges in industrial systems [46].

1.3 Objective of the thesis and main contributions

The main objective of this thesis is to assess the potential and limitation of the use of VSC-HVDC in industrial power systems. The control algorithms of the VSC-HVDC will be designed and the dynamics of industrial systems with VSC-HVDC infeed will be analyzed.

The main contributions are: design of frequency control strategies for a VSC-HVDC to increase the ride-through capability for the VSC-HVDC supplied industrial systems in case of voltage disturbances, investigation of the impact of the converter current limit on the system and study of the VSC-HVDC dynamic performance for industrial plants with and without on-site generation. The details are described as follows:

- a control scheme for a VSC-HVDC connecting two established AC systems is studied. Two different control strategies, AC voltage control and reactive power control, are tested and compared during step changes and faults. The investigation focuses on the ability of the VSC-HVDC to keep in operation and how the system recovers after fault clearing.

- the dynamic performance of a VSC-HVDC system under unbalanced faults in the supplying AC system is investigated. Different control algorithms, such as an inner

current controller, a controller with LCL filter and positive-sequence and negative-sequence current controllers, are presented and analyzed for the most common unbalanced fault, i.e. single-line-to-ground fault (SLGF).

- the thesis describes different frequency controllers and compares the dynamics of a VSC-HVDC supplied industrial plant when different types of frequency controllers are implemented in the inverter station.

- the thesis studies the AC voltage/frequency control of the VSC-HVDC to supply industrial installations. During the investigation the moment of inertia of rotating masses, load characteristics and current limits are included and their effects on the VSC-HVDC's ability to ride through voltage disturbances are investigated during faults and motor starts.

- the thesis investigates a VSC-HVDC supplying an industrial plant with on-site generation. A PI frequency controller and a droop frequency controller are implemented in the VSC-HVDC control system. The dynamics of the system are investigated and compared when the two different frequency controllers are used and when the turbine operates in three different modes, i.e. constant power mode, droop frequency control with and without a reheat model.

1.4 Outline of the thesis

Chapter 2 presents classic HVDC and VSC-HVDC. In this chapter the arrangements of the HVDC system, the configurations, the advantages and applications of classic HVDC and VSC-HVDC are described. Furthermore, the structure of the VSC-HVDC, including its converter, harmonic filter and DC capacitor, is described in detail. The operation of the VSC-HVDC is also explained.

Chapter 3 focuses on the control system of the VSC-HVDC. The overall control structure of the VSC-HVDC is presented. A mathematical model of the control system is described in detail. Different outer controllers are also presented.

Chapter 4 discusses some simulations concerning the VSC-HVDC between two grids and makes the comparison between the complete and simplified VSC-HVDC models. In this chapter step changes, balanced and unbalanced faults are simulated with the complete and simplified models to evaluate and verify the proposed control system of the VSC-HVDC. Moreover, the improvement of the system performance during unbalanced faults is investigated. In all simulations the current limit is considered. Some of the results presented in **[Paper A]** and **[Paper B]** are highlighted in this chapter.

Chapter 5 focuses on the simulation of VSC-HVDC supplied industrial power systems with and without on-site generation. Balanced faults on the grid side, load step

changes and motor starts are investigated. Different frequency control strategies are also studied. Some of the results presented in **[Papers C-I]** will be addressed in this chapter.

Finally, the conclusions of the work and some suggestions for future research are pointed out in Chapter 6.

1.5 List of publications

Apart from the Licentiate thesis [47], the thesis is based on the work contained in the following publications:

A **C. Du**, A. Sannino, and M. Bollen, ”Analysis of the Control Algorithms of Voltage-Source Converter HVDC”, in *Proc. IEEE-PES Power Tech 2005*, St. Petersburg, June 2005.

B **C. Du**, A. Sannino, and M. Bollen, ”Analysis of Response of VSC-Based HVDC to Unbalanced Faults with Different Control Systems”, in *Proc. IEEE/PES Transmission and Distribution Conference and Exhibition: Asia Pacific, 2005*, Dalian, August 2005.

C **C. Du** and E. Agneholm, ”Investigation of Frequency/AC Voltage Control of Inverter Station of VSC-HVDC”, in *Proc. 32nd Annual Conference on IEEE Industrial Electronics, IECON 2006*, Paris, November 2006, pp. 1810 - 1815.

D **C. Du**, M. Bollen, E. Agneholm, and A. Sannino, ”A New Control Strategy of a VSC-HVDC System for High-Quality Supply of Industrial Plants”, accepted by IEEE Transactions on Power Delivery.

E **C. Du** and M. Bollen, ”Power-Frequency Control for VSC-HVDC during Island Operation”, in *Proc. The 8th IEE International Conference on AC and DC Power Transmission, 2006. ACDC 2006*, London, March 2006, pp. 177 - 181.

F **C. Du** and E. Agneholm, ”A Novel Control of VSC-HVDC for Improving Power Quality of an Industrial Plant”, in *Proc. 32nd Annual Conference on IEEE Industrial Electronics, IECON 2006*, Paris, November 2006, pp. 1962 - 1967.

G **C. Du**, E. Agneholm, and G. Olsson, ”Comparison of different frequency controls for VSC-HVDC”, submitted to IEEE Transactions on Power Delivery.

H **C. Du**, E. Agneholm, and G. Olsson, ”VSC-HVDC System for Industrial Plants with On-Site Generators”, submitted to IEE generation, transmission and distribution.

I **C. Du**, E. Agneholm, and G. Olsson, ”Use of VSC-HVDC for Industrial Systems with On-Site Generation with Frequency Control”, submitted to IEEE Transactions on Power Delivery.

Chapter 2

High Voltage Direct Current

This chapter presents general aspects of HVDC transmission. The configurations of HVDC and two different HVDCs, i.e. classic HVDC and VSC-HVDC, are described.

2.1 Introduction

The HVDC technology is a high power electronics technology used in electric power systems. It is an efficient and flexible method to transmit large amounts of electric power over long distances by overhead transmission lines or underground/submarine cables. It can also be used to interconnect asynchronous power systems [48]. The first commercial HVDC connecting two AC systems was a submarine cable link between the Swedish mainland and the island of Gotland. The link was rated 20MW, 100kV, and was commissioned in 1953 [49, 50]. Nowadays, the HVDC is being widely used all around the world. Until recently HVDC based on thyristors, which is called traditional HVDC or classic HVDC, has been used for conversion from AC to DC and vice versa.

Recently a new type of HVDC has become available. It makes use of the more advanced semiconductor technology instead of thyristors for power conversion between AC and DC. The semiconductors used are insulated gate bipolar transistors (IGBTs), and the converters are voltage source converters (VSCs) which operate with high switching frequencies (1-2kHz) utilizing pulse width modulation (PWM). The technology is commercially available as HVDC Light [51] or $\mathrm{HVDC}^{\mathrm{PLUS}}$ (Power Link Universal Systems) [52]. In this thesis the new technology will be referred to as VSC-HVDC (VSC based HVDC). A number of underground transmissions, up to 330 MW, are in commercial operation or being built [15, 35, 53, 54]. Today a maximum power capacity of 1000 MW at $\pm$ 300 kV DC is commercially available [55]. In this chapter a brief overview of classic HVDC is presented. The topology of the VSC-HVDC is discussed in detail. Design considerations and modelling aspects of the VSC-HVDC are addressed.

2.2 Configurations of HVDC

HVDC converter bridges together with lines or cables can be arranged in a number of configurations as shown in Figs. 2.1 and 2.2 [11, 49, 50, 56]:

I. Monopolar HVDC system
In the monopolar configuration, two converters are connected by a single pole line and a positive or a negative DC voltage is used. In Fig. 2.1(a) there is only one insulated transmission conductor installed and the ground or sea provides the path for the return current. For instance, the Konti-Skan (1965) project and Sardinia-Italy (mainland) (1967) project use monopolar links [11]. Alternatively, a metallic return conductor may be used as the return path.

II. Bipolar HVDC system
This is the most commonly used configuration of HVDC transmission systems [11]. The bipolar configuration, shown in Fig. 2.1(b), uses two insulated conductors as positive and negative poles. The two poles can be operated independently if both neutrals are grounded. The bipolar configuration increases the power transfer capacity. Under normal operation, the currents flowing in both poles are identical and there is no ground current. In case of failure of one pole power transmission can continue in the other pole which increases the reliability. Most overhead line HVDC transmission systems use the bipolar configuration [11].

III. Homopolar HVDC system

In the homopolar configuration, shown in Fig. 2.1(c), two or more conductors have the negative polarity and can be operated with ground or a metallic return. With two poles operated in parallel, the homopolar configuration reduces the insulation costs. However, the large earth return current is the major disadvantage [57].

IV. Back-to-back HVDC system
This is the common configuration for connecting two adjacent asynchronous AC systems. Two converter stations are located at the same site and transmission line or cable is not needed. A block diagram of a back-to-back system is shown in Fig. 2.2(a). The two AC systems interconnected may have the same or different nominal frequencies, i.e. 50Hz and 60Hz. Examples of such system configuration can be found in Japan and South America [58].

V. Multiterminal HVDC system
In the multiterminal configuration, three or more HVDC converter stations are geographically separated and interconnected through transmission lines or cables. The system can be either parallel, where all converter stations are connected to the same voltage as shown in Fig. 2.2(b) or series multiterminal system, where one

or more converter stations are connected in series in one or both poles as shown in Fig. 2.2(c). A hybrid multiterminal system contains a combination of parallel and series connections of converter stations. Applications of multiterminal HVDCs include the Sardinia-Corsica-Italy (SACOI) connection, the Pacific Intertie in USA and the Hydro Quebec - New England Hydro from Canada to USA [59, 60].

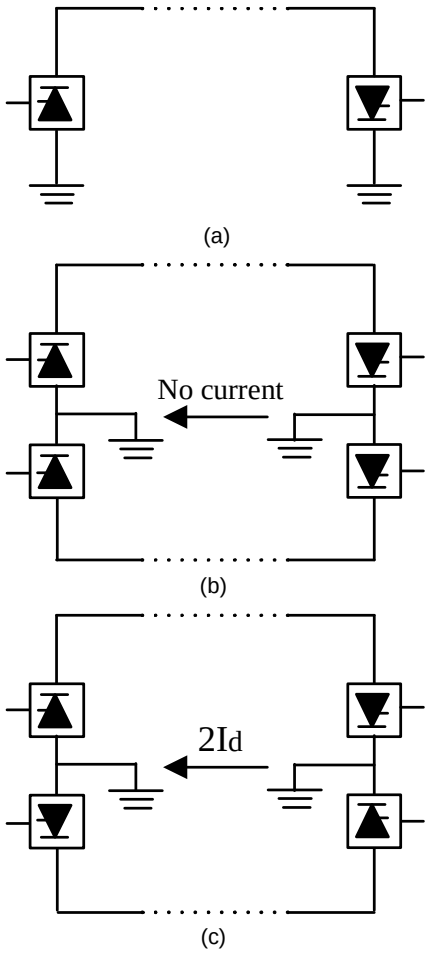

Fig. 2.1 Monopolar (a), bipolar (b) and homopolar (c) HVDC systems.

2.3 Classic HVDC

2.3.1 Components of classic HVDC

A bipolar classic HVDC system, shown in Fig. 2.3, consists of AC filters, shunt capacitor banks or other reactive-compensation equipment, converter transformers, converters, DC reactors, DC filters, and DC lines or cables [12].

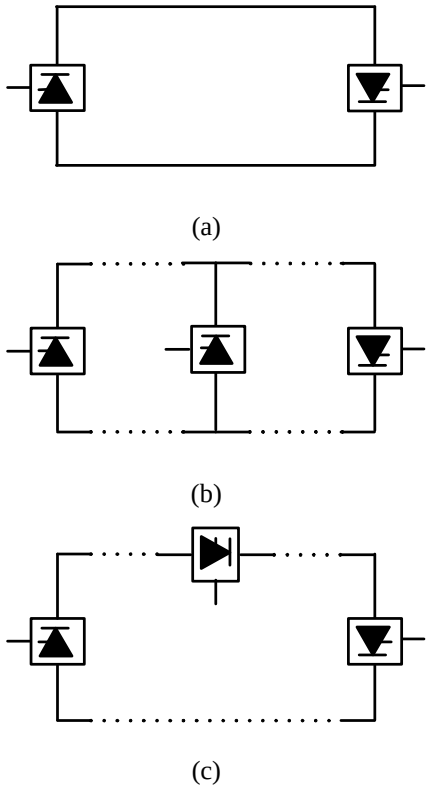

Fig. 2.2 Back-to-back (a), parallel multiterminal (b) and series multiterminal (c) HVDC systems.

Converters

The HVDC converters are the most important part of an HVDC system. They perform the conversion from AC to DC (rectifier) at the sending end and from DC to AC (inverter) at the receiving end. HVDC converters are connected to the AC system through transformers. The classic HVDC converters are current source converters (CSCs) with line-commutated thyristor switches. A six pulse valve bridge, shown in Fig. 2.4, is the basic converter unit of classic HVDC for both conversions, i.e. rectification and inversion. A twelve pulse converter bridge can be built by connecting two six pulse bridges. The bridges are then connected separately to the AC system through transformers, one with Y-Y winding structure and the other with Y-Δ winding structure, as shown in Fig. 2.3. In this way the 5th and 7th harmonic currents through the two transformers are in opposite phase. This significantly reduces the distortion in the AC system caused by the HVDC converters [61, 62].

Transformers

The transformers connect the AC network to the valve bridges and adjust the AC voltage level to a suitable level for the converters. The transformers can be of different design depending on the power to be transmitted and possible transport requirements [12].

AC-side harmonic filters

The HVDC converters produce harmonic currents on the AC side and the harmonic cur-

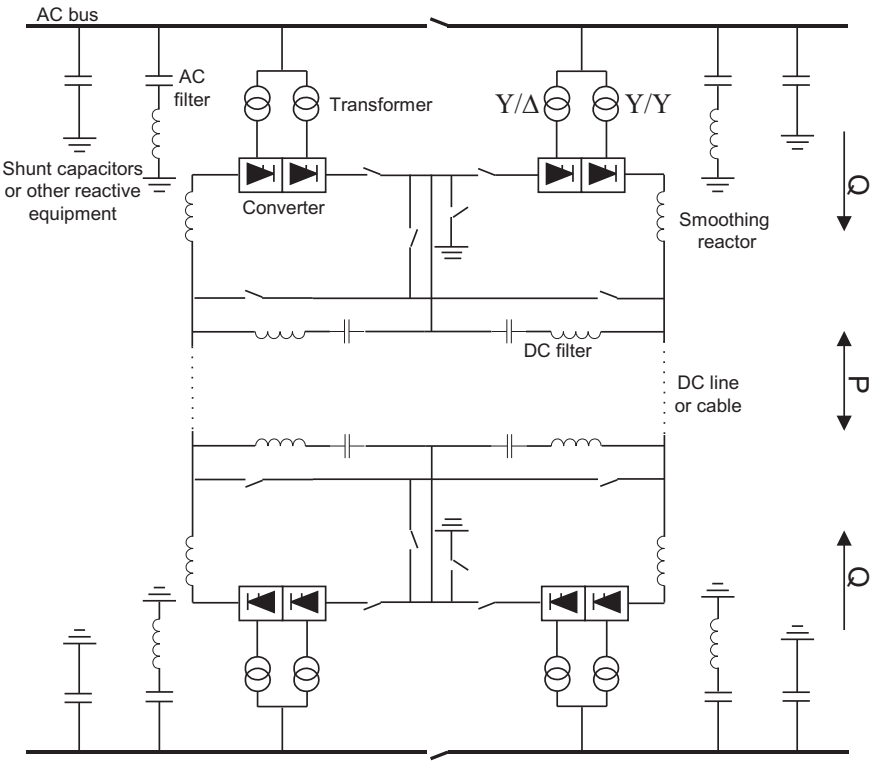

Fig. 2.3 A configuration for a classic HVDC system.

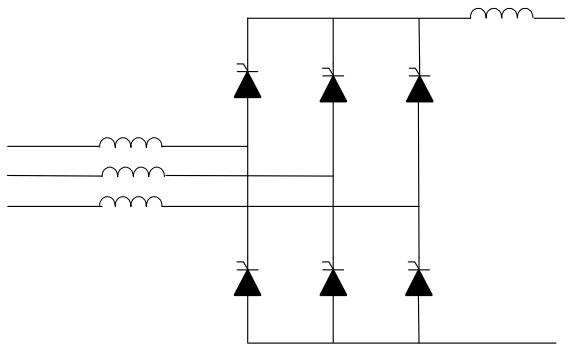

Fig. 2.4 Configuration of a six pulse valve group.

rents entering into the connected AC network are limited by AC filters. For instance, AC filters installed on the AC side of a 12-pulse HVDC converter are tuned such that the 11^{th}, 13^{th}, 23^{th} and 25^{th} harmonic currents are limited. In the conversion process the converters consume reactive power which is partly compensated in the filter banks and the rest is provided by capacitor banks.

DC filters

The HVDC converters produce ripple on the DC voltage. Voltage ripple causes the interference to telephone circuits near the DC line. DC filters can be used to reduce the ripple. Usually no DC filters are needed for pure cable transmission nor for back-to-back HVDC stations. However, it is necessary to install DC filters if overhead lines are used in the transmission system. The filter types used on the DC side are tuned filters and active DC filters [11, 63].

HVDC cables or overhead lines

HVDC cables are normally used for submarine transmission. No serious length limitation exists for HVDC cables. For a back-to-back HVDC system no DC cable or overhead line is needed. For connections over land overhead lines are typically used. However, due to environmental concerns the tendency is to also use cables for connections over land.

2.3.2 Advantages and applications of classic HVDC

Advantages of classic HVDC

It is important to remark that an HVDC system offers not only the capability to transfer electrical power but also a number of advantages as compared to AC transmission [11, 12] such as:

- no limits in transmitted distance. This is valid for both overhead lines and submarine/underground cables.
- fast and accurate control of power flow which improves the power system stability.
- direction of power flow can be changed quickly.
- an HVDC link does not increase the short-circuit power in the point of connection. This implies that it will not be necessary to change other equipment in the existing network from the viewpoint of short-circuit power.
- HVDC can carry more power for a given size of conductor as compared to the AC system, which implies that when transmitting the same amount of active power, the need for right-of-ways (RoWs) is less for an HVDC than for an AC connection.
- power can be transmitted between two AC systems operating at different nominal frequencies or at the same frequency without being synchronized.

Applications of classic HVDC

The purpose of the first classic HVDC application was to provide point to point electrical power interconnections between asynchronous AC power networks. Other applications [56] where HVDC transmission is suitable include:

- delivery of electrical power from large energy sources over long distance, e.g. the connection of remote hydro-stations to load centers.
- import of power into congested load areas, where it is not possible to build new generations to meet the load demand. Underground DC cable transmission is usually used in such application.
- increasing the capacity of existing AC transmission by DC transmission, which eliminates the need of new transmission RoWs.
- power flow control. In AC networks the desired power flow control can be difficult to accomplish. Power marketers and system operators may require the power flow control capability provided by HVDC transmission.

2.4 VSC-HVDC

With continued load growth and the difficulty of obtaining RoWs for new transmission lines, the existing transmission systems are pushed towards their limits. This will deteriorate the power quality and have a negative impact on the network stability. Therefore, it is necessary to adapt existing transmission system to increase the power density on the existing RoWs. The use of VSC-HVDC transmission has the potential to be a part of the solution to these anticipated problems.

The VSC-HVDC is a new DC transmission system technology. The valves are built by IGBTs and PWM is used to create the desired voltage waveform. With PWM it is possible to create any waveform, any phase angle and magnitude of the fundamental frequency component. This high controllability allows for a wide range of applications.

2.4.1 Components of VSC-HVDC

A typical VSC-HVDC system, shown in Fig. 2.5, consists of AC filters, transformers, converters, phase reactors, DC capacitors and DC cables [64].

Converters

The converters are VSCs employing IGBT power semiconductors, one operating as a rectifier and the other as an inverter. The two converters are connected either back-to-back or through a DC cable, depending on the application. This is described in detail in Section 2.4.2.

Transformers

Normally, the converters are connected to the AC system via transformers. The most important function of the transformers is to transform the voltage of the AC system to a level suitable for the converter.

Phase reactors

The phase reactors are used for controlling both the active and the reactive power flow by regulating currents through them. The reactors also function as AC filters to reduce the high frequency harmonic contents of the AC currents which are caused by the switching operation of the VSCs.

AC filters

The AC voltage output contains harmonic components, caused by the switching of the IGBTs. The harmonics emitted into the AC system have to be limited to prevent them from causing malfunction of AC system equipment or radio and telecommunication disturbances. High-pass filter branches are installed to mitigate these high order harmonics. With VSC converters there is no need to compensate any reactive power and the current harmonics on the AC side are related directly to the PWM frequency. Therefore, the amount of filters in this type of converters is reduced as compared with line commutated converters. This is described in detail in Section 2.4.3.

DC capacitors

On the DC side there are two capacitor stacks with the same size. The size of these capacitors depends on the required DC voltage. The objective of the DC capacitors is to provide an energy buffer to keep the power balance during transients and reduce the voltage ripple on the DC side. This is described in detail in Section 2.4.4.

DC cables

The cable used in the VSC-HVDC applications is a new developed type where the insulation is made of an extruded polymer that is particularly resistant to DC voltage. Polymeric cables are the preferred choice for HVDC mainly because of their mechanical strength, flexibility and low weight [65].

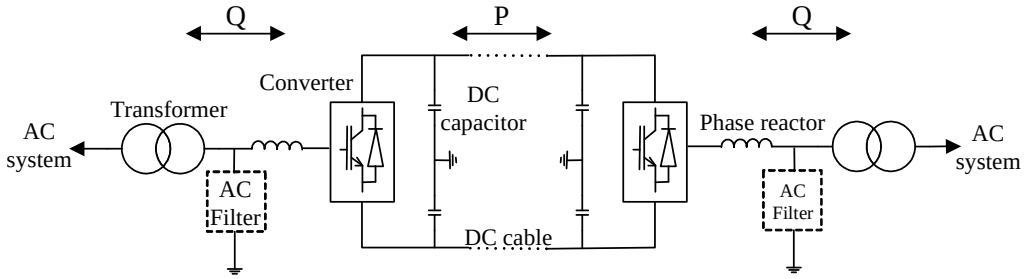

Fig. 2.5 A VSC-HVDC system.

2.4.2 Converters

So far the converters are composed of a number of elementary converters, i.e. three-phase, two-level, six-pulse bridges or three-phase, three-level, twelve-pulse bridges, as shown in Fig. 2.6. Both topologies have been used in the commissioned projects [15–17].

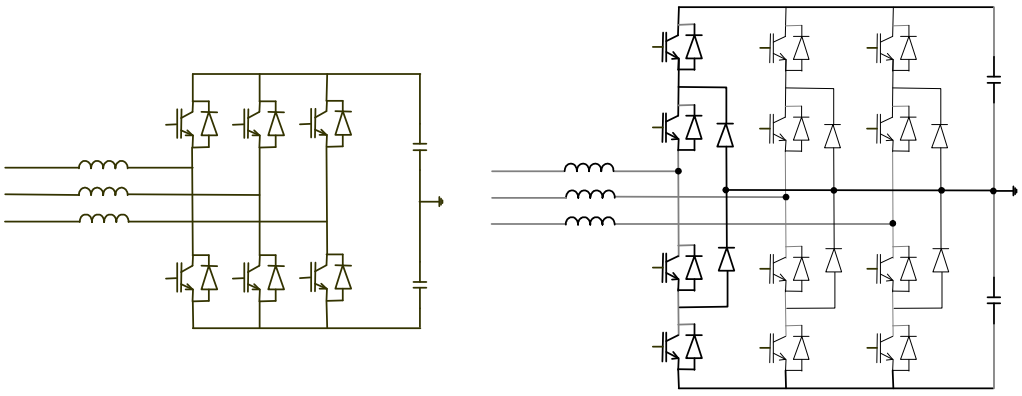

(a) Two-level VSC (b) Three-level VSC

Fig. 2.6 The topology of the VSC.

The two-level bridge is the simplest circuit configuration that can be used for building up a three-phase forced commutated VSC bridge. It has been widely used in many applications at a wide range of power levels. As shown in Fig. 2.6, the two-level converter consists of six valves. It is capable of generating the two voltage levels $-0.5{\cdot}u_{\mathrm{DC}}$ and $+0.5{\cdot}u_{\mathrm{DC}}$ (where u_{DC} is the DC voltage). The three-level converter comprises four valves in one arm of the converter. It can generate the resulting voltage on the AC terminal comprising three voltage levels $-0.5{\cdot}u_{\mathrm{DC}}$, 0 and $+0.5{\cdot}u_{\mathrm{DC}}$. In order to use the two or three-level bridge in high power applications series connection of devices may be necessary and then each valve will be built up of a number of series connected turn-off devices and anti-parallel diodes. The number of devices required is determined by the rated power of the bridge and the power handling capability of the switching devices.

2.4.3 AC filters

As described above, the currents and the voltages at the inverter and rectifier are not sinusoidal due to the commutation valve switching process. These non-sinusoidal current and voltage waveforms consist of the fundamental frequency AC component plus higher-order harmonics. Passive high-pass AC filters are used in the VSC-HVDC to filter the high harmonics. Hence, sinusoidal line currents and voltages can be obtained from the transformer secondary sides. Furthermore, the reactive power compensation may be accomplished by high-pass filters.

As stated in [66], a PWM output waveform contains harmonics $M'f_c \pm N'f_1$, where f_c is the carrier frequency, f_1 is the fundamental grid frequency. M' and N' are integers,

and the sum $M' + N'$ is an odd integer. In addition to the fundamental frequency component, the spectrum of the output voltages contains components around the carrier frequency of the PWM and multiples of the carrier frequency. This is illustrated in Table 2.1, where a summary of the output voltage harmonics obtained by triangular carrier PWM with the frequency modulation ratio m_f equal to 39. Here, m_f is defined as:

$$m_f = \frac{f_c}{f_1} \tag{2.1}$$

The selection of m_f depends on the balance between switching losses and harmonic losses. A higher value of m_f (i.e. a higher number of commutations per second) increases the switching losses but reduces the harmonic losses.

Table 2.1: Spectrum of the output voltage

M'	1	2	3
Harmonic	$39f_1$	$78f_1$	$117f_1$
	$39f_1 \pm 2f_c$	$78f_1 \pm 1f_c$	$117f_1 \pm 2f_c$
	$39f_1 \pm 4f_c$	$78f_1 \pm 3f_c$	$117f_1 \pm 4f_c$
	$39f_1 \pm 6f_c$	$78f_1 \pm 5f_c$	$117f_1 \pm 6f_c$
	etc.	etc.	etc.

From Table 2.1, the harmonic contents can be obtained. The higher m_f, the higher the frequency of the lowest order harmonics produced. Therefore, with the use of PWM, passive high-pass damped filters are selected to filter the high order harmonics. Normally second and third-order passive high-pass filters shown in Fig. 2.7 are used in HVDC schemes [11].

When designing the high damping filters the quality factor Q is chosen to obtain the best characteristic over the required frequency band. The typical value of the quality factor Q is between 0.5 and 5 [11].

2.4.4 Design of DC voltage and DC capacitors

For the converter to be capable of controlling the input current waveforms to be sinusoidal, the nominal DC voltage should be appropriately chosen. As mentioned in subsection 2.4.2, a two-level converter is able to generate two voltage levels $-0.5{\cdot}u_{\mathrm{DC}}$ and $+0.5{\cdot}u_{\mathrm{DC}}$. Therefore, the DC voltage should be larger than 1.634 times the root mean square (rms) AC voltage [61].

The design of DC side capacitor is an important part for the design of an HVDC system. Due to PWM switching action in the VSC-HVDC, the current flowing to the DC side of a converter contains harmonics which will result in a ripple on the DC side voltage. The magnitude of the ripple depends on the DC side capacitor size and the switching frequency.

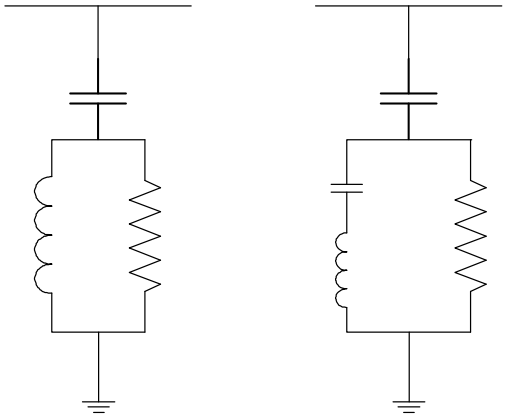

(a) Second-order filter (b) Third-order filter

Fig. 2.7 Passive high-pass filter.

Here, a small DC capacitor C_{DC} can be used, which should theoretically result in a faster converter response. It can also provide an energy storage in order to control the power flow. The DC capacitor size is characterized as a time constant τ, defined as the ratio between the stored energy at the rated DC voltage U_{DCN} and the nominal apparent power of the converter S_{N}:

$$\tau = \frac{\frac{1}{2} C_{\mathrm{DC}} U_{\mathrm{DCN}}^2}{S_N} \tag{2.2}$$

The time constant is equal to the time needed to charge the capacitor from zero to rated voltage U_{DCN} if the converter is supplied with a constant active power equal to S_{N} [67,68]. The time constant τ can be selected to be smaller to satisfy small ripple and small transient overvoltages on the DC voltage. This will be verified in the simulations. The relatively small time constant allows fast control of active and reactive power.

2.4.5 Operation of VSC-HVDC

The operation of a VSC-HVDC can be explained by considering each terminal as a voltage source connected to an AC transmission network via series reactors.

Fig. 2.8 shows a simplified single line diagram of the converter connected to an AC system. As shown in the figure, the AC system and the controlled voltage source are connected via the phase reactor. The converter is modelled as a controlled voltage source u_{v} at the AC side and a controlled current source i_{DC} at the DC side. The current source can be calculated based on the power balance at the AC and DC side of the converter. The controlled voltage source can be derived from the control system of the converter where the amplitude, the phase and the frequency can be controlled independently of each other. The controlled voltage source can be described by the following equation [66]:

$$u_{\mathrm{v}} = \frac{1}{2} u_{\mathrm{DC}} M \sin(\omega t + \delta) + \text{ harmonic terms} \tag{2.3}$$

where M is the modulation index which is defined as the ratio of the peak value of the modulating wave and the peak value of the carrier wave, i.e. the DC voltage. ω is the frequency, δ is the phase shift of the output voltage. Variables M, ω and δ can be adjusted by the VSC controller. As a result, the voltage drop (ΔV shown in Fig. 2.8) across the reactor can be varied to control the active and reactive power flows.

Fig. 2.8 also shows the corresponding fundamental frequency phasor representation for a VSC operating as a rectifier and absorbing reactive power from the AC system. In this case the VSC output voltage has a smaller amplitude and is phase lagged with respect to the AC system. The active power flow between the AC system and the converter

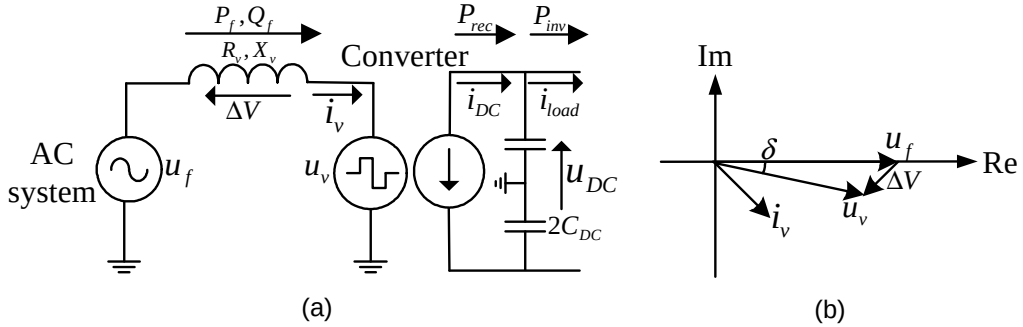

Fig. 2.8 Equivalent circuit (a) and phasor diagram (b) of the converter connected to an AC system.

can be controlled by changing the phase angle (δ) between the fundamental frequency voltage (u_{v}) generated by the VSC and the AC voltage (u_{f}) on the secondary side of the transformer [64, 69]. The active power is calculated according to (2.4) neglect the losses of the phase reactor.

$$P_{\mathrm{f}} = \frac{u_{\mathrm{f}} u_{\mathrm{v}} \sin\delta}{X_{\mathrm{v}}} \tag{2.4}$$

The reactive power is determined by the amplitude of u_{v} [64,69] and calculated according to (2.5).

$$Q_{\mathrm{f}} = \frac{u_{\mathrm{f}}(u_{\mathrm{f}} - u_{\mathrm{v}}\cos\delta)}{X_{\mathrm{v}}} \tag{2.5}$$

In a VSC-HVDC connection the active power on the AC side is equal to the active power transmitted from the DC side at steady state (losses neglected). This can be fulfilled if one of the two converters controls the active power transmitted while the other converter controls the DC voltage. The reactive power generation and consumption can be used to control the AC voltage of the network. Fig. 2.9 illustrates the active/reactive power capabilities of the VSC-HVDC system in a P-Q diagram for two different voltages u_{v1} and u_{v2}, where $u_{\mathrm{v1}} > u_{\mathrm{v2}}$. Several important properties of the VSC-HVDC link can be seen from this figure [52, 70]. For instance, the VSC-HVDC is able to operate at any point within the circle. However, since the radius of the VSC-HVDC represents the converter MVA rating which equals to the production of the maximum current and the actual AC voltage, the MVA capacity will decrease proportionally to the voltage drop.

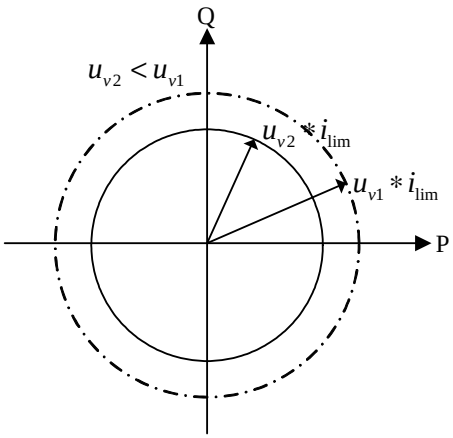

Fig. 2.9 PQ diagram for the VSC-HVDC.

Fig. 2.10 illustrates the active and reactive power flow for the grid and the VSC transmission system in a power circle diagram. From Fig. 2.10, it can be obtained that the crossing between the capability curve of the VSC transmission and the grid circle indicates the stable operation for that particular voltage level. Furthermore, Fig. 2.10 also shows the change of the transferred active and reactive power flow during voltage dips. It can be obtained that the stable transferred active power is reduced (i.e. $P_{\mathrm{AC2}} < P_{\mathrm{AC1}}$) when the grid voltage drops.

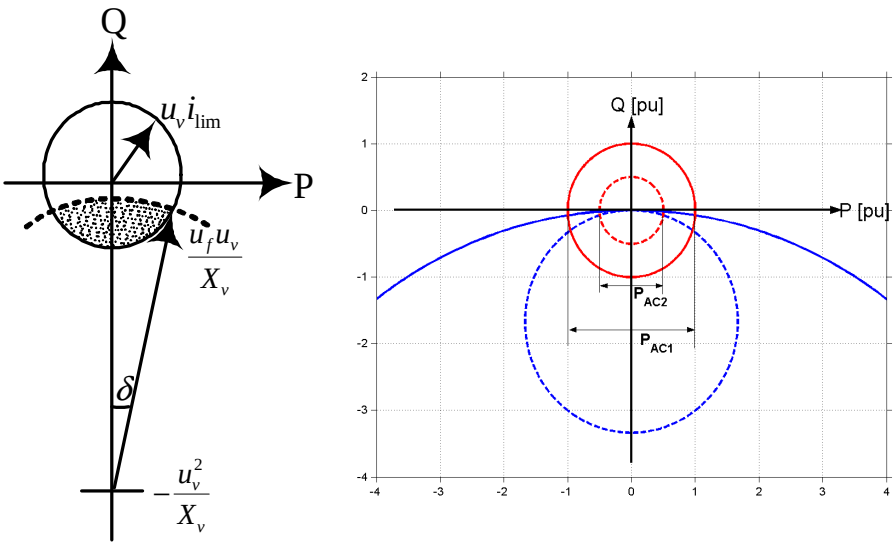

Fig. 2.10 The power circle plane for a VSC transmission in series with an AC network at normal operation (a) and during faults (b).

2.4.6 Advantages and applications of VSC-HVDC

The main operation difference between classic HVDC and VSC-HVDC is the higher controllability of the latter. This leads to a number of potential advantages and applications, where some are given below [12, 65, 71]:

- independent control of active and reactive power without extra compensating equipment. With the use of PWM, the VSC-HVDC can control both active and reactive power independently. While the transmitted active power is kept constant the AC voltage controller can control the voltage in the AC network. Reactive power generation and consumption of a VSC-HVDC converter can be used for voltage control to compensate the needs of the connected network within the rating of a converter.

- mitigation of power quality disturbances. The reactive power capabilities of the VSC-HVDC can be used to control the AC network voltage and thereby contribute to an enhanced power quality. Furthermore, the faster response, due to increased switching frequency (PWM), offers new levels of performance regarding power quality control such as flickers and harmonics. Power quality problems are issues of priority for owners of industrial plants, grid operators and for the public [72].

- reduced risk of commutation failures. Disturbances in the AC system may lead to commutation failures in a classic HVDC system. As the VSC-HVDC uses self-commutating semiconductor devices, it is no longer necessary to present a sufficiently-high AC voltage. This significantly reduces the risk of commutation failures and extends the application of the VSC-HVDC for stability control.

- communication not needed. As the control systems on the rectifier and inverter sides operate independently, they do not depend on a telecommunication connection, which in turn improves the speed and the reliability of the controller.

- feeding islands and passive AC networks. The VSC converter is able to create its own AC voltage at any predetermined frequency without the presence of rotating machines. Therefore, it may be used to supply industrial installations or to connect large wind farms.

- multiterminal DC grid. The VSC converters are suitable for creating a DC grid with a number of converters since little coordination is needed between the VSC-HVDC converters. One potential application of multiterminal DC grids is to provide power supply to city centers.

2.5 Summary

In this chapter an overview of the HVDC system has been presented. Different configurations of the HVDC have been described. The function of each component, advantages and applications of the classic HVDC and the VSC-HVDC have been presented in detail. Moreover, the design and operation of the VSC-HVDC system have been discussed. It can be concluded that the bipolar HVDC link is the most common HVDC configuration. The higher controllability of the VSC-HVDC leads to many new potential advantages and applications, which makes it more attractive for the future.

Chapter 3

Control System of the VSC-HVDC

This chapter describes a cascaded control system of the VSC-HVDC. Different vector controllers and outer controllers are presented.

3.1 Introduction

With classic HVDC the reactive power cannot be controlled independently of the active power. With VSC-HVDC there is an additional degree of freedom. As described in Chapter 2, the VSC-HVDC can control the active and reactive power independently. The reactive power can be controlled separately in each converter by the required AC voltage or set manually. The active power flow can be controlled by the DC voltage, the variation of frequency at the AC side or set manually. This means that the active power flow, the reactive power flow, the AC voltage, the DC voltage and the frequency can be controlled when using VSC-HVDC.

The control system of the VSC-HVDC is a cascade control system, it typically consists of a faster vector controller. Furthermore, the vector controller is completed by additional controllers which supply the references for the vector controller. Thus, the vector controller will be the inner loop and additional controllers will be the outer loop. In this thesis the additional controllers will be referred to as the outer controllers. The outer controllers include the DC voltage controller, the AC voltage controller, the active power controller, the reactive power controller or the frequency controller. For example, as shown in Fig. 3.1, either side of the link can choose between AC voltage controller and reactive power controller. Each of these controllers generates a reference value for the vector controller.

Obviously not all controllers can be used at the same time. The choice of different kinds of controllers will depend on the application and may require advanced power system studies. For example, the VSC-HVDC can control frequency and AC voltage if the load is a passive system, the VSC-HVDC can control AC voltage and active power flow if the load is an established AC system. However, since the active power flow into the DC

link must be balanced, the DC voltage controller is necessary in order to achieve active power balance. Active power out from the DC link must equal the active power into the DC link minus the losses in the DC link. Any difference would result in a rapid change of the DC voltage. The other converter can set any active power value within the limits for the system.

In this chapter the vector controller and various outer controllers will be described in detail. Simulation results will be presented in the next chapter.

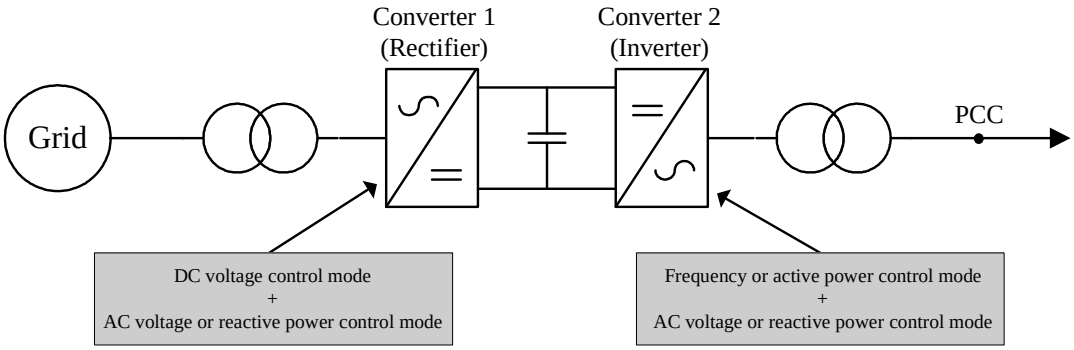

Fig. 3.1 Overall control structure of the VSC-HVDC.

3.2 Vector controller

The vector controller is based on the basic relationship of the circuit shown in Fig. 3.2 and can be implemented in the dq-coordinate system. In order to have a detailed overview of the vector controller, its derivation is presented in this section.

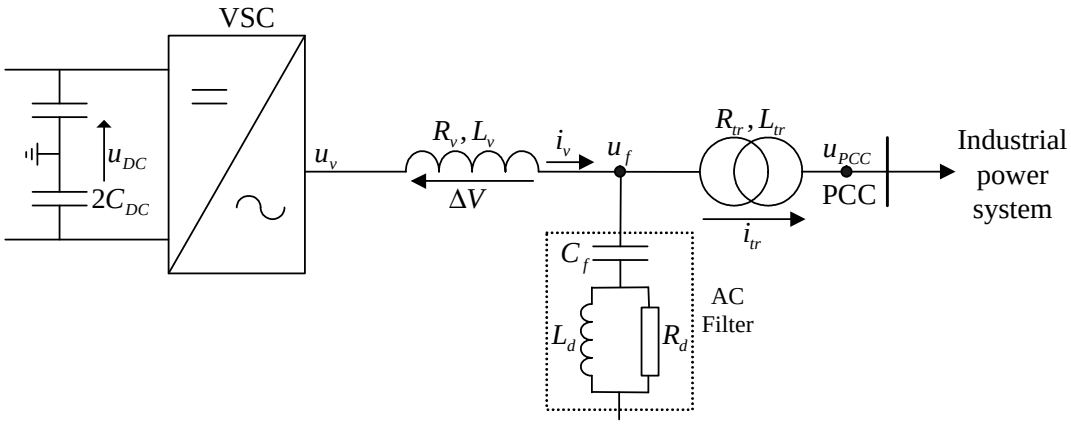

Fig. 3.2 The inverter station of the VSC-HVDC.

Fig. 3.3 shows the frequency response from the converter voltage u_{v} to the filter-bus voltage u_{f} and from the converter voltage u_{v} to the current through transformer i_{tr} with and without R_{d} and L_{d}. It is shown that the same responses at low frequencies

are achieved both with and without R_d and L_d which means that the AC filter is purely capacitive at low frequencies. Therefore, the control algorithms, described in [73–75], can be used in this application. The AC filter is considered as a pure capacitor, i.e. R_d and L_d neglected, in the following derivation of the vector controller.

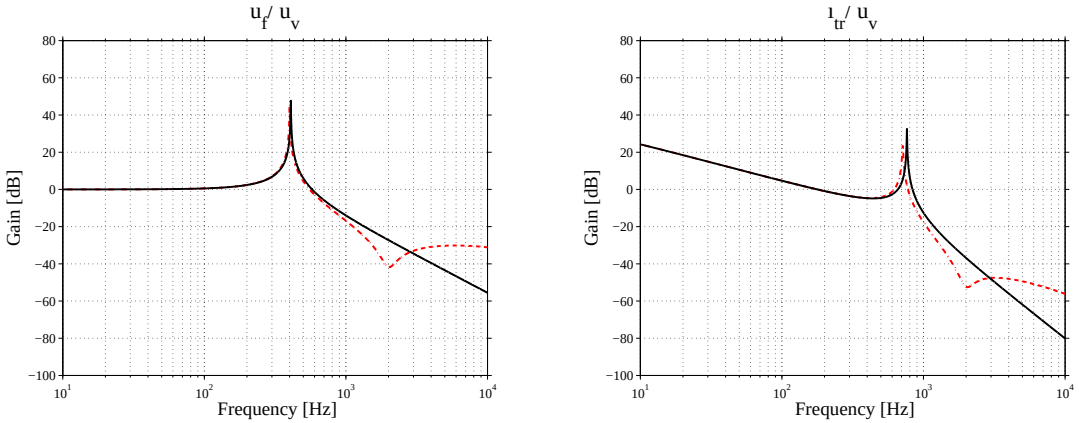

(a) (b)

Fig. 3.3 Frequency response of $u_\mathrm{f}/u_\mathrm{v}$ (a) and $i_\mathrm{tr}/u_\mathrm{v}$ (b) with [dash-dotted] and without $R_\mathrm{d}, L_\mathrm{d}$ [solid].

From the circuit shown in Fig. 3.2, the voltage over the transformer, the current through the AC filter and the voltage over the phase reactor can be obtained in the three-phase system:

$$u_\mathrm{f}^{(\mathrm{abc})}(t) - u_\mathrm{PCC}^{(\mathrm{abc})}(t) = L_\mathrm{tr}\frac{\mathrm{d}}{\mathrm{d}t}i_\mathrm{tr}^{(\mathrm{abc})}(t) + R_\mathrm{tr}i_\mathrm{tr}^{(\mathrm{abc})}(t) \tag{3.1}$$

$$i_\mathrm{v}^{(\mathrm{abc})}(t) - i_\mathrm{tr}^{(\mathrm{abc})}(t) = C_\mathrm{f}\frac{\mathrm{d}}{\mathrm{d}t}u_\mathrm{f}^{(\mathrm{abc})}(t) \tag{3.2}$$

$$u_\mathrm{v}^{(\mathrm{abc})}(t) - u_\mathrm{f}^{(\mathrm{abc})}(t) = L_\mathrm{v}\frac{\mathrm{d}}{\mathrm{d}t}i_\mathrm{v}^{(\mathrm{abc})}(t) + R_\mathrm{v}i_\mathrm{v}^{(\mathrm{abc})}(t) \tag{3.3}$$

According to (3.1), (3.2) and (3.3) the following differential equations are derived:

$$\frac{\mathrm{d}}{\mathrm{d}t}i_\mathrm{tr}^{(\mathrm{abc})}(t) = -\frac{R_\mathrm{tr}}{L_\mathrm{tr}}i_\mathrm{tr}^{(\mathrm{abc})}(t) + \frac{1}{L_\mathrm{tr}}(u_\mathrm{f}^{(\mathrm{abc})}(t) - u_\mathrm{PCC}^{(\mathrm{abc})}(t)) \tag{3.4}$$

$$\frac{\mathrm{d}}{\mathrm{d}t}u_\mathrm{f}^{(\mathrm{abc})}(t) = -\frac{1}{C_\mathrm{f}}i_\mathrm{tr}^{(\mathrm{abc})}(t) + \frac{1}{C_\mathrm{f}}i_\mathrm{v}^{(\mathrm{abc})}(t) \tag{3.5}$$

$$\frac{\mathrm{d}}{\mathrm{d}t}i_\mathrm{v}^{(\mathrm{abc})}(t) = -\frac{R_\mathrm{v}}{L_\mathrm{v}}i_\mathrm{v}^{(\mathrm{abc})}(t) + \frac{1}{L_\mathrm{v}}(u_\mathrm{v}^{(\mathrm{abc})}(t) - u_\mathrm{f}^{(\mathrm{abc})}(t)) \tag{3.6}$$

By using the transformation from abc to $\alpha\beta$, i.e. $x^{(\alpha\beta)} = \sqrt{\frac{2}{3}}[x^{(\mathrm{a})} + x^{(\mathrm{b})}e^{j\frac{2\pi}{3}} + x^{(\mathrm{c})}e^{j\frac{4\pi}{3}}]$,

(3.4), (3.5) and (3.6) can be transformed to the $\alpha\beta$-coordinate system as:

$$\frac{\mathrm{d}}{\mathrm{d}t}i_{\mathrm{tr}}^{(\alpha\beta)}(t) = -\frac{R_{\mathrm{tr}}}{L_{\mathrm{tr}}}i_{\mathrm{tr}}^{(\alpha\beta)}(t) + \frac{1}{L_{\mathrm{tr}}}(u_{\mathrm{f}}^{(\alpha\beta)}(t) - u_{\mathrm{PCC}}^{(\alpha\beta)}(t)) \tag{3.7}$$

$$\frac{\mathrm{d}}{\mathrm{d}t}u_{\mathrm{f}}^{(\alpha\beta)}(t) = -\frac{1}{C_{\mathrm{f}}}i_{\mathrm{tr}}^{(\alpha\beta)}(t) + \frac{1}{C_{\mathrm{f}}}i_{\mathrm{v}}^{(\alpha\beta)}(t) \tag{3.8}$$

$$\frac{\mathrm{d}}{\mathrm{d}t}i_{\mathrm{v}}^{(\alpha\beta)}(t) = -\frac{R_{\mathrm{v}}}{L_{\mathrm{v}}}i_{\mathrm{v}}^{(\alpha\beta)}(t) + \frac{1}{L_{\mathrm{v}}}(u_{\mathrm{v}}^{(\alpha\beta)}(t) - u_{\mathrm{f}}^{(\alpha\beta)}(t)) \tag{3.9}$$

By using the transformation angle θ derived from a phase-locked loop (PLL), (3.7), (3.8) and (3.9) are further transferred into the rotating dq-coordinate system as:

$$\frac{\mathrm{d}}{\mathrm{d}t}i_{\mathrm{tr}}^{(\mathrm{dq})}(t) = -\frac{R_{\mathrm{tr}}}{L_{\mathrm{tr}}}i_{\mathrm{tr}}^{(\mathrm{dq})}(t) - j\omega i_{\mathrm{tr}}^{(\mathrm{dq})}(t) + \frac{1}{L_{\mathrm{tr}}}(u_{\mathrm{f}}^{(\mathrm{dq})}(t) - u_{\mathrm{PCC}}^{(\mathrm{dq})}(t)) \tag{3.10}$$

$$\frac{\mathrm{d}}{\mathrm{d}t}u_{\mathrm{f}}^{(\mathrm{dq})}(t) = -\frac{1}{C_{\mathrm{f}}}i_{\mathrm{tr}}^{(\mathrm{dq})}(t) + \frac{1}{C_{\mathrm{f}}}i_{\mathrm{v}}^{(\mathrm{dq})}(t) - j\omega u_{\mathrm{f}}^{(\mathrm{dq})}(t) \tag{3.11}$$

$$\frac{\mathrm{d}}{\mathrm{d}t}i_{\mathrm{v}}^{(\mathrm{dq})}(t) = -\frac{R_{\mathrm{v}}}{L_{\mathrm{v}}}i_{\mathrm{v}}^{(\mathrm{dq})}(t) - j\omega i_{\mathrm{v}}^{(\mathrm{dq})}(t) + \frac{1}{L_{\mathrm{v}}}(u_{\mathrm{v}}^{(\mathrm{dq})}(t) - u_{\mathrm{f}}^{(\mathrm{dq})}(t)) \tag{3.12}$$

The voltage of the AC filter, the current through the phase reactor $R_{\mathrm{v}} + j\omega L_{\mathrm{v}}$ and the voltage of the VSC side can be expressed:

$$u_{\mathrm{f}}^{(\mathrm{dq})}(t) = u_{\mathrm{PCC}}^{(\mathrm{dq})}(t) + R_{\mathrm{tr}}i_{\mathrm{tr}}^{(\mathrm{dq})}(t) + j\omega L_{\mathrm{tr}}i_{\mathrm{tr}}^{(\mathrm{dq})}(t) + L_{\mathrm{tr}}\frac{\mathrm{d}}{\mathrm{d}t}i_{\mathrm{tr}}^{(\mathrm{dq})}(t) \tag{3.13}$$

$$i_{\mathrm{v}}^{(\mathrm{dq})}(t) = i_{\mathrm{tr}}^{(\mathrm{dq})}(t) + j\omega C_{\mathrm{f}}u_{\mathrm{f}}^{(\mathrm{dq})}(t) + C_{\mathrm{f}}\frac{\mathrm{d}}{\mathrm{d}t}u_{\mathrm{f}}^{(\mathrm{dq})}(t) \tag{3.14}$$

$$u_{\mathrm{v}}^{(\mathrm{dq})}(t) = u_{\mathrm{f}}^{(\mathrm{dq})}(t) + R_{\mathrm{v}}i_{\mathrm{v}}^{(\mathrm{dq})}(t) + j\omega L_{\mathrm{v}}i_{\mathrm{v}}^{(\mathrm{dq})}(t) + L_{\mathrm{v}}\frac{\mathrm{d}}{\mathrm{d}t}i_{\mathrm{v}}^{(\mathrm{dq})}(t) \tag{3.15}$$

The mean voltages and currents over the sample period k to $k+1$ are derived by integrating (3.13), (3.14) and (3.15) from kT_{s} to $(k+1)\,T_{\mathrm{s}}$ and dividing by T_{s} (where T_{s} is the sampling time).

$$\begin{aligned} u_{\mathrm{f}}^{(\mathrm{dq})}(k,k+1) &= u_{\mathrm{PCC}}^{(\mathrm{dq})}(k,k+1) + R_{\mathrm{tr}}i_{\mathrm{tr}}^{(\mathrm{dq})}(k,k+1) + j\omega L_{\mathrm{tr}}i_{\mathrm{tr}}^{(\mathrm{dq})}(k,k+1) \\ &\quad + \frac{L_{\mathrm{tr}}}{T_{\mathrm{s}}}(i_{\mathrm{tr}}^{(\mathrm{dq})}(k+1) - i_{\mathrm{tr}}^{(\mathrm{dq})}(k)) \end{aligned} \tag{3.16}$$

$$\begin{aligned} i_{\mathrm{v}}^{(\mathrm{dq})}(k,k+1) &= i_{\mathrm{tr}}^{(\mathrm{dq})}(k,k+1) + j\omega C_{\mathrm{f}}u_{\mathrm{f}}^{(\mathrm{dq})}(k,k+1) \\ &\quad + \frac{C_{\mathrm{f}}}{T_{\mathrm{s}}}(u_{\mathrm{f}}^{(\mathrm{dq})}(k+1) - u_{\mathrm{f}}^{(\mathrm{dq})}(k)) \end{aligned} \tag{3.17}$$

$$\begin{aligned} u_{\mathrm{v}}^{(\mathrm{dq})}(k,k+1) &= u_{\mathrm{f}}^{(\mathrm{dq})}(k,k+1) + R_{\mathrm{v}}i_{\mathrm{v}}^{(\mathrm{dq})}(k,k+1) + j\omega L_{\mathrm{v}}i_{\mathrm{v}}^{(\mathrm{dq})}(k,k+1) \\ &\quad + \frac{L_{\mathrm{v}}}{T_{\mathrm{s}}}(i_{\mathrm{v}}^{(\mathrm{dq})}(k+1) - i_{\mathrm{v}}^{(\mathrm{dq})}(k)) \end{aligned} \tag{3.18}$$

where $u_{\mathrm{PCC}}^{(\mathrm{dq})}(k,k+1)$, $i_{\mathrm{tr}}^{(\mathrm{dq})}(k,k+1)$, $u_{\mathrm{f}}^{(\mathrm{dq})}(k,k+1)$, $i_{\mathrm{v}}^{(\mathrm{dq})}(k,k+1)$ and $u_{\mathrm{v}}^{(\mathrm{dq})}(k,k+1)$ are the average values of $u_{\mathrm{PCC}}^{(\mathrm{dq})}$, $i_{\mathrm{tr}}^{(\mathrm{dq})}$, $u_{\mathrm{f}}^{(\mathrm{dq})}$, $i_{\mathrm{v}}^{(\mathrm{dq})}$ and $u_{\mathrm{v}}^{(\mathrm{dq})}$ over the sampling period [76].

During one sample period T_{s}, it can be assumed that:

- in (3.16) the current $i_{\mathrm{tr}}^{(\mathrm{dq})}(k,k+1)$ is changed linearly, the voltage $u_{\mathrm{PCC}}(k,k+1)$ changes slowly as compared with the dynamics of $i_{\mathrm{tr}}^{(\mathrm{dq})}(k,k+1)$ and can be considered constant.
- in (3.17) the voltage $u_{\mathrm{f}}^{(\mathrm{dq})}(k,k+1)$ is changed linearly and the current $i_{\mathrm{tr}}^{(\mathrm{dq})}(k,k+1)$ changes slowly as compared with the dynamics of $u_{\mathrm{f}}^{(\mathrm{dq})}(k,k+1)$ and can be considered constant.
- in (3.18) the current $i_{\mathrm{v}}^{(\mathrm{dq})}(k,k+1)$ is changed linearly and the voltage $u_{\mathrm{f}}(k,k+1)$ changes slowly as compared with the dynamics of $i_{\mathrm{v}}^{(\mathrm{dq})}(k,k+1)$ and can be considered constant.
- the controller uses dead-beat gain of the proportional regulator, thus the current through the transformer, the voltage of the AC filter and the current through the phase reactor will track the reference values with one sample delay, i.e. $i_{\mathrm{tr}}^{(\mathrm{dq})}(k+1)=i_{\mathrm{tr}}^{(\mathrm{dq})^*}(k)$, $u_{\mathrm{f}}^{(\mathrm{dq})}(k+1)=u_{\mathrm{f}}^{(\mathrm{dq})^*}(k)$ and $i_{\mathrm{v}}^{(\mathrm{dq})}(k+1)=i_{\mathrm{v}}^{(\mathrm{dq})^*}(k)$.

Under the above assumptions it can be derived that:

$$\begin{aligned} u_{\mathrm{f}}^{(\mathrm{dq})}(k,k+1) &= u_{\mathrm{PCC}}^{(\mathrm{dq})}(k)+\frac{R_{\mathrm{tr}}}{2}\left[i_{\mathrm{tr}}^{(\mathrm{dq})^*}(k)+i_{\mathrm{tr}}^{(\mathrm{dq})}(k)\right]+j\frac{\omega L_{\mathrm{tr}}}{2}\left[i_{\mathrm{tr}}^{(\mathrm{dq})^*}(k)+i_{\mathrm{tr}}^{(\mathrm{dq})}(k)\right] \\ &\quad +\frac{L_{\mathrm{tr}}}{T_{\mathrm{s}}}\left[i_{\mathrm{tr}}^{(\mathrm{dq})^*}(k)-i_{\mathrm{tr}}^{(\mathrm{dq})}(k)\right] \qquad (3.19) \\ i_{\mathrm{v}}^{(\mathrm{dq})}(k,k+1) &= i_{\mathrm{tr}}^{(\mathrm{dq})}(k)+j\frac{\omega C_{\mathrm{f}}}{2}\left[u_{\mathrm{f}}^{(\mathrm{dq})^*}(k)+u_{\mathrm{f}}^{(\mathrm{dq})}(k)\right] \\ &\quad +\frac{C_{\mathrm{f}}}{T_{\mathrm{s}}}\left[u_{\mathrm{f}}^{(\mathrm{dq})^*}(k)-u_{\mathrm{f}}^{(\mathrm{dq})}(k)\right] \qquad (3.20) \\ u_{\mathrm{v}}^{(\mathrm{dq})}(k,k+1) &= u_{\mathrm{f}}^{(\mathrm{dq})}(k)+\frac{R_{\mathrm{v}}}{2}\left[i_{\mathrm{v}}^{(\mathrm{dq})^*}(k)+i_{\mathrm{tr}}^{(\mathrm{dq})}(k)\right]+j\frac{\omega L_{\mathrm{v}}}{2}\left[i_{\mathrm{v}}^{(\mathrm{dq})^*}(k)+i_{\mathrm{v}}^{(\mathrm{dq})}(k)\right] \\ &\quad +\frac{L_{\mathrm{v}}}{T_{\mathrm{s}}}\left[i_{\mathrm{v}}^{(\mathrm{dq})^*}(k)-i_{\mathrm{v}}^{(\mathrm{dq})}(k)\right] \qquad (3.21) \end{aligned}$$

It is assumed that the produced average currents and voltages between sample k and $k+1$ become the reference currents and voltages at sample k. Finally the following proportional control equations can be derived as:

$$\begin{aligned} u_{\mathrm{f}}^{(\mathrm{dq})^*}(k) &= u_{\mathrm{PCC}}^{(\mathrm{dq})}(k)+R_{\mathrm{tr}}i_{\mathrm{tr}}^{(\mathrm{dq})}(k)+\mathrm{j}\frac{\omega L_{\mathrm{tr}}}{2}\left[i_{\mathrm{tr}}^{(\mathrm{dq})^*}(k)+i_{\mathrm{tr}}^{(\mathrm{dq})}(k)\right] \\ &\quad +k_{\mathrm{p,pcc}}\left[i_{\mathrm{tr}}^{(\mathrm{dq})^*}(k)-i_{\mathrm{tr}}^{(\mathrm{dq})}(k)\right] \qquad (3.22) \\ i_{\mathrm{v}}^{(\mathrm{dq})^*}(k) &= i_{\mathrm{tr}}^{(\mathrm{dq})}(k)+\mathrm{j}\frac{\omega C_{\mathrm{f}}}{2}\left[u_{\mathrm{f}}^{(\mathrm{dq})^*}(k)+u_{\mathrm{f}}^{(\mathrm{dq})}(k)\right] \\ &\quad +k_{\mathrm{p,u_f}}\left[u_{\mathrm{f}}^{(\mathrm{dq})^*}(k)-u_{\mathrm{f}}^{(\mathrm{dq})}(k)\right] \qquad (3.23) \\ u_{\mathrm{v}}^{(\mathrm{dq})^*}(k) &= u_{\mathrm{f}}^{(\mathrm{dq})}(k)+R_{\mathrm{v}}i_{\mathrm{v}}^{(\mathrm{dq})}(k)+\mathrm{j}\frac{\omega L_{\mathrm{v}}}{2}\left[i_{\mathrm{v}}^{(\mathrm{dq})^*}(k)+i_{\mathrm{v}}^{(\mathrm{dq})}(k)\right] \\ &\quad +k_{\mathrm{p,i_v}}\left[i_{\mathrm{v}}^{(\mathrm{dq})^*}(k)-i_{\mathrm{v}}^{(\mathrm{dq})}(k)\right] \qquad (3.24) \end{aligned}$$

The proportional gains are equal to:

$$k_{\mathrm{p,pcc}} = k_{\mathrm{pf1}} \cdot \left(\frac{L_{\mathrm{tr}}}{T_{\mathrm{s}}} + \frac{R_{\mathrm{tr}}}{2} \right) \tag{3.25}$$

$$k_{\mathrm{p,u_f}} = k_{\mathrm{pf2}} \cdot \left(\frac{C_{\mathrm{f}}}{T_{\mathrm{s}}} \right) \tag{3.26}$$

$$k_{\mathrm{p,i_v}} = k_{\mathrm{pf3}} \cdot \left(\frac{L_{\mathrm{v}}}{T_{\mathrm{s}}} + \frac{R_{\mathrm{v}}}{2} \right) \tag{3.27}$$

In order to stabilize the controller, the gain of the P-parts are altered from the dead beat gain by the constants k_{pf1}, k_{pf2} and k_{pf3}. Stability analysis of the system can give the proper values for the gain factors of the P-controller. It is known that the stability boundary for a discrete time system is defined as the unit circle. Hence, if the poles of the system are inside the unit circle, the discrete system is stable.

In the following subsections three different algorithms for the vector controller are analyzed. All three algorithms are based on (3.22), (3.23) and (3.24).

3.2.1 Inner current controller

The inner current controller is obtained directly from (3.24). An integral part is included to avoid a steady state error. The resulting control equation reads as follows:

$$\begin{aligned} u_{\mathrm{v}}^{(\mathrm{dq})^*}(k) = \; & u_{\mathrm{f}}^{(\mathrm{dq})}(k) + R_{\mathrm{v}} i_{\mathrm{v}}^{(\mathrm{dq})}(k) + \mathrm{j}\frac{\omega L_{\mathrm{v}}}{2}\left[i_{\mathrm{v}}^{(\mathrm{dq})^*}(k) + i_{\mathrm{v}}^{(\mathrm{dq})}(k) \right] \\ & + k_{\mathrm{p,i_v}}\left[i_{\mathrm{v}}^{(\mathrm{dq})^*}(k) - i_{\mathrm{v}}^{(\mathrm{dq})}(k) \right] + \Delta u_{\mathrm{I,v}}^{(\mathrm{dq})}(k) \end{aligned} \tag{3.28}$$

and the integral term can be written as:

$$\Delta u_{\mathrm{I,v}}^{(\mathrm{dq})}(k+1) = \Delta u_{\mathrm{I,v}}^{(\mathrm{dq})}(k) + k_{\mathrm{I,i_v}}\left[i_{\mathrm{v}}^{(\mathrm{dq})^*}(k) - i_{\mathrm{v}}^{(\mathrm{dq})}(k) \right] \tag{3.29}$$

where the integral gain [77] is:

$$k_{\mathrm{I,i_v}} = k_{\mathrm{p,i_v}} T_{\mathrm{s}} R_{\mathrm{v}} / L_{\mathrm{v}} \tag{3.30}$$

The reference values of the currents through the phase reactor in the dq-plane, i.e. $i_{\mathrm{v}}^{(\mathrm{dq})^*}$, are given from the outer controllers. The $k_{\mathrm{p,i_v}}$ is obtained from (3.27). In (3.27) k_{pf3} is chosen to render a stable controller according to stability analysis. It should be mentioned that a one-sample delay is implemented in the controller due to the calculation time. Figs. 3.4 and 3.5 show the frequency responses from the current reference $i_{\mathrm{v}}^{(\mathrm{q})^*}$ to the actual current $i_{\mathrm{v}}^{(\mathrm{q})}$ for different k_{pf3} with and without a one-sample delay. As shown in Fig. 3.5, the use of a high k_{pf3} may result in a poor performance or instability of the system. Therefore, a low value of k_{pf3} can be used without a one-sample delay compensation in a slow current controller. However, a high k_{pf3} should be chosen in a fast current

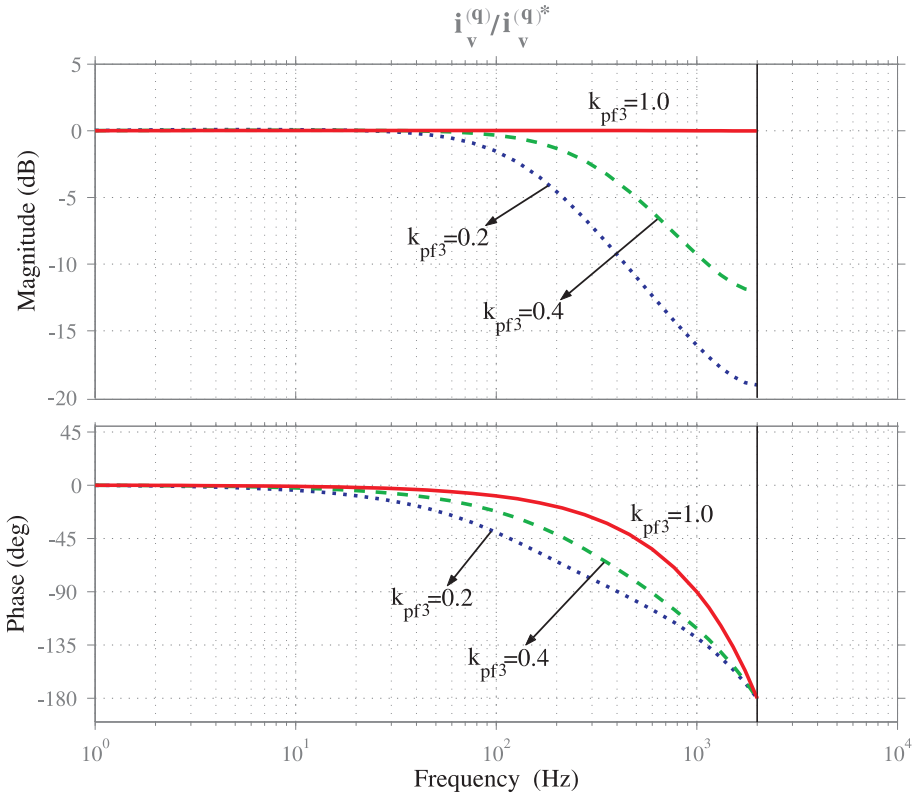

Fig. 3.4 Frequency response from the current reference $i_{\mathrm{v}}^{(\mathrm{q})^*}$ to the actual current $i_{\mathrm{v}}^{(\mathrm{q})}$ without a one-sample delay.

controller and the one-sample delay has to be compensated for. A Smith predictor [78] can be used to compensate for the time delay. The derived predicted current $\hat{i}_{\mathrm{v}}^{(\mathrm{dq})}$ is given as:

$$\begin{aligned}\hat{i}_{\mathrm{v}}^{(\mathrm{dq})}(k+1) &= \frac{T_{\mathrm{s}}}{L_{\mathrm{v}}}\left(u_{\mathrm{v}}^{(\mathrm{dq})^*}(k) - u_{\mathrm{f}}^{(\mathrm{dq})}(k)\right) + \left(1 - \frac{R_{\mathrm{v}}T_{\mathrm{s}}}{L_{\mathrm{v}}} - \mathrm{j}\omega\mathrm{T_s}\right)\hat{i}_{\mathrm{v}}^{(\mathrm{dq})}(k) \\ &+ k_{\mathrm{ps}}\left(i_{\mathrm{v}}^{(\mathrm{dq})}(k) - \hat{i}_{\mathrm{v}}^{(\mathrm{dq})}(k)\right) \end{aligned} \tag{3.31}$$

where k_{ps} is a proportional gain of the Smith predictor.

The control equation of the inner current controller (3.28) is modified as:

$$\begin{aligned}u_{\mathrm{v}}^{(\mathrm{dq})^*}(k) = u_{\mathrm{f}}^{(\mathrm{dq})}(k) + R_{\mathrm{v}}i_{\mathrm{v}}^{(\mathrm{dq})}(k) + \mathrm{j}\frac{\omega L_{\mathrm{v}}}{2}\left[i_{\mathrm{v}}^{(\mathrm{dq})^*}(k) + i_{\mathrm{v}}^{(\mathrm{dq})}(k)\right] \\ + k_{\mathrm{p,i_v}}e(k) + \Delta u_{\mathrm{I,v}}^{(\mathrm{dq})}(k)\end{aligned} \tag{3.32}$$

where

$$e(k) = \left(i_{\mathrm{v}}^{(\mathrm{dq})^*}(k) - i_{\mathrm{v}}^{(\mathrm{dq})}(k)\right) - \left(\hat{i}_{\mathrm{v}}^{(\mathrm{dq})}(k) - \hat{i}_{\mathrm{v}}^{(\mathrm{dq})}(k-1)\right) \tag{3.33}$$

and the integral term can be rewritten as:

$$\Delta u_{\mathrm{I,v}}^{(\mathrm{dq})}(k+1) = \Delta u_{\mathrm{I,v}}^{(\mathrm{dq})}(k) + k_{\mathrm{I,i_v}}e(k) \tag{3.34}$$

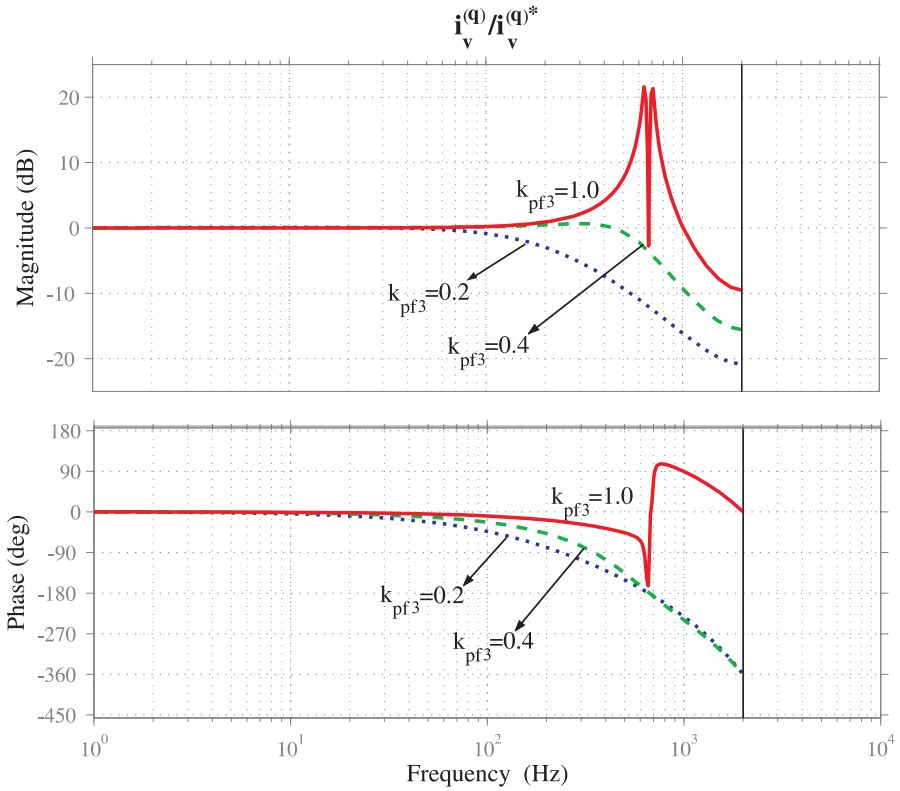

Fig. 3.5 Frequency response from the current reference $i_{\mathrm{v}}^{(\mathrm{q})^*}$ to the actual current $i_{\mathrm{v}}^{(\mathrm{q})}$ with a one-sample delay.

3.2.2 Dual vector controller

The dual vector controller is based on (3.23) and (3.24). It consists of a filter-bus voltage outer controller for the voltage u_{f}, and an inner current control loop for the current i_{v} which has been described in the above subsection. In this subsection the inner current controller will be described again together with the filter-bus voltage controller for clarity.

The resulting control equations of the dual vector controller can be written as:

$$\begin{aligned} i_{\mathrm{v}}^{(\mathrm{dq})^*}(k) &= i_{\mathrm{tr}}^{(\mathrm{dq})}(k) + \mathrm{j}\frac{\omega C_{\mathrm{f}}}{2}\left[u_{\mathrm{f}}^{(\mathrm{dq})^*}(k) + u_{\mathrm{f}}^{(\mathrm{dq})}(k)\right] \\ &\quad + k_{\mathrm{p,u_f}}\left[u_{\mathrm{f}}^{(\mathrm{dq})^*}(k) - u_{\mathrm{f}}^{(\mathrm{dq})}(k)\right] + \Delta i_{\mathrm{I,v}}^{(\mathrm{dq})}(k) \end{aligned} \tag{3.35}$$

$$\begin{aligned} u_{\mathrm{v}}^{(\mathrm{dq})^*}(k) &= u_{\mathrm{f}}^{(\mathrm{dq})}(k) + R_{\mathrm{v}} i_{\mathrm{v}}^{(\mathrm{dq})}(k) + \mathrm{j}\frac{\omega L_{\mathrm{v}}}{2}\left[i_{\mathrm{v}}^{(\mathrm{dq})^*}(k) + i_{\mathrm{v}}^{(\mathrm{dq})}(k)\right] \\ &\quad + k_{\mathrm{p,i_v}}\left[i_{\mathrm{v}}^{(\mathrm{dq})^*}(k) - i_{\mathrm{v}}^{(\mathrm{dq})}(k)\right] + \Delta u_{\mathrm{I,v}}^{(\mathrm{dq})}(k) \end{aligned} \tag{3.36}$$

where the integral terms are:

$$\Delta i_{\mathrm{I,v}}^{(\mathrm{dq})}(k+1) = \Delta i_{\mathrm{I,v}}^{(\mathrm{dq})}(k) + k_{\mathrm{I,u_f}}\left[u_{\mathrm{f}}^{(\mathrm{dq})^*}(k) - u_{\mathrm{f}}^{(\mathrm{dq})}(k)\right] \tag{3.37}$$

$$\Delta u_{\mathrm{I,v}}^{(\mathrm{dq})}(k+1) = \Delta u_{\mathrm{I,v}}^{(\mathrm{dq})}(k) + k_{\mathrm{I,i_v}}\left[i_{\mathrm{v}}^{(\mathrm{dq})^*}(k) - i_{\mathrm{v}}^{(\mathrm{dq})}(k)\right] \tag{3.38}$$

where $k_{\mathrm{I,u_f}} = k_{\mathrm{p,u_f}} \frac{T_\mathrm{s}}{T_{\mathrm{i,u_f}}}$ and $T_{\mathrm{i,u_f}}$ is the integral time constant. Again $k_{\mathrm{p,u_f}}$ and $k_{\mathrm{p,i_v}}$ are calculated from (3.26) and (3.27) while $k_{\mathrm{I,i_v}}$ is given from (3.30). The reference values of the filter-bus voltages in the dq-plane, i.e. $u_\mathrm{f}^{(\mathrm{dq})^*}$, can be set to $u_\mathrm{f}^{(\mathrm{d})^*} = 0.0\ \mathrm{pu}$ and $u_\mathrm{f}^{(\mathrm{q})^*} = 1.0\ \mathrm{pu}$ in a flux-oriented system to control the filter-bus voltage to the rated value. In (3.35) and (3.36) the factors k_{pf2} and k_{pf3} are chosen to tune the proportional gains of the controller.

The effect on the stability of the controller when changing the gain factors k_{pf2} and k_{pf3} is examined. The zeros and poles of the complete system's transfer function are shown in Fig. 3.6 where k_{pf2} is varied between 0 and 1 (The directions of the arrows in the figure indicate the directions of increasing k_{pf2}). From the study it can be concluded that the poles are attracted into the unit circle more quickly when decreasing k_{pf3}. When k_{pf2} is set to be the dead-beat gain ($k_{\mathrm{pf2}} = 1$) the system can be stable when k_{pf3} is set to be 0.3 or less. However, a high value of k_{pf3} will lead to an unstable behavior even though k_{pf2} is chosen to be low. As shown in Fig. 3.6, k_{pf3} should be chosen to be less than 0.5 to keep the system stable when k_{pf2} is set to be lower.

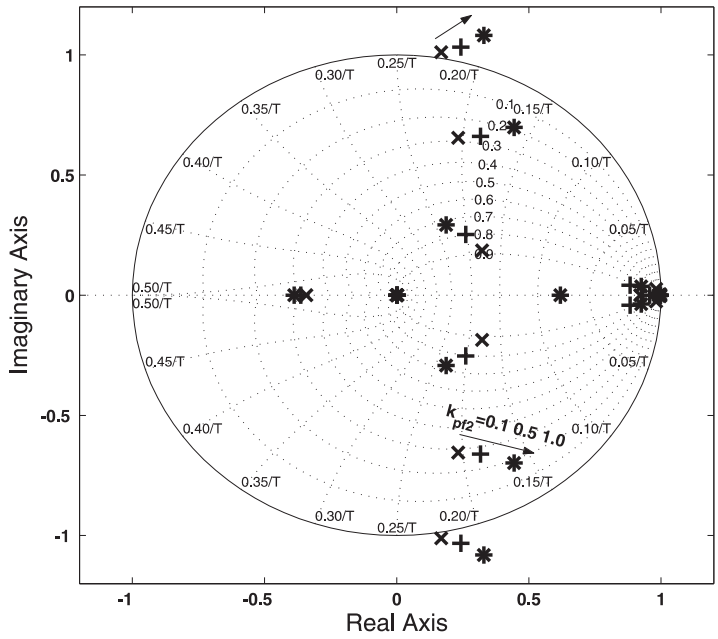

Fig. 3.6 Poles and zeros of the discrete time closed loop system with k_{pf2} increasing from 0 to 1 and $k_{\mathrm{pf3}} = 0.5$ ($\times : \mathrm{k_{pf2}} = 0.1, + : \mathrm{k_{pf2}} = 0.5$ and $* : \mathrm{k_{pf2}} = 1.0$).

3.2.3 Vector controller with LCL filter

The purpose of the vector controller with LCL filter is to generate the controlled voltage value u_v^* such that the AC voltage and frequency at the PCC keep their reference values when $i_\mathrm{tr}^{(\mathrm{dq})^*}$ are obtained from the PCC voltage and frequency controllers. The vector controller with LCL filter [75] comprises a PCC current control loop for the current through

the transformer, i.e. (3.22), a filter-bus voltage controller for the filter capacitor voltage, i.e. (3.23), and an inner current control loop for the current through the phase reactor, i.e. (3.24). All together, the vector controller with LCL filter consists of two P controllers and one PI controller with additional feed forward and feed back terms. The filter-bus voltage controller and the inner current controller, described in the previous subsections, will be described again together with a PCC current controller for clarity.

The derived vector controller with LCL filter are formulated as:

$$u_{\mathrm{f}}^{(\mathrm{dq})^*}(k) = u_{\mathrm{PCC}}^{(\mathrm{dq})}(k) + R_{\mathrm{tr}} i_{\mathrm{tr}}^{(\mathrm{dq})}(k) + \mathrm{j}\frac{\omega L_{\mathrm{tr}}}{2}\left[i_{\mathrm{tr}}^{(\mathrm{dq})^*}(k) + i_{\mathrm{tr}}^{(\mathrm{dq})}(k)\right] + k_{\mathrm{p,pcc}}\left[i_{\mathrm{tr}}^{(\mathrm{dq})^*}(k) - i_{\mathrm{tr}}^{(\mathrm{dq})}(k)\right] \tag{3.39}$$

$$i_{\mathrm{v}}^{(\mathrm{dq})^*}(k) = i_{\mathrm{tr}}^{(\mathrm{dq})}(k) + \mathrm{j}\frac{\omega C_{\mathrm{f}}}{2}\left[u_{\mathrm{f}}^{(\mathrm{dq})^*}(k) + u_{\mathrm{f}}^{(\mathrm{dq})}(k)\right] + k_{\mathrm{p,u_f}}\left[u_{\mathrm{f}}^{(\mathrm{dq})^*}(k) - u_{\mathrm{f}}^{(\mathrm{dq})}(k)\right] \tag{3.40}$$

$$u_{\mathrm{v}}^{(\mathrm{dq})^*}(k) = u_{\mathrm{f}}^{(\mathrm{dq})}(k) + R_{\mathrm{v}} i_{\mathrm{v}}^{(\mathrm{dq})}(k) + \mathrm{j}\frac{\omega L_{\mathrm{v}}}{2}\left[i_{\mathrm{v}}^{(\mathrm{dq})^*}(k) + i_{\mathrm{v}}^{(\mathrm{dq})}(k)\right] + k_{\mathrm{p,i_v}}\left[i_{\mathrm{v}}^{(\mathrm{dq})^*}(k) - i_{\mathrm{v}}^{(\mathrm{dq})}(k)\right] + \Delta u_{\mathrm{I,v}}^{(\mathrm{dq})}(k) \tag{3.41}$$

The overall structure of the vector controller with LCL filter is shown in Fig. 3.7. As described in (3.25), (3.26) and (3.27), the proportional gains are scaled by the gain factors $k_{\mathrm{pf1}}, k_{\mathrm{pf2}}$ and k_{pf3} to stabilize the closed loop system.

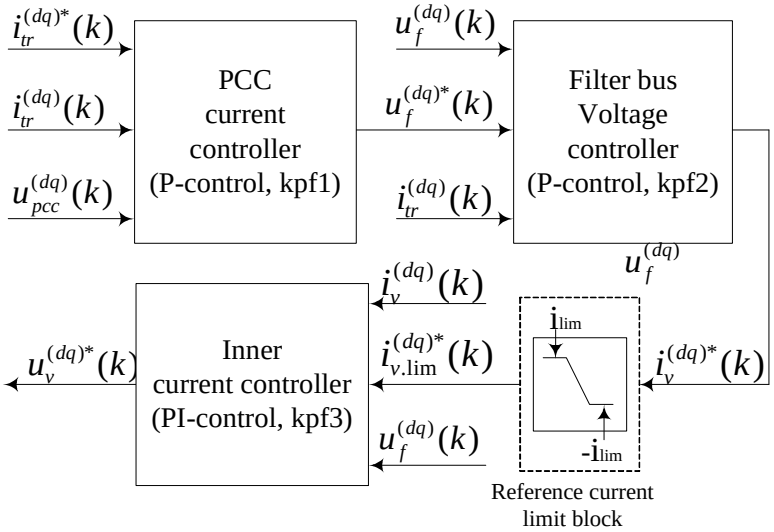

Fig. 3.7 Schematic diagram of the vector controller with LCL filter.

To investigate the influence of the gain factors k_{pf1}, k_{pf2} and k_{pf3} on the stability of the vector controller with LCL filter, the zeros and poles of the complete system's transfer function are computed with the gain factors varied between 0 and 1. The variation of zeros and poles are plotted in Fig. 3.8 when k_{pf3} is changed (The direction of the arrow in the

figure indicates the direction of increasing k_{pf3}). From the results of the stability analysis it can be obtained that k_{pf2} and k_{pf3} have significant effects on the poles of the system. The two poles close to the border of the stability region are moving faster when the gain factor k_{pf3} is changed as compared to if k_{pf2} is changed. A high value of k_{pf2} or k_{pf3} will lead to an unstable behavior. The influence of the gain factor k_{pf1} on the system performance is negligible.

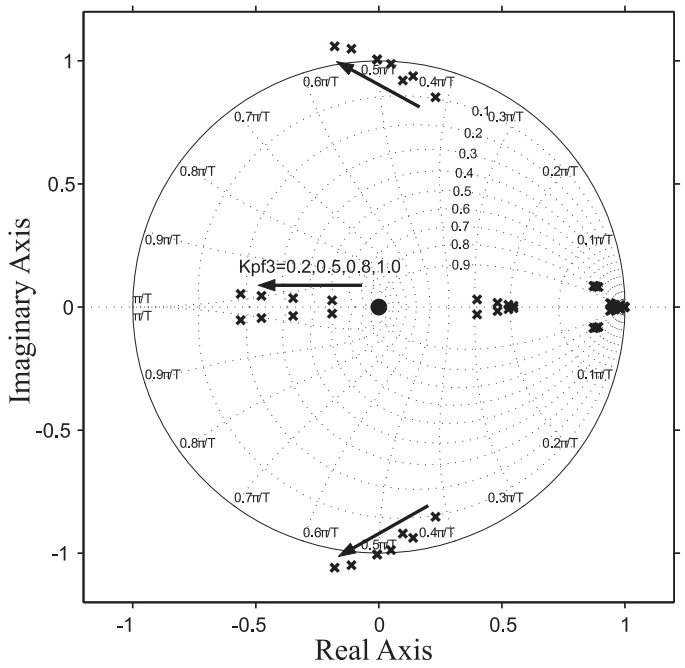

Fig. 3.8 Poles and zeros of the closed loop system with $k_{\mathrm{pf1}} = 1.0$, $k_{\mathrm{pf2}} = 0.2$ and varied k_{pf3}.

3.2.4 Limitation

Since the VSC-HVDC does not have any overload capability as synchronous generators have, a large transient current due to disturbances will stress or damage the valves. Therefore, a current limit must be implemented in the control system. Moreover, since the maximum output voltage amplitude out of the VSC is limited by the VSC voltage capability, the produced reference voltage from the vector controller must be appropriately limited.

The current limit i_{lim} is compared with the current magnitude computed from the active and reactive reference currents. When the current limit is exceeded, both the active and reactive reference currents have to be limited. The choice of how to limit both reference currents will depend on the application. For instance, if the converter is connected to a strong grid used for transmission, the active reference current will be given high priority, when the current limit is exceeded, to produce more active power. The produced active power may be estimated from the equation $P_{\max} = \sqrt{u_{\mathrm{v}}^2 * i_{\mathrm{lim}}^2}$. If the converter is

connected to a weak grid or used to supply an industrial plant, the VSC will give high priority to the reactive reference current to keep up the AC voltage when the current limit is exceeded. The remaining capability is then available for active power production. The produced reactive and active power may be estimated from the following equations:

$$\begin{aligned} Q_{\max} &= u_{\mathrm{v}} * i_{\mathrm{lim}}^{(\mathrm{d})} \\ P_{\max} &= \sqrt{u_{\mathrm{v}}^2 * i_{\mathrm{lim}}^2 - Q_{\max}^2} \end{aligned} \tag{3.42}$$

where $i_{\mathrm{lim}}^{(\mathrm{d})}$ is the pre-set maximum reactive reference current.

In order to maintain a proper control and reduce the lower-frequency harmonics, the maximum output voltage amplitude out of the VSC is limited inside the hexagon shown in Fig. 3.9. The amplitude of u_{lim}^* is equal to $\frac{1}{2}\sqrt{\frac{3}{2}}u_{\mathrm{DC}}$ [79]. It should be mentioned that when the limits are reached the back-calculation [80] is used to avoid integrator windup.

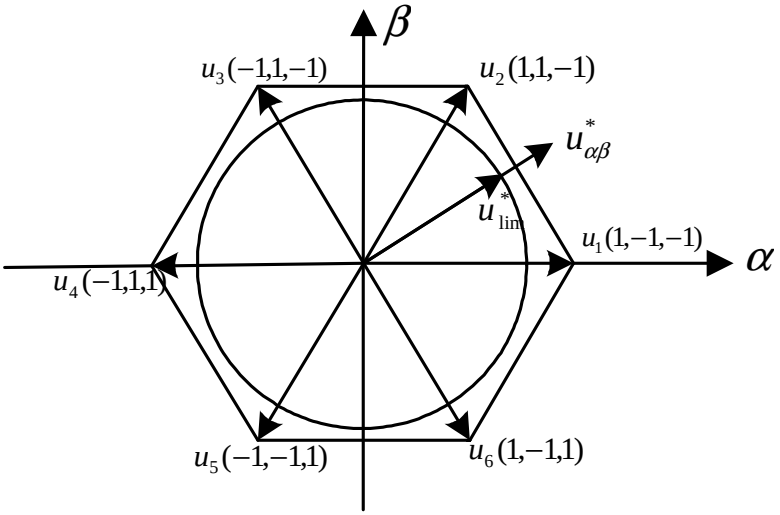

Fig. 3.9 Hexagon including eight realizable voltage vectors of three-phase VSC and the voltage limit method.

3.3 Outer controller

As previously mentioned the outer controller consists of the DC voltage controller, the AC voltage controller, the active and reactive power controller and the frequency controller. In this section different outer controllers are described.

3.3.1 DC voltage controller

As shown in Fig. 2.8 the instantaneous active power $P_{\mathrm{f}}^{(\mathrm{dq})}$ and reactive power $Q_{\mathrm{f}}^{(\mathrm{dq})}$ together with the power P_{rec} transmitted on the DC side of the VSC are expressed as:

$$P_{\mathrm{f}}^{(\mathrm{dq})}(t) = u_{\mathrm{f}}^{(\mathrm{d})}(t) \cdot i_{\mathrm{v}}^{(\mathrm{d})}(t) + u_{\mathrm{f}}^{(\mathrm{q})}(t) \cdot i_{\mathrm{v}}^{(\mathrm{q})}(t) \tag{3.43}$$

$$Q_{\mathrm{f}}^{(\mathrm{dq})}(t) = u_{\mathrm{f}}^{(\mathrm{q})}(t) \cdot i_{\mathrm{v}}^{(\mathrm{d})}(t) - u_{\mathrm{f}}^{(\mathrm{d})}(t) \cdot i_{\mathrm{v}}^{(\mathrm{q})}(t) \tag{3.44}$$

$$P_{\mathrm{rec}}(t) = u_{\mathrm{DC}}(t) \cdot i_{\mathrm{DC}}(t) \tag{3.45}$$

where i_{DC} is the current on the DC side of the converter.

For balanced steady state operation, the dq-voltages are constant at the rated value. Therefore, the voltage $u_{\mathrm{f}}^{(\mathrm{d})}$ will be zero and $u_{\mathrm{f}}^{(\mathrm{q})}$ will be the rated voltage in a flux-oriented system. In order to ensure stability, the outer controller must be much slower than the vector controller [81]. At the time-scale of interest for the DC voltage controller, the currents may thus be assumed equal to their reference values. Under these assumptions, the expressions for active and reactive power become:

$$P_{\mathrm{f}}^{(\mathrm{dq})}(t) = u_{\mathrm{f}}^{(\mathrm{q})}(t) \cdot i_{\mathrm{v}}^{(\mathrm{q})^*}(t) \tag{3.46}$$

$$Q_{\mathrm{f}}^{(\mathrm{dq})}(t) = u_{\mathrm{f}}^{(\mathrm{q})}(t) \cdot i_{\mathrm{v}}^{(\mathrm{d})^*}(t) \tag{3.47}$$

Neglecting the losses in the converter and the phase reactor and equating the power transmitted on the AC and DC side of the converter yields from (3.45) and (3.46):

$$i_{\mathrm{DC}}(t) = \frac{u_{\mathrm{f}}^{(\mathrm{q})}(t) \cdot i_{\mathrm{v}}^{(\mathrm{q})^*}(t)}{u_{\mathrm{DC}}(t)} \tag{3.48}$$

Any unbalance between AC and DC power leads to a change in voltage over the DC link capacitors, given by:

$$C_{\mathrm{DC}} \frac{\mathrm{d}}{\mathrm{d}t} u_{\mathrm{DC}}(t) = i_{\mathrm{DC}}(t) - i_{\mathrm{load}}(t) \tag{3.49}$$

where i_{load} is the current out from the DC system, as shown in Fig. 2.8. By applying the forward Euler method and assuming that i_{DC} and i_{load} are constant during the interval and that the DC voltage tracks the reference, the following equation is obtained:

$$\frac{C_{\mathrm{DC}}}{T_{\mathrm{s}}} \{u_{\mathrm{DC}}^*(k) - u_{\mathrm{DC}}(k)\} = i_{\mathrm{DC}}(k) - i_{\mathrm{load}}(k) \tag{3.50}$$

Substituting (3.48) into (3.50) yields:

$$\begin{aligned} \frac{C_{\mathrm{DC}}}{T_{\mathrm{s}}} \cdot (u_{\mathrm{DC}}^*(k) - u_{\mathrm{DC}}(k)) &= \frac{u_{\mathrm{f}}^{(\mathrm{q})}(k) \cdot i_{\mathrm{v}}^{(\mathrm{q})^*}(k)}{u_{\mathrm{DC}}(k)} - i_{\mathrm{load}}(k) \\ &= \frac{u_{\mathrm{f}}^{(\mathrm{q})}(k) \cdot i_{\mathrm{v}}^{(\mathrm{q})^*}(k)}{u_{\mathrm{DC}}^*(k)} - i_{\mathrm{load}}(k) \end{aligned} \tag{3.51}$$

From (3.51) a control equation for the current reference $i_{\mathrm{v}}^{(\mathrm{q})^*}(k)$ is obtained as:

$$i_{\mathrm{v}}^{(\mathrm{q})^*}(k) = \frac{u_{\mathrm{DC}}^*(k)}{u_{\mathrm{f}}^{(\mathrm{q})}(k)}\{k_{\mathrm{p,DC}} \cdot (u_{\mathrm{DC}}^*(k) - u_{\mathrm{DC}}(k)) + i_{\mathrm{load}}(k)\} \tag{3.52}$$

where

$$k_{\mathrm{p,DC}} \quad = \quad k_{\mathrm{pf,DC}} \cdot \frac{C_{\mathrm{DC}}}{T_{\mathrm{s}}} \tag{3.53}$$

The factor $k_{\mathrm{pf,DC}}$ adjusts the gain $k_{\mathrm{p,DC}}$ to ensure stability.

3.3.2 Active power controller

A simple method to control the active power is an open-loop controller. The reactive current reference is obtained from (3.46) as:

$$i_{\mathrm{v}}^{(\mathrm{q})^*} = \frac{P_{\mathrm{f}}^*}{u_{\mathrm{f}}^{(\mathrm{q})}} \tag{3.54}$$

where P_{f}^* is the desired (reference) active power. If an accurate control of the active power is needed, a combination of a feedback loop and an open loop can be used [18]:

$$i_{\mathrm{v}}^{(\mathrm{q})^*} = \frac{P_{\mathrm{f}}^*}{u_{\mathrm{f}}^{(\mathrm{q})}} + (k_{\mathrm{p,P_f}} + \frac{k_{\mathrm{I,P_f}}}{s})(P_{\mathrm{f}}^* - P_{\mathrm{f}}) \tag{3.55}$$

where $k_{\mathrm{p,P_f}}$ and $k_{\mathrm{I,P_f}}$ are the proportional and integral gains of the active power controller.

3.3.3 Reactive power controller

A reactive power controller similar to the active power controller is obtained from (3.47) as:

$$i_{\mathrm{v}}^{(\mathrm{d})^*} = \frac{Q_{\mathrm{f}}^*}{u_{\mathrm{f}}^{(\mathrm{q})}} \tag{3.56}$$

where Q_{f}^* is the reference reactive power. Another method is to combine a feedback loop with an open loop [18]:

$$i_{\mathrm{v}}^{(\mathrm{d})^*} = \frac{Q_{\mathrm{f}}^*}{u_{\mathrm{f}}^{(\mathrm{q})}} + (k_{\mathrm{p,Q_f}} + \frac{k_{\mathrm{I,Q_f}}}{s})(Q_{\mathrm{f}}^* - Q_{\mathrm{f}}) \tag{3.57}$$

where $k_{\mathrm{p,Q_f}}$ and $k_{\mathrm{I,Q_f}}$ are the proportional and integral gains of the reactive power controller.

3.3.4 AC voltage controller

The voltage drop ΔV over the reactance $R_{\mathrm{v}} + \mathrm{j}\omega L_{\mathrm{v}}$ in Fig. 2.8 can be approximated as:

$$\Delta V = u_{\mathrm{f}} - u_{\mathrm{v}} \approx \frac{R_{\mathrm{v}} P_{\mathrm{f}} + X_{\mathrm{v}} Q_{\mathrm{f}}}{u_{\mathrm{f}}} \tag{3.58}$$

For the phase reactor $X_{\mathrm{v}} \gg R_{\mathrm{v}}$, thus the voltage drop ΔV depends only on the reactive power flow Q_{f}. According to (3.47), the voltage can then be regulated by controlling the d-component of the current.

3.3.5 Frequency controller

In this subsection four different frequency controllers will be described as follows.

Frequency controller I

Frequency controller I can be considered as a fixed frequency controller. A fixed frequency f^*_{VSC} equal to the nominal frequency is supplied to the VSC output voltage. The dual vector controller, as described in Section 3.2.2, can be used directly to produce the reference voltage. It should be noted that such a frequency controller can only be used for the supply to a system without other sources of frequency control.

Frequency controller II

Frequency controller II is also a fixed frequency controller. A new fixed frequency f^*_{VSC} is given to the VSC output voltage. This new fixed frequency is obtained from the voltage dynamics in the DC link. As known, the electrical energy in the capacitor is:

$$W_{\mathrm{DC}} = \frac{1}{2} C_{\mathrm{DC}} u^2_{\mathrm{DC}} \tag{3.59}$$

If the switching losses of both converters are neglected, the dynamics in the capacitor will be the difference between the power into the DC system P_{rec} and the power out from the DC system P_{inv}, given by:

$$\frac{\mathrm{d}}{\mathrm{d}t} W_{\mathrm{DC}} = \frac{1}{2} C_{\mathrm{DC}} \frac{\mathrm{d}}{\mathrm{d}t} u^2_{\mathrm{DC}} = P_{\mathrm{rec}} - P_{\mathrm{inv}} \tag{3.60}$$

According to the active power-frequency characteristics in an interconnected system [82,83], the new fixed frequency reference for frequency controller II can be produced from the following equation:

$$f^\star = f_0 - k_{\mathrm{FCII}} ({u^*_{\mathrm{DC}}}^2 - u^2_{\mathrm{DC}}) \tag{3.61}$$

where u^*_{DC} is the reference value, k_{FCII} is a gain and f_0 is the nominal frequency value. The frequency controller II is therefore of a proportional type.

Frequency controller III

The principle of frequency controller III [84, 85] is based on the active power-frequency characteristics in an interconnected system. An integral part is introduced in frequency controller III to avoid the steady state error, i.e. a PI controller [86, 87]. The input to frequency controller III is an estimated frequency from the phase locked loop (PLL) [80].

Improvement of frequency controller III

The principle of the VSC frequency controller is based on the relationship of the generator speed and the mismatch of the mechanical power provided by the turbine and the generator electric power [83]. The frequency dynamics of the VSC can be described by the following differential equation:

$$2H_{\mathrm{sys}}\frac{\mathrm{d}}{\mathrm{d}t}\Delta\omega = (\Delta P_{\mathrm{VSC}} - \Delta P_{\mathrm{L}}) - D * \Delta\omega \tag{3.62}$$

where H_{sys} is the equivalent inertia constant of the VSC supplied industrial system, $\Delta\omega$ is the system frequency deviation, D is the damping coefficient, ΔP_{VSC} is the active power change of the VSC and ΔP_{L} is the load change. As the VSC has no kinetic energy the only kinetic energies in the VSC supplied system are in the loads and production units. Therefore the inertia constant of a VSC supplied system can be defined as follows:

$$H_{\mathrm{sys}} = \sum H_{\mathrm{SM}} + \sum H_{\mathrm{IM}} \tag{3.63}$$

where H_{SM} is the inertia constant of the synchronous machines, turbines and gear boxes while H_{IM} is the inertia constant of the induction machines and their mechanical loads.

The simplified block diagram of the VSC's frequency controller is shown in Fig. 3.10. The controller is chosen to be a PI controller described by:

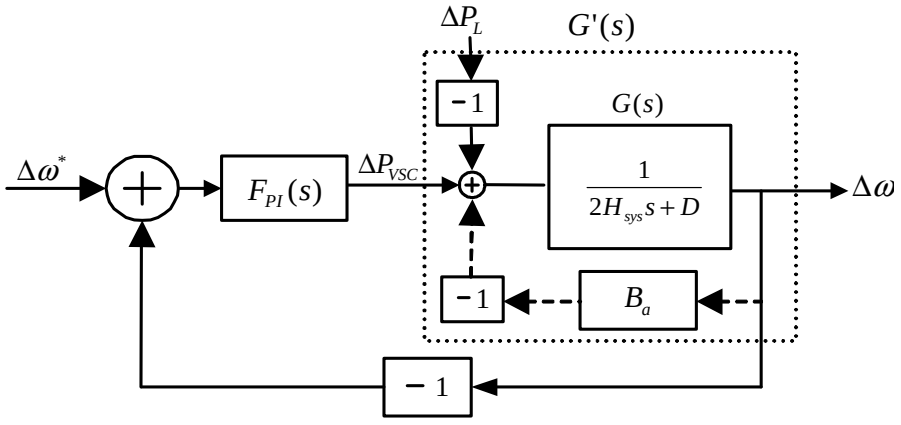

Fig. 3.10 Simplified block diagram of the improved frequency controller III.

$$F_{\mathrm{PI}}(s) = k_{\mathrm{p,fre}} + \frac{k_{\mathrm{I,fre}}}{s} \tag{3.64}$$

and an "active damping" term [80], B_{a}, is introduced to improve the rejection of disturbances. By using internal model control (IMC) [80], the proportional $k_{\mathrm{p,fre}}$ and integral gain $k_{\mathrm{I,fre}}$ of the improved frequency controller III can be derived as:

$$k_{\mathrm{p,fre}} = 2\alpha_{\mathrm{F}}\hat{H}_{\mathrm{sys}} \tag{3.65}$$

$$k_{\mathrm{I,fre}} = 2\alpha_{\mathrm{F}}^2\hat{H}_{\mathrm{sys}} \tag{3.66}$$

$$B_{\mathrm{a}} = 2\alpha_{\mathrm{F}}\hat{H}_{\mathrm{sys}} \tag{3.67}$$

where α_{F} is the bandwidth of the frequency control loop, $\hat{H}_{\mathrm{sys}}$ is the estimated inertia constant of the VSC supplied industrial plant. The transfer function of the closed loop system can be derived as:

$$\begin{aligned}
\frac{\Delta\omega}{\Delta\omega^*} &= \frac{F_{\mathrm{PI}}(s)G'(s)}{1+F_{\mathrm{PI}}(s)G'(s)} \\
&= \frac{sk_{\mathrm{p,fre}}+k_{\mathrm{I,fre}}}{s^2 2H_{\mathrm{sys}}+s(k_{\mathrm{p,fre}}+D+B_{\mathrm{a}})+k_{\mathrm{I,fre}}} \\
&= \frac{s(2\alpha_{\mathrm{F}}\hat{H}_{\mathrm{sys}})+2\alpha_{\mathrm{F}}^2\hat{H}_{\mathrm{sys}}}{s^2 2H_{\mathrm{sys}}+s(4\alpha_{\mathrm{F}}\hat{H}_{\mathrm{sys}}+D)+2\alpha_{\mathrm{F}}^2\hat{H}_{\mathrm{sys}}} \\
&\approx \frac{s(\alpha_{\mathrm{F}}\hat{H}_{\mathrm{sys}})+\alpha_{\mathrm{F}}^2\hat{H}_{\mathrm{sys}}}{s^2 H_{\mathrm{sys}}+s(2\alpha_{\mathrm{F}}\hat{H}_{\mathrm{sys}})+\alpha_{\mathrm{F}}^2\hat{H}_{\mathrm{sys}}}
\end{aligned} \tag{3.68}$$

In the last expression the damping term D has been considered negligible in comparison with the other term $4\alpha_{\mathrm{F}}\hat{H}_{\mathrm{sys}}$. As can be seen an accurately estimated inertia constant $\hat{H}_{\mathrm{sys}}$ has a significant effect on the system behavior. However, it is difficult to always have access to the accurate inertia constant of the system since it may change drastically such as before and after the trip of a synchronous generator. Therefore, it is important to investigate the impact on the system behavior with respect to different values of the estimated inertia constant. Fig. 3.11 shows the poles and zeros of the closed loop system depicted in Fig. 3.10 when varying the estimated inertia $\hat{H}_{\mathrm{sys}}$. It can be seen that the complex-conjugate pole pairs move towards the right half plane when $\hat{H}_{\mathrm{sys}}$ is underestimated, whereas the poles of the closed loop system are negative and real when $\hat{H}_{\mathrm{sys}}$ is equal to the actual H_{sys} or overestimated. It should be mentioned that with the overestimated $\hat{H}_{\mathrm{sys}}$ in Fig. 3.11 the poles also move slowly towards the right half plane. Therefore, a suitable overestimation of H_{sys} is chosen in this study in order to create a larger stability margin.

Frequency controller IV

Frequency controller IV is a droop frequency controller and can be used when the system can tolerate small frequency deviations at steady state conditions or the system contains

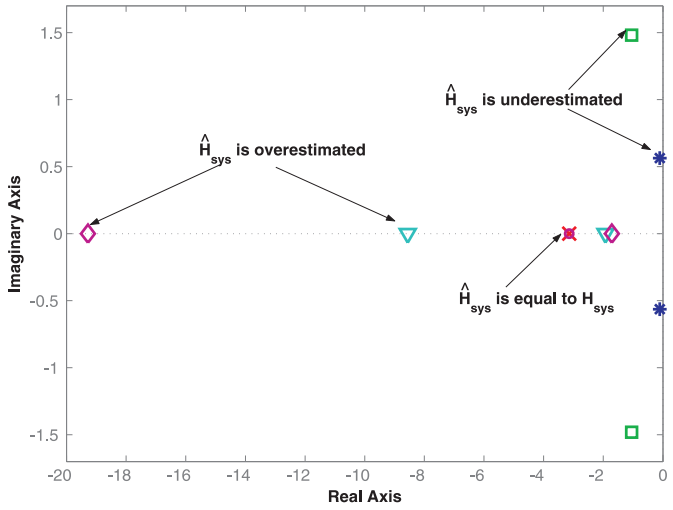

Fig. 3.11 Poles and zeros of the closed loop system having different estimates of H_{sys}.

other units with own frequency controllers. The transfer function of a droop controller $F_{\mathrm{droop}}(s)$, shown in Fig. 3.12, can be implemented as follows [39, 88, 89]:

$$\begin{aligned} F_{\mathrm{droop}}(s) &= k_{\mathrm{p,fre}} + k_{\mathrm{I,fre}} \frac{\omega_{\mathrm{cut}}}{s + \omega_{\mathrm{cut}}} \\ &= (k_{\mathrm{p,fre}} + k_{\mathrm{I,fre}}) \frac{1 + s\gamma T_{\mathrm{cut}}}{1 + sT_{\mathrm{cut}}} \end{aligned} \tag{3.69}$$

where $\gamma = \frac{k_{\mathrm{p,fre}}}{k_{\mathrm{p,fre}} + k_{\mathrm{I,fre}}} < 1$ and $T_{\mathrm{cut}} = \frac{1}{\omega_{\mathrm{cut}}}$.
$\Delta\omega$ will be equal to:

$$\begin{aligned} \Delta\omega &= \frac{-\Delta P_{\mathrm{L}}}{F_{\mathrm{droop}}(s) + 2H_{\mathrm{sys}}s + D} \\ &= \frac{-\Delta P_{\mathrm{L}}}{(k_{\mathrm{p,fre}} + k_{\mathrm{I,fre}}) \frac{1 + s\gamma T_{\mathrm{cut}}}{1 + sT_{\mathrm{cut}}} + 2H_{\mathrm{sys}}s + D} \end{aligned} \tag{3.70}$$

where $\Delta\omega^* = 0$.

By applying the final-value theorem to (3.70) the steady state error can be derived as:

$$\begin{aligned} \Delta\omega_{\mathrm{ss}} &= \frac{-\Delta P_{\mathrm{L}}}{k_{\mathrm{p,fre}} + k_{\mathrm{I,fre}} + D} \\ &\approx \frac{-\Delta P_{\mathrm{L}}}{k_{\mathrm{VSC}}} \end{aligned} \tag{3.71}$$

where the static gain $k_{\mathrm{VSC}} = \frac{1}{R_{\mathrm{VSC}}} = k_{\mathrm{p,fre}} + k_{\mathrm{I,fre}}$ as the damping D is very small and can be negligible. R_{VSC} denotes the frequency droop of the VSC.

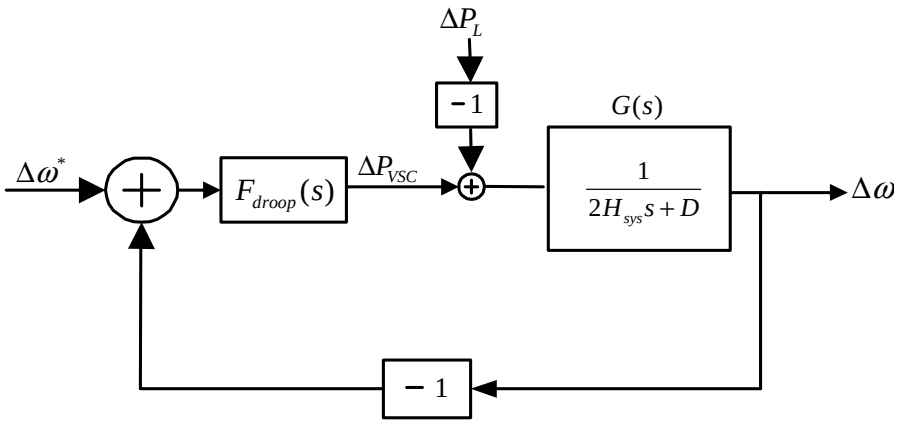

Fig. 3.12 Block diagram of frequency controller IV.

3.4 Summary

This chapter has focused on the control system structure of the VSC-HVDC. A cascade control structure including a fast vector controller and outer controllers has been presented. Three different vector controllers, i.e. the inner current controller, the dual vector controller and the vector controller with LCL filter, and different outer controllers, such as the DC and AC voltage controllers, the active power and reactive power controllers and four different frequency controllers, have been described. Furthermore, some analyses of the control system have been carried out.

Chapter 4

VSC-HVDC Connecting Two Grids

This chapter focuses on the performances of the complete and simplified VSC-HVDC models at steady state, load changes and disturbances in the supplying network. Some results are included in the published papers ***[Paper A]*** *and* ***[Paper B]****.*

4.1 Introduction

As discussed in Chapters 2 and 3, the high controllability of the VSC-HVDC gives a number of advantages and applications. Different applications require different choices of the control strategy. This chapter focuses on the performances of the complete VSC-HVDC model at steady state, subjected to load changes and disturbances in the supplying network. Moreover, since the control of the HVDC transmission based on voltage source converter uses PWM it is necessary to simulate the VSC-HVDC system with a small time step. This will reduce the simulation speed resulting in an increase of the time required to get valid and useful simulation results. Therefore, an equivalent but simplified simulation model of a VSC-HVDC system is evaluated during various disturbances in the supplying network.

In the complete model the converter consists of a three-phase, two-level, six-pulse bridge. The converter bridge valves are represented by ideal switches, where on-state losses and switching losses are neglected and phase reactors and transformers are assumed linear (saturation is not considered). In the simplified model the switching actions of the valves are neglected [26,28]. As can be noticed from Figs. 2.5 and 2.8, the only difference between the complete and simplified model is the connection between the AC and the DC side.

The behavior of the VSC-HVDC, using the complete model, during disturbances such as faults (balanced and unbalanced faults) and step changes (AC voltage, active and reactive power) is thoroughly investigated in **[Paper A]** and **[Paper B]**. In this chapter, the key results are illustrated together with supplementary details. Simulations are also performed to verify the simplified model against the complete model.

The studied system is shown in Fig. 4.1 and the system parameters are listed in Table 4.1. The current limit i_{lim} is set to $1.0\,\text{pu}$. Two different control strategies are implemented to evaluate the performance:

Strategy 1: AC-voltage control

- converter 1 controls the DC and AC voltages.
- converter 2 controls the active power and the AC voltage.

Strategy 2: reactive-power control

- converter 1 controls the DC voltage and the reactive power.
- converter 2 controls the active power and the reactive power.

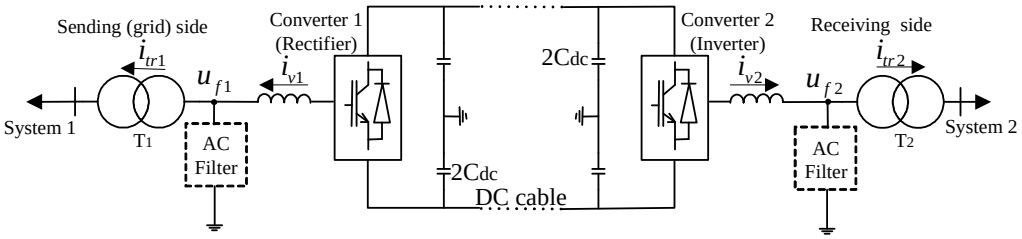

Fig. 4.1 The studied system.

Table 4.1: System parameters

Constant	Symbol	Actual value	Value in pu
Rated (base) voltage	U_1	$150\ \text{kV}$	1.0
Rated (base) voltage	U_2	$33\ \text{kV}$	1.0
DC voltage	U_{DC}	$160\ \text{kV}$	1.0
Rated (base) power	P	$60\ \text{MW}$	1.0
Reactor inductance	L_{v}	$0.049\ \mu\text{H}$	0.15
Reactor resistance	R_{v}	$0.5133\ \Omega$	0.005
DC capacitor	$2C_{\text{DC}}$	$75.2\ \mu\text{F}$	$4ms$
System frequency	f	$50\ \text{Hz}$	
Switching frequency	f_{sw}	$2000\ \text{Hz}$	

4.2 Performance during step changes of active and reactive power

This section will show the performance of the complete and simplified VSC-HVDC system models with two different control strategies during step changes in active and reactive power.

4.2.1 Strategy 1: AC-voltage control

Step in active power

Step changes in active power are performed by changing the active current reference value. The response of the system is shown in Figs. 4.2, 4.3 and 4.4. First the converter 2 active current reference value is changed from $+0.0\,\mathrm{pu}$ to $-0.5\,\mathrm{pu}$ at $t = 0.02\,\mathrm{s}$ and then set to $0.9\,\mathrm{pu}$ at $t = 0.12\,\mathrm{s}$. As can be seen from Fig. 4.3 the active current can track the reference current. The DC voltage is changed when the step is applied and then returns to the reference value due to the DC voltage controller (Fig. 4.4). The voltages at the filter-bus 1 and 2 (see Fig. 4.2), in the dq-coordinate system, can be kept constant except for some transients that occur when both the step changes are applied. It can be noticed that for the second step the total current reaches the current limit at around 0.13s (Fig. 4.3) and consequently the DC voltage drops deeply (Fig. 4.4). The active power step changes affect the direction of the transmitted power. When the second step change is applied the active power flow is adjusted to the new setting within 30 ms (Fig. 4.4).

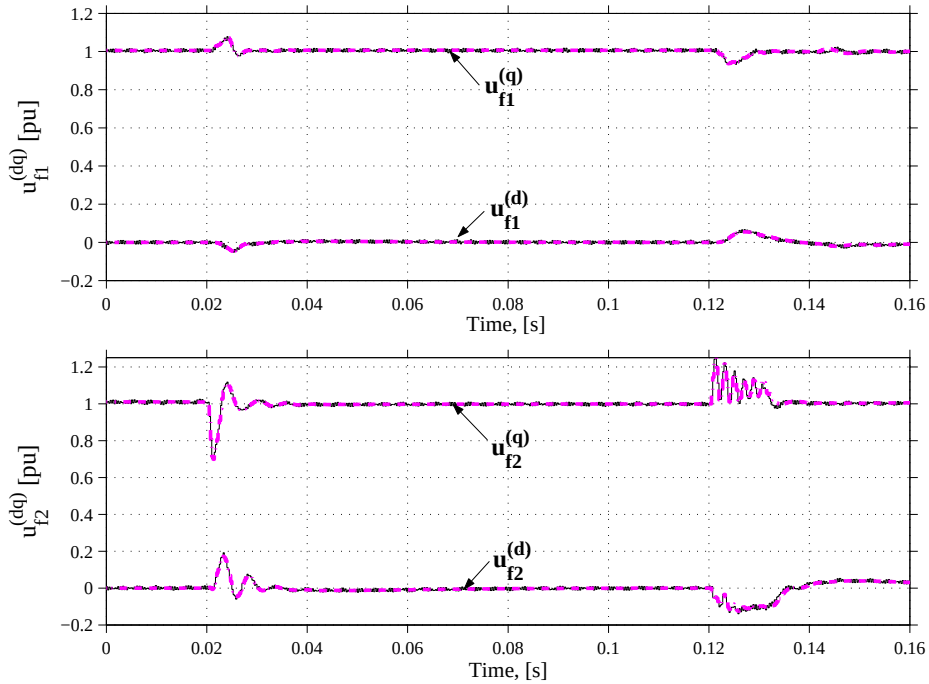

Fig. 4.2 Steps in active power using an AC-voltage control strategy for the complete (solid line) and simplified (dash-dotted line) VSC-HVDC systems: voltages in dq-plane at the filter-bus 1 (top) and at the filter-bus 2 (bottom).

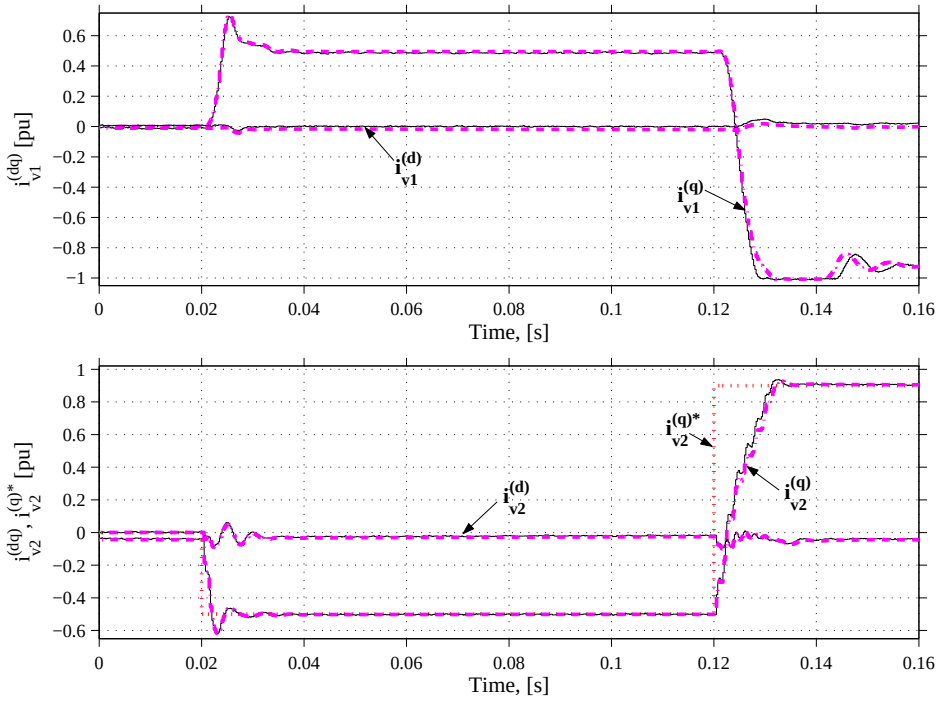

Fig. 4.3 Steps in active power using an AC-voltage control strategy for the complete (solid line) and simplified (dash-dotted line) VSC-HVDC systems: currents in dq-plane at converter 1 (top) and at converter 2 (bottom).

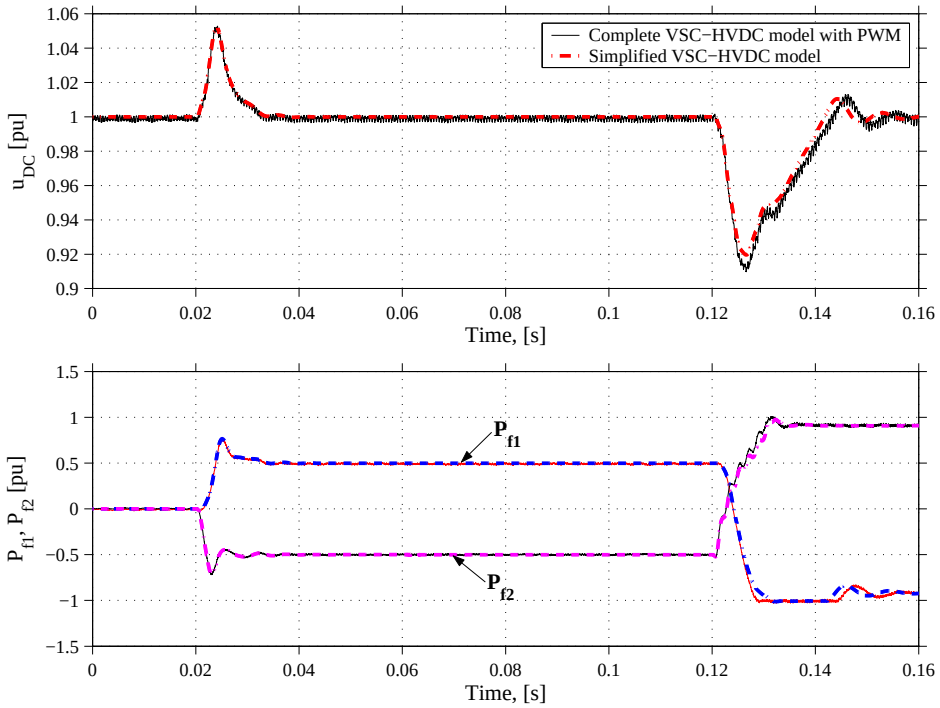

Fig. 4.4 Steps in active power using an AC-voltage control strategy for the complete (solid line) and simplified (dash-dotted line) VSC-HVDC systems: DC voltages (top) and active powers (bottom).

In Figs. 4.2, 4.3 and 4.4 a comparison is also made between the complete and simplified models. As can be seen high frequency ripples are only shown in the complete model. The reason is that the switching valves with PWM technology are modelled in the complete model. It is also found that the most obvious difference is shown in the DC voltage when the current limit is reached. However, the maximum absolute error of the DC voltage is only 0.0096 pu (1%). Therefore, it is clearly demonstrated that there is no significant difference in the performances of the complete and simplified models.

4.2.2 Strategy 2: reactive-power control

Steps in active and reactive power

The changes in active and reactive power are done by adjusting the reference values of the active and reactive converter current. Simulation results are shown for three changes in the power settings, as demonstrated in Figs. 4.5, 4.6, 4.7 and 4.8:

- at $t = 0.02\,\mathrm{s}$ the reactive current setting of converter 2 is changed from $+0.3\,\mathrm{pu}$ to $-0.3\,\mathrm{pu}$.

- at $t = 0.07\,\mathrm{s}$ the active current setting of converter 2 is changed from $-0.5\,\mathrm{pu}$ to $+0.5\,\mathrm{pu}$.

- at $t = 0.12\,\mathrm{s}$ the reactive current setting of converter 1 is changed from $-0.5\,\mathrm{pu}$ to $+0.5\,\mathrm{pu}$.

As shown in Figs. 4.5, 4.6 and 4.7 when the reactive current step change of converter 2 is applied at 0.02s (Fig. 4.6), the q-component of the voltage at the filter-bus 2 in the dq-coordinate system drops which is shown in Fig. 4.5. The similar phenomenon can be observed at the filter-bus 1 (Fig. 4.5) when the reactive current step is applied at converter 1 at 0.12s (Fig. 4.6). When the active current step change is applied at 0.07s (Fig. 4.6), the transferred active powers at both sides change the direction (Fig. 4.7). Fig. 4.8 shows the response of the DC voltage. The step changes cause transients on the DC voltage, but, as expected, the step change of the active power causes a much higher transient than that with the change in reactive current. It can be clearly noticed that both the transient and the steady state responses of the simplified model agree well with the responses of the complete model. As previously mentioned and expected, the DC voltage high frequency ripple is found in Fig. 4.8 when the complete model is used in the simulation. This is also a result of using the switching valves that are replaced as the voltage and current sources in the simplified model.

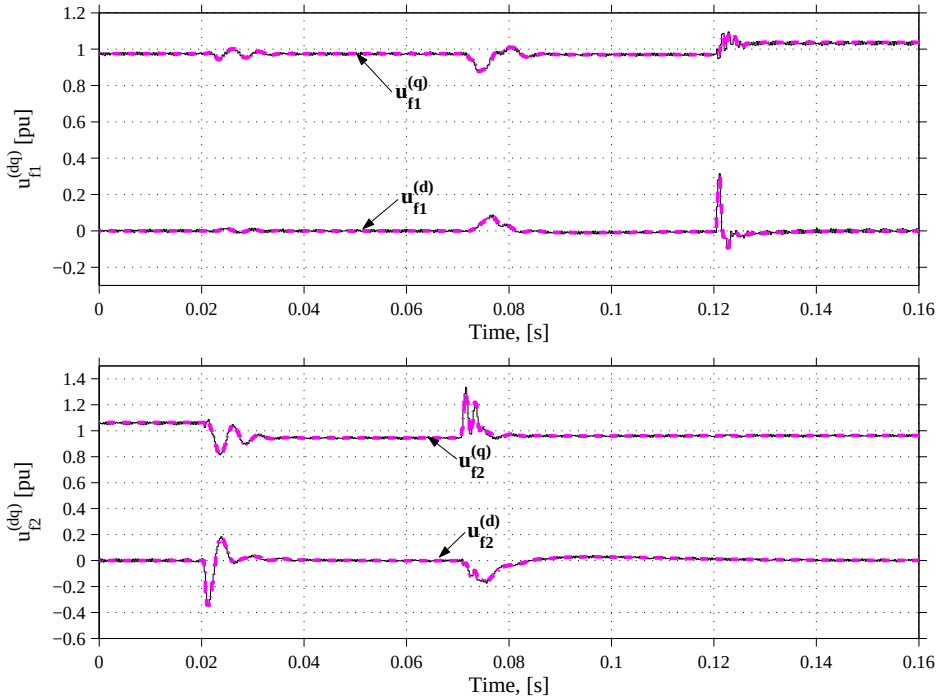

Fig. 4.5 Steps in active and reactive power using a reactive-power control strategy for the complete (solid line) and simplified (dash-dotted line) VSC-HVDC systems: voltages in dq-plane at the filter-bus 1 (top) and at the filter-bus 2 (bottom).

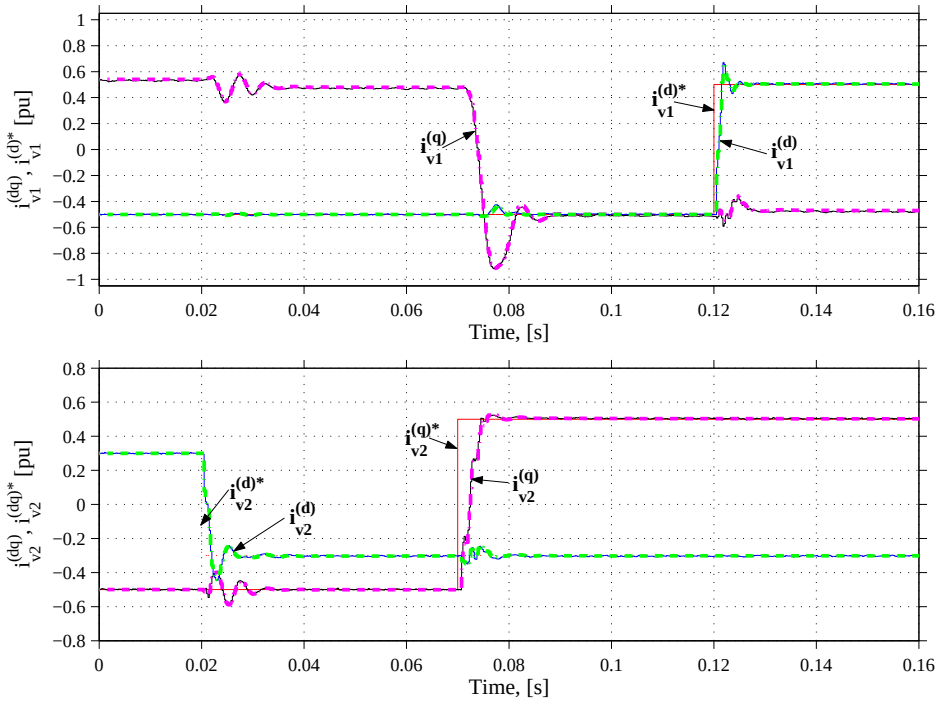

Fig. 4.6 Steps in active and reactive power using a reactive-power control strategy for the complete (solid line) and simplified (dash-dotted line) VSC-HVDC systems: currents in dq-plane at converter 1 (top) and at converter 2 (bottom).

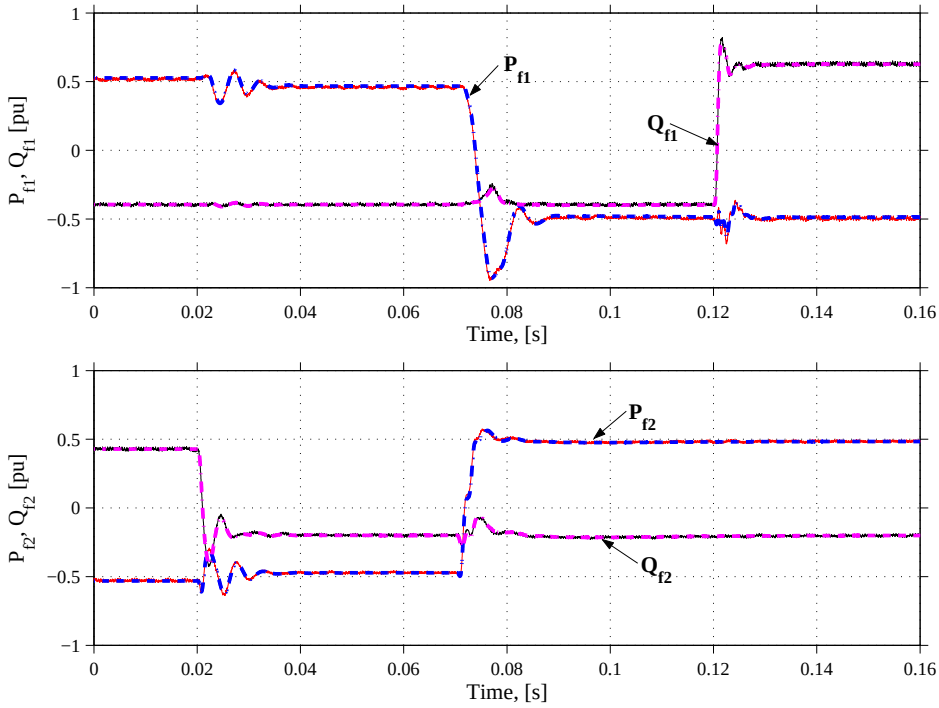

Fig. 4.7 Steps in active and reactive power using a reactive-power control strategy for the complete (solid line) and simplified (dash-dotted line) VSC-HVDC systems: active and reactive powers at the filter-bus 1 (top) and at the filter-bus 2 (bottom).

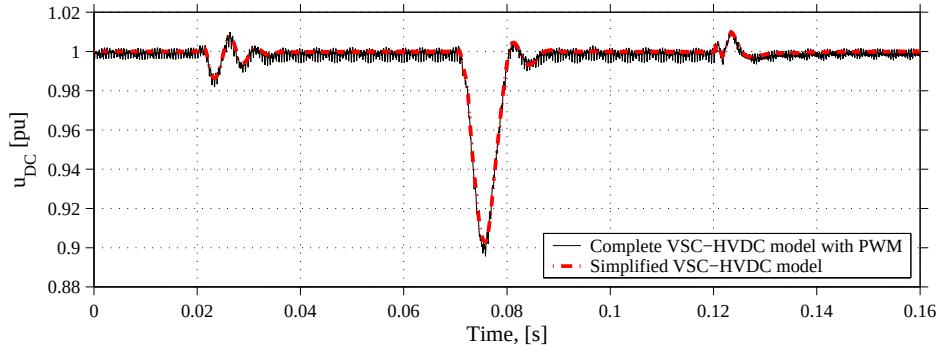

Fig. 4.8 Steps in active and reactive power using a reactive-power control strategy: DC voltages u_{DC}.

4.3 Performance during balanced faults - using AC-voltage control

A 50% three-phase balanced voltage dip with a duration of 100 ms is applied at $0.02\,\mathrm{s}$ at the grid side and its response is illustrated in Figs. 4.9, 4.10 and 4.11. The active current reference is $0.8\,\mathrm{pu}$ from converter 1 to converter 2 and is not changed during the fault.

Both control strategies are tested for the same fault conditions. Only the simulation results are presented in this section when using control strategy 1, i.e. AC-voltage control.

As shown in Figs. 4.9, 4.10 and 4.11 the q-component voltage at the filter-bus 1 decreases to $0.5\,\mathrm{pu}$ during the fault and recovers to the reference voltage after the fault is cleared (Fig. 4.9). The reactive and active current at converter 1 increase due to the AC voltage controller and active current setting (Fig. 4.10). Since the total current of the converter 1 increases to the current limit, the DC voltage drops (Fig. 4.11). Consequently the active power flows through both converters together with the active current of converter 2 are reduced to low values during the fault and recover to the desired value after the fault (Fig. 4.11). The voltage at the filter-bus 2 in the dq-coordinate system, which is also controlled to keep the terminal voltage at $1.0\,\mathrm{pu}$, is maintained except small transients in the beginning of the fault and after the fault is cleared (Fig. 4.9). It is also demonstrated that during a three-phase fault, the decreased voltage at the grid reduces the transferred active power through the DC link. When the fault is cleared, normal operation is recovered. Therefore, the severity of a three-phase short circuit is reduced as compared with an AC interconnection. By comparing the performances of the complete and simplified models it can be obtained that the maximum absolute difference, which is shown in the DC voltage when the current limit is reached, is only 0.0133 pu (1.8%).

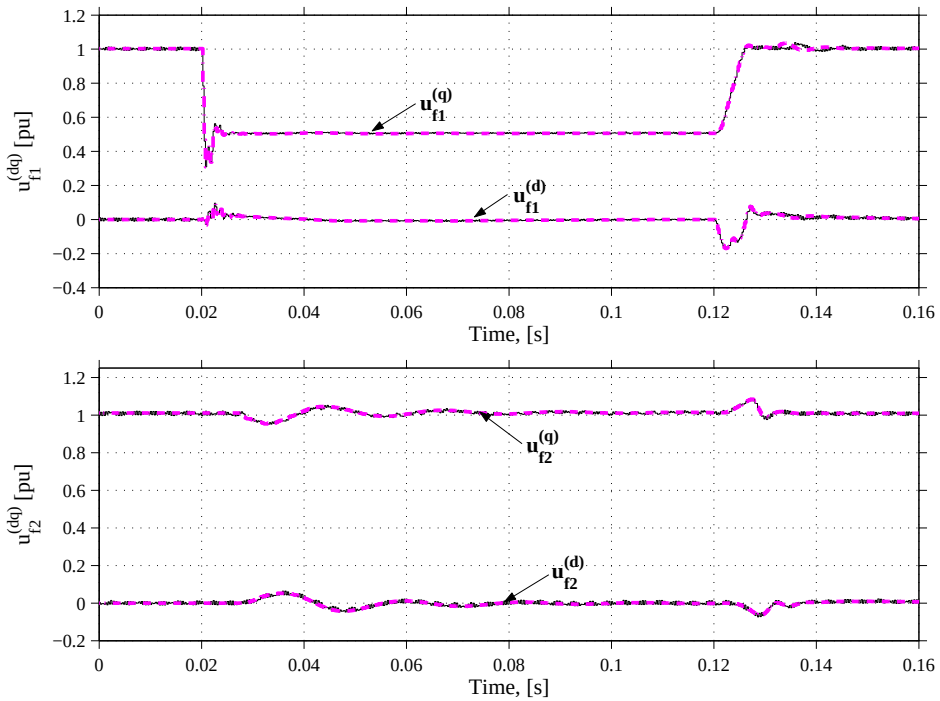

Fig. 4.9 Three-phase fault at the grid side using an AC-voltage control strategy for the complete (solid line) and simplified (dash-dotted line) VSC-HVDC systems: voltages in dq-plane at the filter-bus 1 (top) and at the filter-bus 2 (bottom).

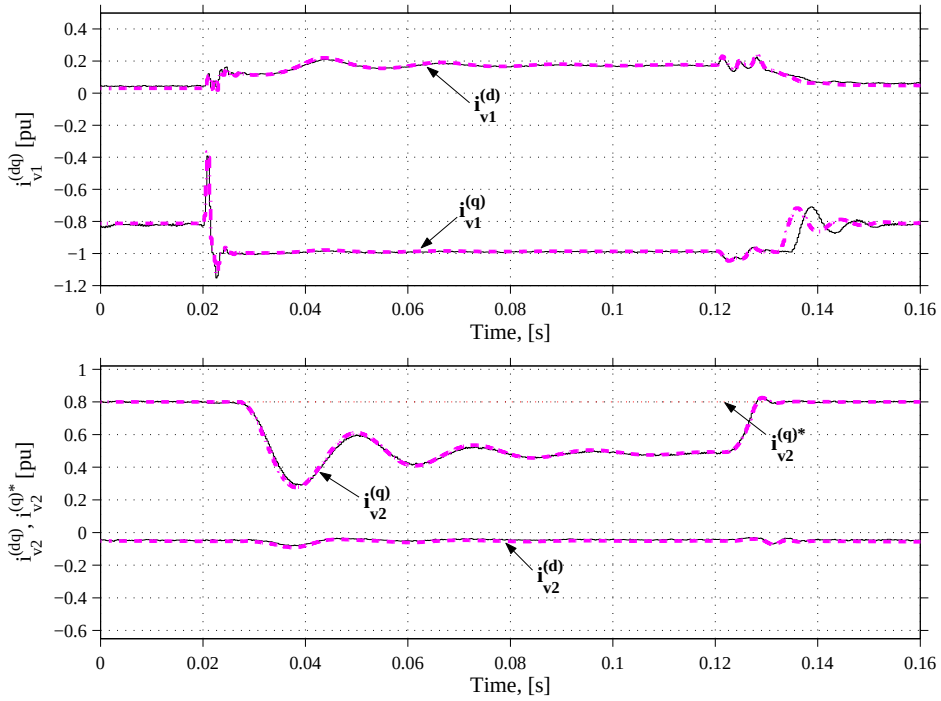

Fig. 4.10 Three-phase fault at the grid side using an AC-voltage control strategy for the complete (solid line) and simplified (dash-dotted line) VSC-HVDC systems: currents in dq-plane at converter 1 (top) and at converter 2 (bottom).

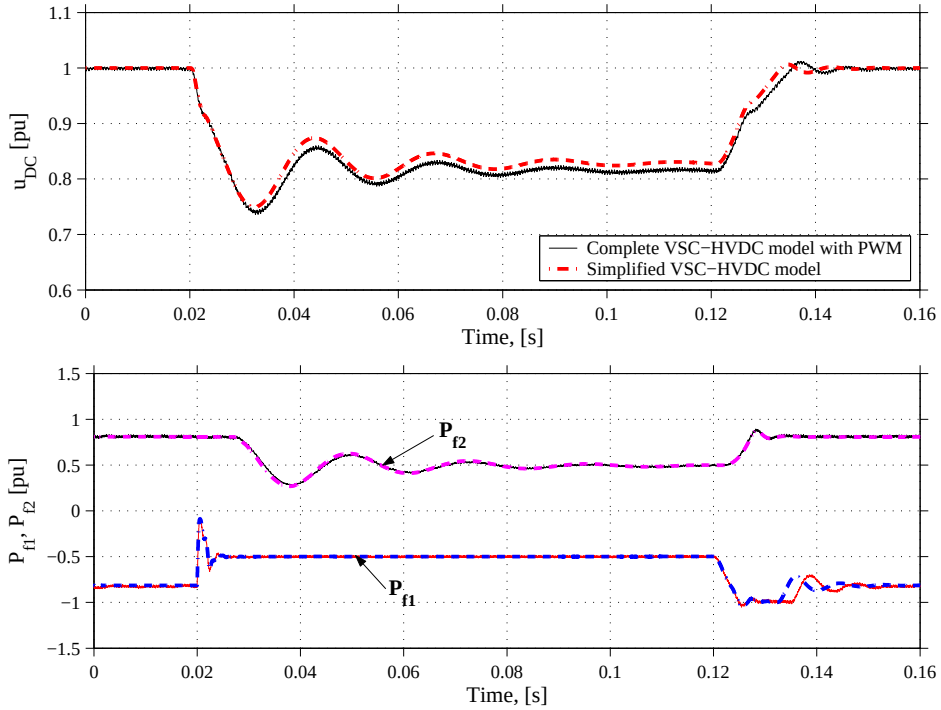

Fig. 4.11 Three-phase fault at the grid side using an AC-voltage control strategy for the complete (solid line) and simplified (dash-dotted line) VSC-HVDC systems: DC voltages (top) and active powers (bottom).

4.4 Performance during unbalanced faults - using AC-voltage control

To investigate the behavior of the VSC-HVDC system during unbalanced faults, a 5-cycle single-line-to-ground fault (SLGF) is applied in phase a at the grid side at $0.02\,\mathrm{s}$ (see Fig. 4.12). The active power flow is $0.8\,\mathrm{pu}$, transmitted from converter 1 to converter 2, and is kept constant during the fault.

As shown in Figs. 4.12, 4.13 and 4.14 the voltages at the filter-bus 1 in the dq-coordinate system are affected by a 100 Hz oscillation (Fig. 4.12). The currents of converter 1, in the dq-coordinate system, increase with a large oscillation and the maximum transient current of converter 1 is $1.15\,\mathrm{pu}$ (Fig. 4.13). This exceeds the current limit, as also shown in Fig. 4.15. The DC voltage drops and it contains an oscillation during the fault (Fig. 4.14). Consequently the transferred active power is reduced and also contains the oscillation (Fig. 4.14). During the grid side fault the voltages at the filter-bus 2, in the dq-coordinate system, can be kept constant except a small oscillation (Fig. 4.12). The currents at converter 2, in the dq-coordinate system, are reduced with an oscillation during the fault (Fig. 4.13). All oscillations in voltages and currents at both systems, in the dq-coordinate system, means that the phase voltages and currents at both systems are unbalanced.

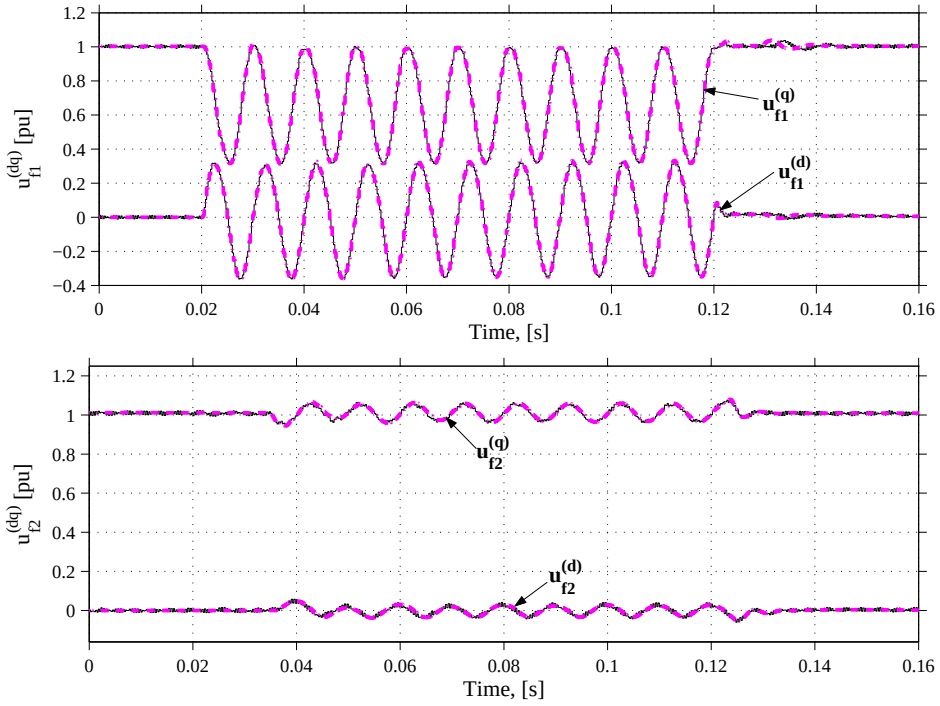

Fig. 4.12 SLGF at the grid side using an AC-voltage control strategy for the complete (solid line) and simplified (dash-dotted line) VSC-HVDC systems with $i_{v2}^{(q)^*} = 0.8\,\mathrm{pu}$: voltages in dq-plane at the filter-bus 1 (top) and at the filter-bus 2 (bottom).

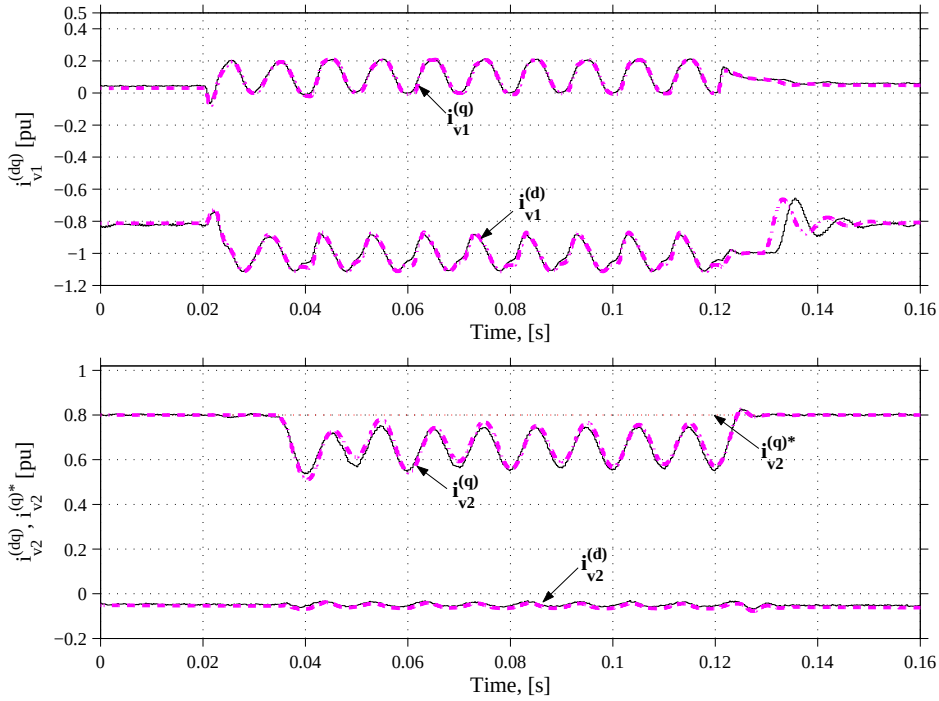

Fig. 4.13 SLGF at the grid side using an AC-voltage control strategy for the complete (solid line) and simplified (dash-dotted line) VSC-HVDC systems with $i_{\mathrm{v2}}^{(\mathrm{q})^*} = 0.8\ \mathrm{pu}$: currents in dq-plane at converter 1 (top) and at converter 2 (bottom).

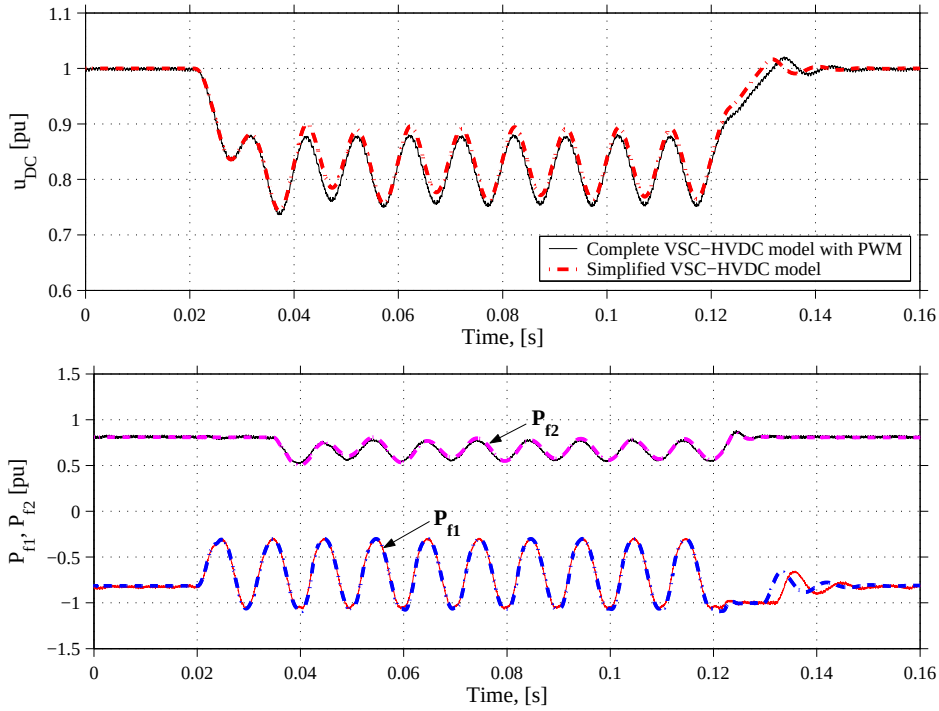

Fig. 4.14 SLGF at the grid side using an AC-voltage control strategy for the complete (solid line) and simplified (dash-dotted line) VSC-HVDC systems with $i_{\mathrm{v2}}^{(\mathrm{q})^*} = 0.8\ \mathrm{pu}$: DC voltages (top) and active powers (bottom).

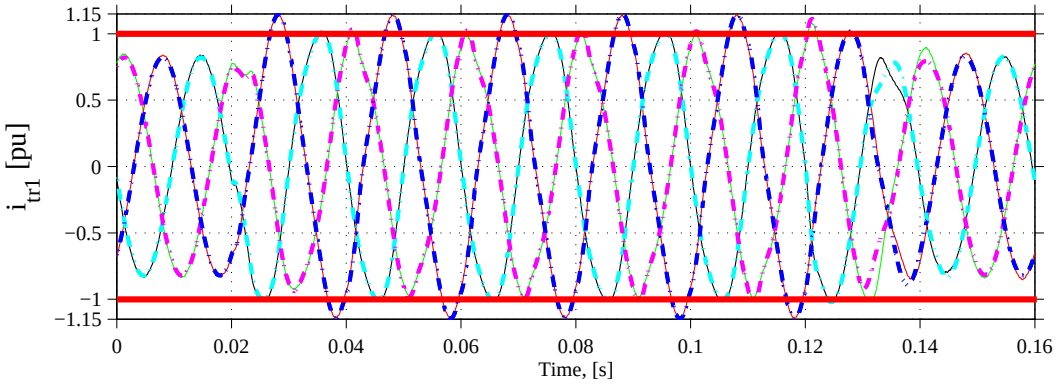

Fig. 4.15 SLGF at the grid side using AC-voltage control strategy for the complete (solid line) and simplified (dash-dotted line) VSC-HVDC systems with $i_{\mathrm{v2}}^{(\mathrm{q})^*} = 0.8\ \mathrm{pu}$: phase currents at T_1.

From Figs. 4.12, 4.13 and 4.14 it can be obtained that the unbalance is transferred from system 1 to system 2. This unbalance can be reduced either by decreasing the transferred active power or increasing the current limit of converter 1 [90]. As shown in Figs. 4.16 and 4.17, when the active power flow is set to $0.4\,\mathrm{pu}$ (Fig. 4.16), the DC voltage contains a large oscillation without a drop during the fault (Fig. 4.17) which implies that system 1 can still transfer the required active power to system 2.

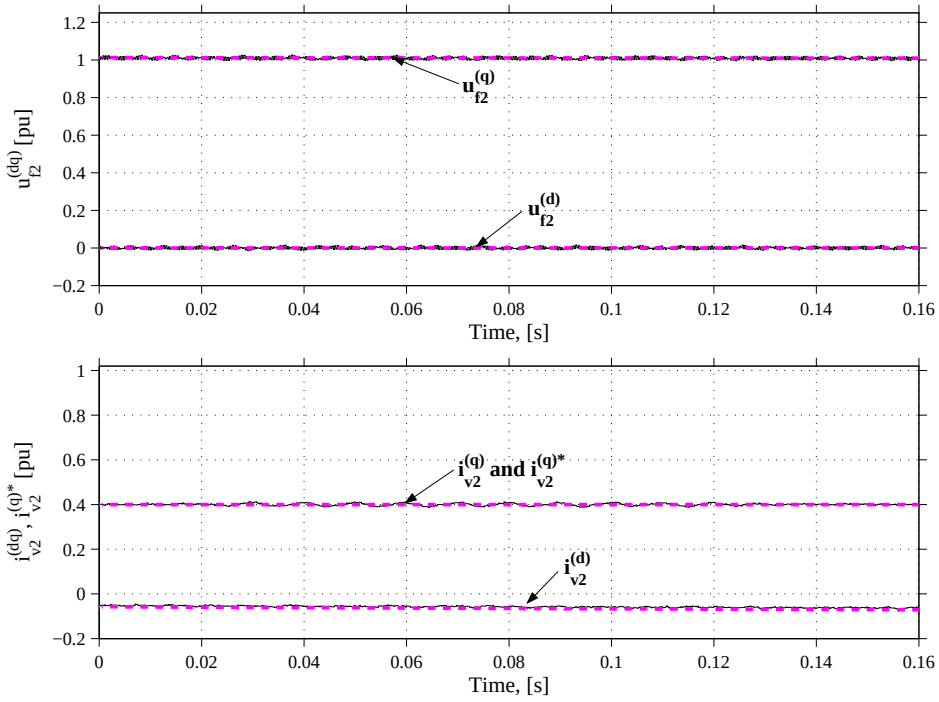

Fig. 4.16 SLGF at the grid side using AC-voltage control strategy for the complete (solid line) and simplified (dash-dot line) VSC-HVDC systems with $i_{\mathrm{v2}}^{(\mathrm{q})^*} = 0.4\ \mathrm{pu}$: voltages at the filter-bus 2 (top) and currents at converter 2 (bottom) in dq-plane.

As shown in Fig. 4.17 the active power flow at the faulted side (P_{f1}) of the DC link shows a large oscillation during the fault. However, the oscillation of the active power at the non-faulted side (P_{f2}) is less which clearly demonstrates that the DC link filters out the unbalance at system 1 and system 2 is operating close to normal.

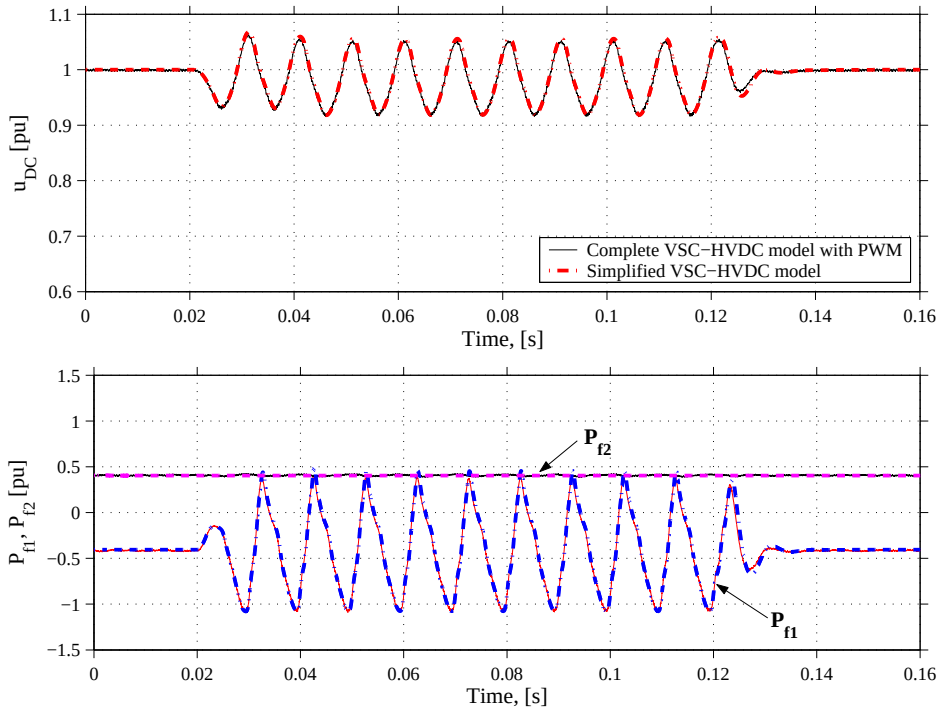

Fig. 4.17 SLGF at the grid side using AC-voltage control strategy for the complete (solid line) and simplified (dash-dot line) VSC-HVDC systems with $i_{\mathrm{v2}}^{(\mathrm{q})^*} = 0.4$ pu: DC voltages (top) and active powers at the filter-bus 1 and 2 (bottom).

4.5 Improvement of the system performance during unbalanced faults

As shown and mentioned in the above section, the AC currents at converter 1, shown in Fig. 4.15, exceed the current limit during SLGF and this may cause the overcurrent protection of the VSC to trigger. A trip of the DC link would significantly reduce the reliability of the supply. In order to avoid a triggering, two modified controllers are used at converter 1 to improve the performance of system 1. In these two modified controllers the positive and negative sequence components of the AC system are considered separately.

In both modified controllers the inner current controller, described in Chapter 3, is modified and divided into two parts: the positive-sequence current controller and the negative-sequence current controller. The method that is derived in [91] and used in [68] to separate positive-sequence and negative-sequence components is adopted. This method

implemented in the digital control system can be defined as:

$$x_{\mathrm{pos}}^{(\alpha\beta)}(k) = \frac{1}{2}\left(x^{(\alpha\beta)}(k) + jx^{(\alpha\beta)}(k - \frac{1}{4}\frac{T}{T_s})\right) \tag{4.1}$$

$$x_{\mathrm{neg}}^{(\alpha\beta)}(k) = \frac{1}{2}\left(x^{(\alpha\beta)}(k) - jx^{(\alpha\beta)}(k - \frac{1}{4}\frac{T}{T_s})\right) \tag{4.2}$$

where $x_{\mathrm{pos}}^{(\alpha\beta)}$ and $x_{\mathrm{neg}}^{(\alpha\beta)}$ are the positive-sequence and negative-sequence components in the $\alpha\beta$-plane, respectively. T is the period of the grid fundamental frequency.

The control equations of the modified inner current controller are shown in (4.3) and (4.4).

$$\begin{aligned} u_{\mathrm{v,pos}}^{(\mathrm{dq})^*}(k) = {} & u_{\mathrm{f,pos}}^{(\mathrm{dq})}(k) + R_{\mathrm{v}} i_{\mathrm{v,pos}}^{(\mathrm{dq})}(k) + \mathrm{j}\frac{\omega L_{\mathrm{v}}}{2}\left[i_{\mathrm{v,pos}}^{(\mathrm{dq})^*}(k) + i_{\mathrm{v,pos}}^{(\mathrm{dq})}(k)\right] \\ & + k_{\mathrm{p,i_v}}\left[i_{\mathrm{v,pos}}^{(\mathrm{dq})^*}(k) - i_{\mathrm{v,pos}}^{(\mathrm{dq})}(k)\right] + \Delta u_{\mathrm{I,v,pos}}^{(\mathrm{dq})}(k) \end{aligned} \tag{4.3}$$

$$\begin{aligned} u_{\mathrm{v,neg}}^{(\mathrm{dq})^*}(k) = {} & u_{\mathrm{f,neg}}^{(\mathrm{dq})}(k) + R_{\mathrm{v}} i_{\mathrm{v,neg}}^{(\mathrm{dq})}(k) - \mathrm{j}\frac{\omega L_{\mathrm{v}}}{2}\left[i_{\mathrm{v,neg}}^{(\mathrm{dq})^*}(k) + i_{\mathrm{v,neg}}^{(\mathrm{dq})}(k)\right] \\ & + k_{\mathrm{p,i_v}}\left[i_{\mathrm{v,neg}}^{(\mathrm{dq})^*}(k) - i_{\mathrm{v,neg}}^{(\mathrm{dq})}(k)\right] + \Delta u_{\mathrm{I,v,neg}}^{(\mathrm{dq})}(k) \end{aligned} \tag{4.4}$$

where $\Delta u_{\mathrm{I,v,pos}}^{(\mathrm{dq})}$ and $\Delta u_{\mathrm{I,v,neg}}^{(\mathrm{dq})}$ are the integral terms. $i_{\mathrm{v,pos}}^{(\mathrm{dq})^*}(k)$ and $i_{\mathrm{v,neg}}^{(\mathrm{dq})^*}(k)$ are the positive-sequence and negative-sequence current references in the dq-coordinate system, respectively. The block scheme of the modified inner current controller for converter 1 of the VSC-HVDC is displayed in Fig. 4.18. Reference values of the positive-sequence reactive and active currents are obtained from outer controllers, i.e. the AC voltage controller and the DC voltage controller. For the negative-sequence reactive and active current references two different algorithms are proposed.

4.5.1 Improved controller with zero negative-sequence reference currents

Balanced currents can be implemented by eliminating the negative-sequence currents. Therefore, in the improved controller, the negative-sequence current references in the dq-coordinate system are set to zero, i.e. $i_{\mathrm{v,neg}}^{(\mathrm{dq})^*} = 0$, to achieve balanced currents during unbalanced faults.

In Fig. 4.19 three phase currents at T_1 have less oscillations than those shown in Fig. 4.15. Moreover, the maximum transient current is almost equal to the current limit i_{lim}. The DC voltage shows an oscillation. As clearly shown in Fig. 4.22, the oscillation of the DC voltage using improved controller with $i_{\mathrm{v,neg}}^{(\mathrm{dq})^*} = 0$ is less than the oscillation of the DC voltage with the original controller.

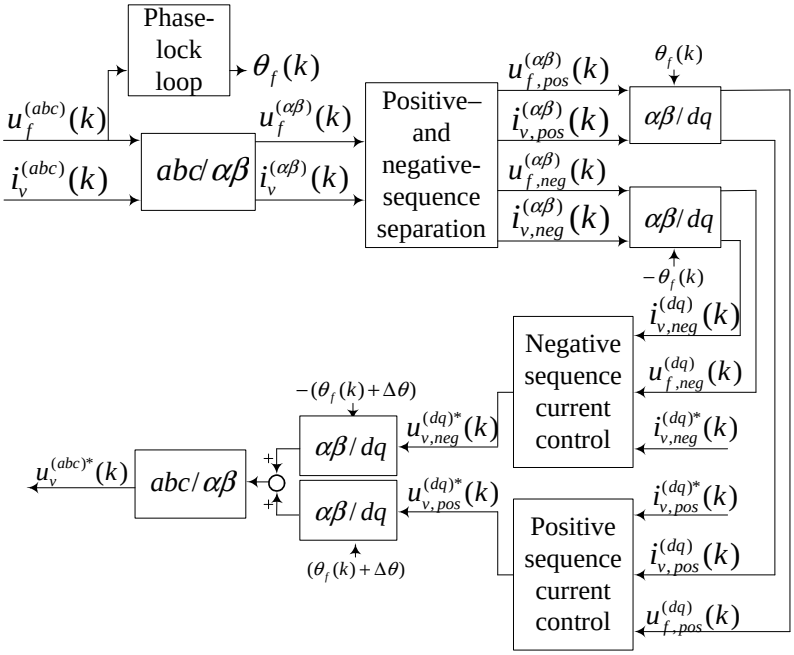

Fig. 4.18 Block scheme of the improved inner current controller for the VSC-HVDC converter 1.

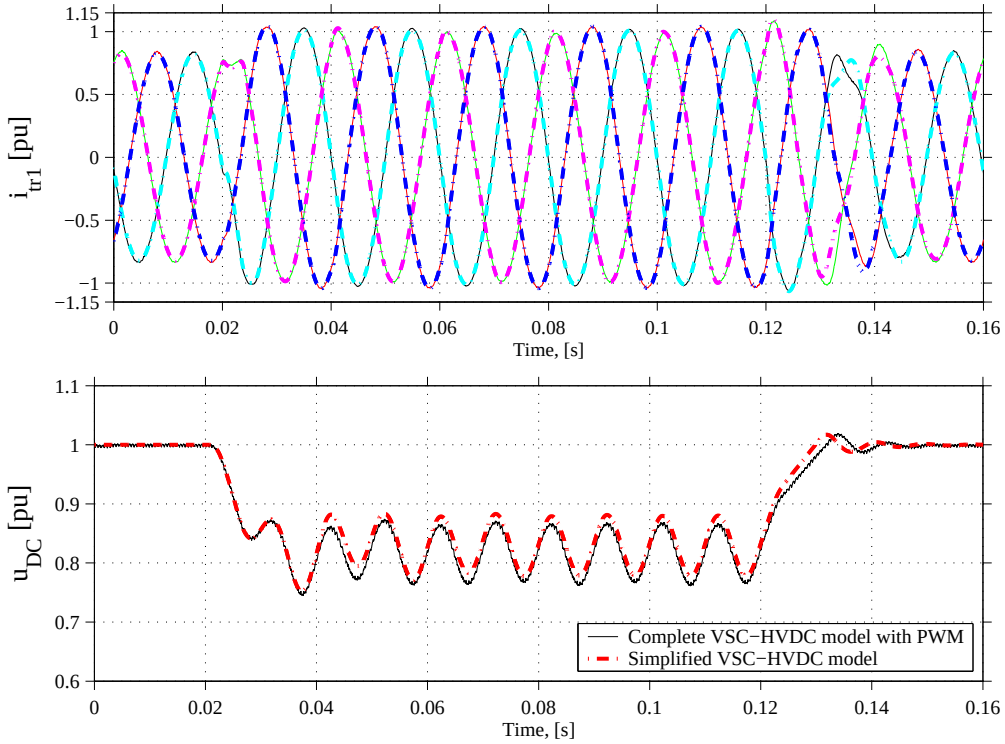

Fig. 4.19 SLGF at the grid side using improved controller with $i_{v,neg}^{(dq)*} = 0$ for the complete (solid line) and simplified (dash-dotted line) VSC-HVDC systems: AC currents at T_1 (top) and DC voltages (bottom).

4.5.2 Improved controller with negative-sequence reference currents

The improved controller with negative-sequence reference currents $i_{\mathrm{v,neg}}^{(\mathrm{dq})^*}$ introduces different reference values for the negative-sequence active and reactive currents [92].

In the system shown in Fig. 4.1, the transmitted instantaneous apparent power $S(t)$ is given by:

$$\begin{aligned} S(t) &= P(t) + \mathrm{j}Q(t) \\ &= \left[e^{\mathrm{j}\omega t}(u_{\mathrm{f,pos}}^{(\mathrm{d})} + \mathrm{j}u_{\mathrm{f,pos}}^{(\mathrm{q})}) + e^{-\mathrm{j}\omega t}(u_{\mathrm{f,neg}}^{(\mathrm{d})} + \mathrm{j}u_{\mathrm{f,neg}}^{(\mathrm{q})})\right] \\ &\quad \times \left[e^{-\mathrm{j}\omega t}(i_{\mathrm{v,pos}}^{(\mathrm{d})} - \mathrm{j}i_{\mathrm{v,pos}}^{(\mathrm{q})}) + e^{\mathrm{j}\omega t}(i_{\mathrm{v,neg}}^{(\mathrm{d})} - \mathrm{j}i_{\mathrm{v,neg}}^{(\mathrm{q})})\right] \end{aligned} \tag{4.5}$$

From (4.5) it follows that the instantaneous real power $P(t)$ and reactive power $Q(t)$ can be expressed as:

$$P(t) = P_0 + P_{\mathrm{c2}}\cos(2\omega t) + P_{\mathrm{s2}}\sin(2\omega t) \tag{4.6}$$

$$Q(t) = Q_0 + Q_{\mathrm{c2}}\cos(2\omega t) + Q_{\mathrm{s2}}\sin(2\omega t) \tag{4.7}$$

where

$$P_0 = (u_{\mathrm{f,pos}}^{(\mathrm{d})} i_{\mathrm{v,pos}}^{(\mathrm{d})} + u_{\mathrm{f,pos}}^{(\mathrm{q})} i_{\mathrm{v,pos}}^{(\mathrm{q})} + u_{\mathrm{f,neg}}^{(\mathrm{d})} i_{\mathrm{v,neg}}^{(\mathrm{d})} + u_{\mathrm{f,neg}}^{(\mathrm{q})} i_{\mathrm{v,neg}}^{(\mathrm{q})}) \tag{4.8}$$

$$P_{\mathrm{c2}} = (u_{\mathrm{f,pos}}^{(\mathrm{d})} i_{\mathrm{v,neg}}^{(\mathrm{d})} + u_{\mathrm{f,pos}}^{(\mathrm{q})} i_{\mathrm{v,neg}}^{(\mathrm{q})} + u_{\mathrm{f,neg}}^{(\mathrm{d})} i_{\mathrm{v,pos}}^{(\mathrm{d})} + u_{\mathrm{f,neg}}^{(\mathrm{q})} i_{\mathrm{v,pos}}^{(\mathrm{q})}) \tag{4.9}$$

$$P_{\mathrm{s2}} = (u_{\mathrm{f,neg}}^{(\mathrm{q})} i_{\mathrm{v,pos}}^{(\mathrm{d})} - u_{\mathrm{f,neg}}^{(\mathrm{d})} i_{\mathrm{v,pos}}^{(\mathrm{q})} - u_{\mathrm{f,pos}}^{(\mathrm{q})} i_{\mathrm{v,neg}}^{(\mathrm{d})} + u_{\mathrm{f,pos}}^{(\mathrm{d})} i_{\mathrm{v,neg}}^{(\mathrm{q})}) \tag{4.10}$$

$$Q_0 = (u_{\mathrm{f,pos}}^{(\mathrm{q})} i_{\mathrm{v,pos}}^{(\mathrm{d})} - u_{\mathrm{f,pos}}^{(\mathrm{d})} i_{\mathrm{v,pos}}^{(\mathrm{q})} + u_{\mathrm{f,neg}}^{(\mathrm{q})} i_{\mathrm{v,neg}}^{(\mathrm{d})} - u_{\mathrm{f,neg}}^{(\mathrm{d})} i_{\mathrm{v,neg}}^{(\mathrm{q})}) \tag{4.11}$$

During disturbances in the AC systems, e.g. faults and switching actions, large power oscillations may occur between the AC and DC side. This will result in oscillations in the DC voltage and a DC overvoltage which may stress the valves. In order to eliminate the DC voltage oscillation, P_{c2} and P_{s2} should be equal to zero. By applying this condition into (4.9) and (4.10), the negative-sequence reactive and active current references ($i_{\mathrm{v,neg}}^{(\mathrm{d})^*}$ and $i_{\mathrm{v,neg}}^{(\mathrm{q})^*}$) are:

$$i_{\mathrm{v,neg}}^{(\mathrm{d})^*} = -\frac{\mathrm{u}_{\mathrm{f,neg}}^{(\mathrm{d})}\mathrm{P}_0}{\mathrm{D}_0} + \frac{\mathrm{u}_{\mathrm{f,neg}}^{(\mathrm{q})}\mathrm{Q}_0}{\mathrm{D}_1} \tag{4.12}$$

$$i_{\mathrm{v,neg}}^{(\mathrm{q})^*} = -\frac{\mathrm{u}_{\mathrm{f,neg}}^{(\mathrm{q})}\mathrm{P}_0}{\mathrm{D}_0} - \frac{\mathrm{u}_{\mathrm{f,neg}}^{(\mathrm{d})}\mathrm{Q}_0}{\mathrm{D}_1} \tag{4.13}$$

where

$$D_0 = (u_{\mathrm{f,pos}}^{(\mathrm{d})})^2 + (u_{\mathrm{f,pos}}^{(\mathrm{q})})^2 - (u_{\mathrm{f,neg}}^{(\mathrm{d})})^2 - (u_{\mathrm{f,neg}}^{(\mathrm{q})})^2 \tag{4.14}$$

$$D_1 = (u_{\mathrm{f,pos}}^{(\mathrm{d})})^2 + (u_{\mathrm{f,pos}}^{(\mathrm{q})})^2 + (u_{\mathrm{f,neg}}^{(\mathrm{d})})^2 + (u_{\mathrm{f,neg}}^{(\mathrm{q})})^2 \tag{4.15}$$

With these choices of reference values for the negative-sequence active and reactive currents, the coefficients P_{c2} and P_{s2} will be zero.

Figs. 4.20 and 4.21 illustrate the responses of the phase currents at T_1 and the DC voltages when converter 1 uses the improved controller with unlimited and limited $i_{\mathrm{v,neg}}^{(\mathrm{dq})^*}$. By comparing both the DC voltage and the phase currents at T_1 it can be obtained that the oscillation amplitude of the DC voltage with unlimited negative-sequence current references is less whereas the maximum transient current with unlimited negative-sequence current references is higher. It can be noticed that the phase currents at T_1 exceed the current limit for both cases. Fig. 4.22 compares the DC voltage during the same fault in system 1 using three different controllers, i.e. the original controller, the improved controller with $i_{\mathrm{v,neg}}^{(\mathrm{dq})^*} = 0$ and the improved controller with limited $i_{\mathrm{v,neg}}^{(\mathrm{dq})^*}$. It can be seen that the oscillation of the DC voltage using improved controller with limited $i_{\mathrm{v,neg}}^{(\mathrm{dq})^*}$ is the smallest one.

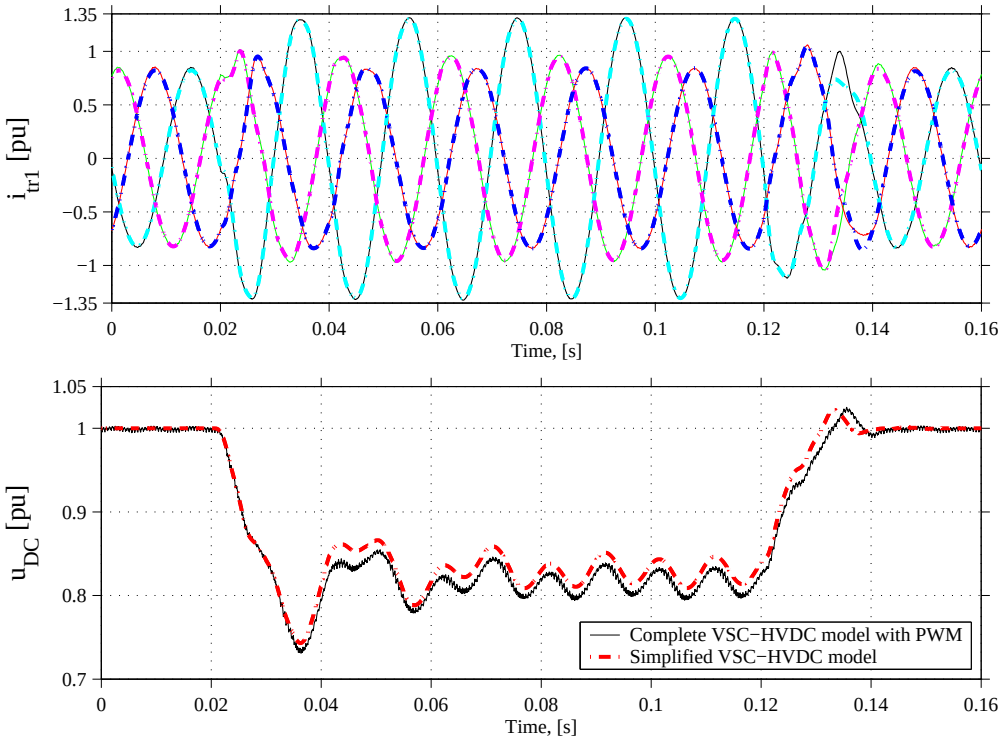

Fig. 4.20 SLGF at the grid side using the improved controller with unlimited $i_{\mathrm{v,neg}}^{(\mathrm{dq})^*}$ for the complete (solid line) and simplified (dash-dotted line) VSC-HVDC systems. AC currents at T_1 (top) and DC voltages (bottom).

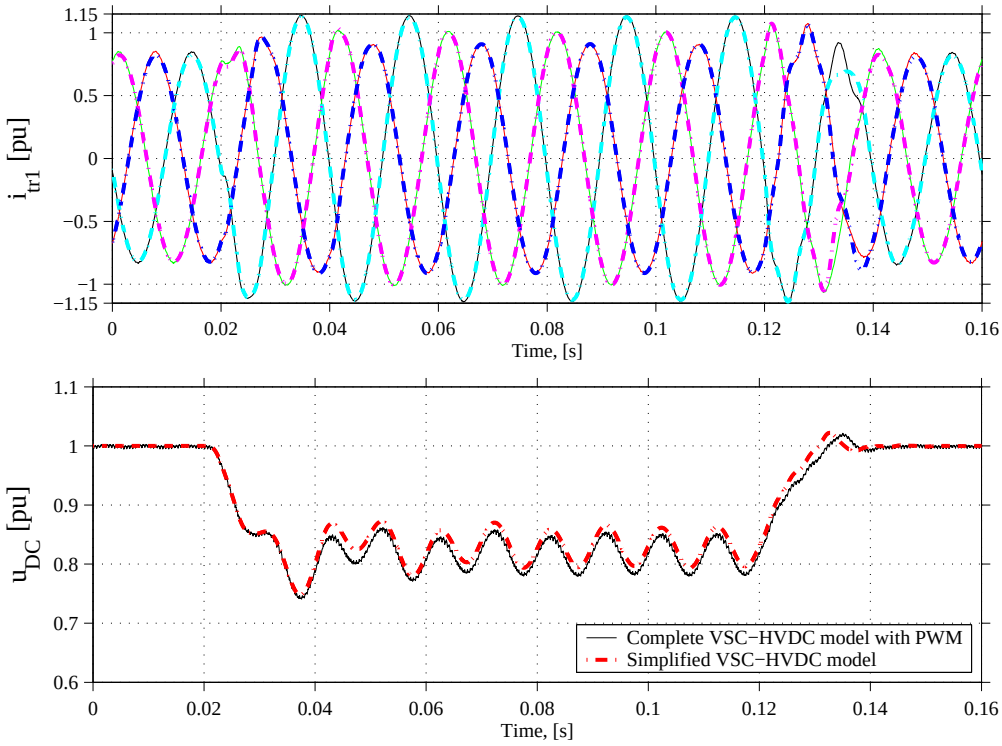

Fig. 4.21 SLGF at the grid side using the improved controller with limited $i_{\mathrm{v,neg}}^{(\mathrm{dq})^*}$ for the complete (solid line) and simplified (dash-dotted line) VSC-HVDC systems. AC currents at T_1 (top) and DC voltages (bottom).

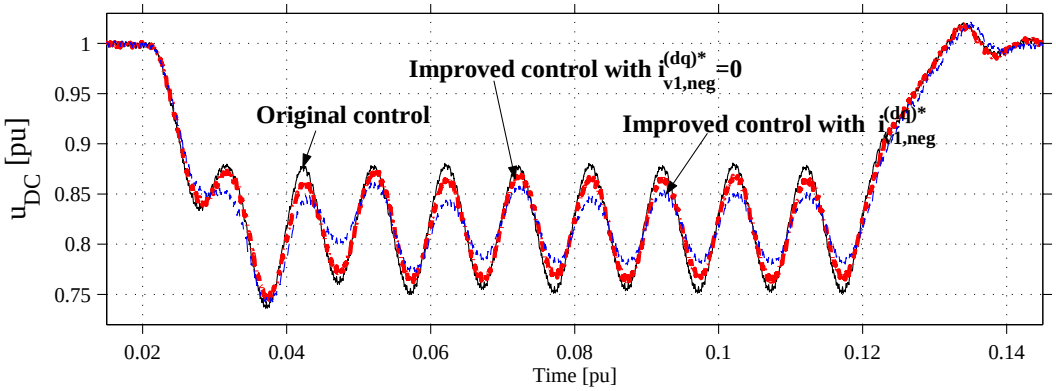

Fig. 4.22 DC voltages of the complete VSC-HVDC system during SLGF at the grid side using the original controller, improved controller with $i_{\mathrm{v,neg}}^{(\mathrm{dq})^*} = 0$ and improved controller with limited $i_{\mathrm{v,neg}}^{(\mathrm{dq})^*}$.

4.6 Summary

This chapter has presented the dynamic performances of the complete and simplified VSC-HVDC models during step changes of the active and reactive powers, balanced and

unbalanced faults. From simulation results it can be obtained that the VSC-HVDC can fulfill fast and bi-directional power transfers and AC voltage adjustment. The VSC-HVDC control strategies can be varied regarding different objectives. The simplified VSC-HVDC model agrees well with the complete model during transients and in steady state. Furthermore, two modified controllers have been presented and implemented in the VSC-HVDC control system to improve the system performance during unbalanced faults in the grid.

Chapter 5

VSC-HVDC System for Industrial Plants

*In this chapter the performance of a VSC-HVDC supplying an industrial system with and without on-site generation is investigated. Some additional results are included in the papers **[Papers C-I]**.*

5.1 Introduction

As discussed in Chapter 1 large industries have a high electricity consumption and are typically supplied directly from the sub-transmission grid. This results in a very reliable supply to the plant. Moreover, many industrial customers, such as pulp and paper industries, refineries and steel factories, have facilities with on-site generation. The on-site generation has several benefits for the industries as well as the utility grid such as reducing electricity costs and improving the power quality. However, power-quality disturbances can still spread directly from the supplying grid to the industrial installation and vice versa. A VSC-HVDC link is capable of transferring the active power from the grid and, at the same time, decreasing the disturbances from the utility grid.

When a VSC-HVDC supplies the industrial network, the inverter of the VSC-HVDC can use the AC voltage and frequency controllers to keep the load side AC voltage and frequency constant. In this way power-quality disturbances like voltage dips do not reach the industrial installation. However, due to the low inertia in the industrial network, the control and operation of industrial installations differ considerably from that of large transmission or sub-transmission networks [93]. Hence, in this chapter the performance of the industrial system when supplied by a VSC-HVDC is investigated in different situations. It should be mentioned that the VSC-HVDC model used in the simulations is the simplified model presented in Chapter 4, where it was demonstrated that the simplified model is a very good approximation of the complete model both during transients and in steady state.

5.2 VSC-HVDC system for industrial plants without on-site generation

In this section, a VSC-HVDC supplied industrial plant without on-site generators is investigated. Initially the VSC supplying different load compositions are simulated to analyze the impact of various loads on the voltage and frequency response of the system. During these studies the VSC utilizes the AC voltage and frequency controllers.

5.2.1 Investigation of frequency/AC voltage control for the VSC

Some simulation results and analysis presented in this section have been presented in **[Paper C]**.

Fig. 5.1 shows a VSC and two different industrial plants. System I comprises a resistive load, an induction motor IM_1 and an aggregate induction motor IM which represents the rest of the load. System II includes the same resistive load, the same induction motor IM_1 and an aggregate synchronous motor SM which represents the rest of the load.

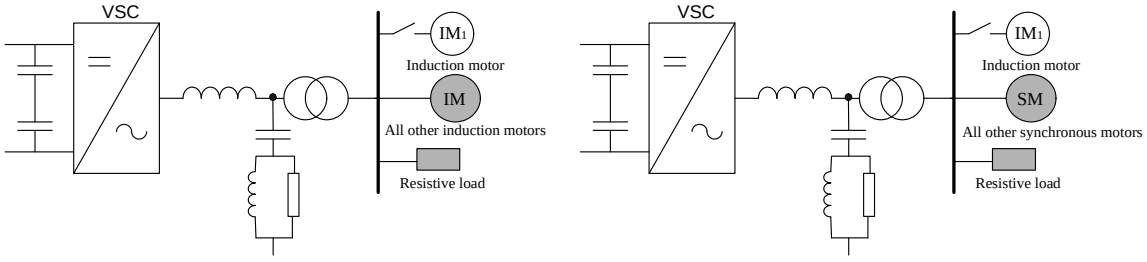

(a) System I (b) System II

Fig. 5.1 System I (a): an HVDC infeed and mainly induction motor loads. System II (b): an HVDC infeed and mainly synchronous motor loads.

Figs. 5.2 and 5.3 show the minimum frequency at the PCC as functions of the converter current limit under several different rotating motor inertia constants. In both systems the size of IM_1 is 0.113 pu (total load 1.0 pu). As expected, when the current limit increases, the minimum frequency increases. Furthermore, with an increase of the rotating motor inertia the frequency deviation decreases. The intersection points of the acceptable minimum frequency and the minimum frequency are the critical VSC current limits. As an example the acceptable minimum frequency is assumed to be 48 Hz. In Fig. 5.2 it can be seen that the intersection points E and F are the minimum VSC current limits for frequencies $\geq 48\mathrm{Hz}$ when H_{IM} is 2.8s and 1.4s respectively. However, there is no intersection point in Fig. 5.3 in this simulated case. This implies that the converter of system II does not need to be overrated to meet the frequency requirement in the power

system. It should be mentioned that the minimum current limit of the VSC increases with an increase of the size of IM_1.

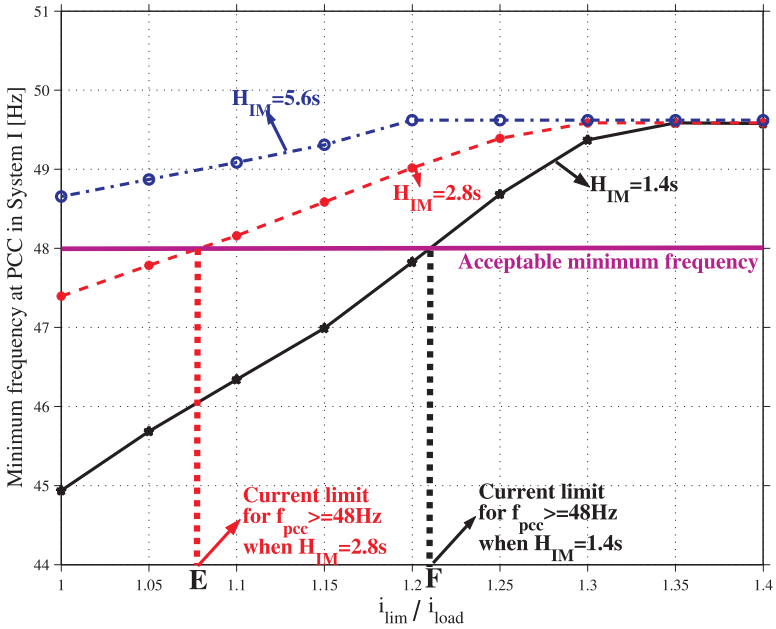

Fig. 5.2 Minimum frequency at PCC as functions of VSC current limit i_{lim} under different induction machine inertia constant $\mathrm{H_{IM}}$ in System I during an IM_1 start.

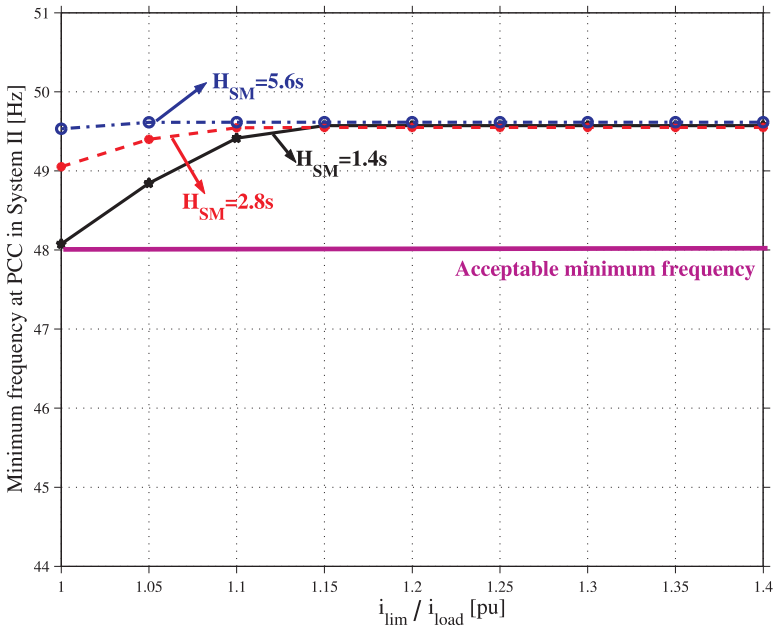

Fig. 5.3 Minimum frequency at PCC as functions of VSC current limit i_{lim} under different synchronous machine inertia constant $\mathrm{H_{SM}}$ in System II during an IM_1 start.

5.2.2 A VSC-HVDC supplied industrial plant

Last subsection illustrates the impact of rotating machines, i.e. induction and synchronous motors, on the voltage and frequency response of the VSC supplied industrial plants when the VSC uses the voltage and frequency controllers. This subsection will further investigate a case where the VSC-HVDC supplies an industrial plant with mainly induction motors, as shown in Fig. 5.4. The control strategy is designed to control the AC and DC voltages on the rectifier side and to control the AC voltage and frequency at the inverter side. Various disturbances such as load changes, balanced and unbalanced faults from the grid have been tested. Detailed simulation results and analysis have been included in **[Paper D]**. In this subsection the system dynamics due to grid faults and motor starts are shown to emphasize the significance of the VSC-HVDC current limit and the benefits and limitations of the VSC-HVDC.

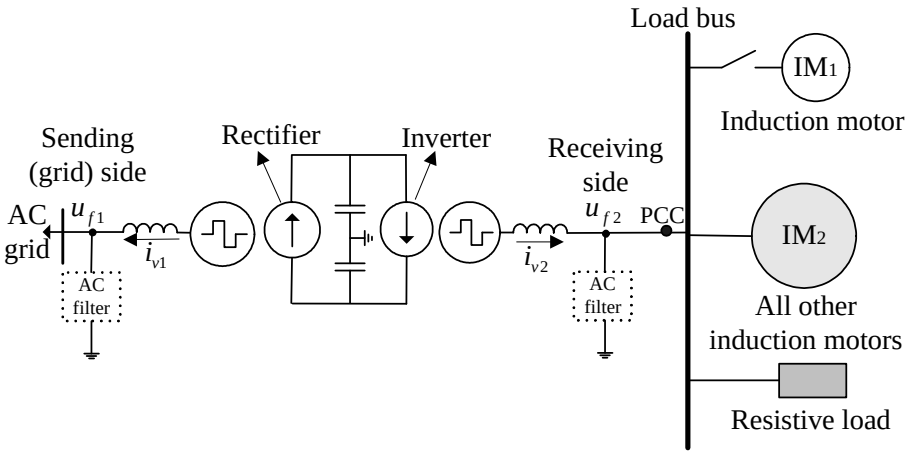

Fig. 5.4 Model for a VSC-HVDC system with different loads.

Three-phase faults at the sending side

A voltage dip with a retained voltage of 0.5 pu and a duration of 0.1s is simulated at the sending side of the VSC-HVDC. The dynamics of the link during and after the dip depend on the remaining control margin, i.e. on the difference between the pre-event load current and the current limit. The simulations have been repeated for different values of the current limit. The results are shown in Figs. 5.5 - 5.7. The fault is applied at $0.02\,\mathrm{s}$ and is cleared 5 cycles later.

As shown in Figs. 5.5 - 5.7, when the current i_{v1} reaches the current limit, the DC voltage decreases and the transferred active power is reduced. This significantly affects the frequency but also slightly affects the voltage at the PCC. For instance, when the current limit of the VSC is equal to 1.1 times the total load, the current i_{v1} increases to i_{lim} during the fault (see Fig. 5.5), the DC voltage drops to about 0.85 pu and the transferred active power is reduced to about 0.5 pu which is not enough to supply the total load at the

receiving side of the VSC-HVDC. The estimated frequency at the PCC then drops to less than 49 Hz (Fig. 5.6). With the drop of the estimated frequency at the PCC, the speed, absorbed active and reactive power of both the induction motors are reduced (Fig. 5.7). With an increase of the VSC current limit, the power quality of the load bus or PCC is improved. When the rating or the current limit of the VSC is two times the total load, the DC link can transfer enough active power during the fault such that the AC voltage and estimated frequency at the PCC can be kept at their reference values. In order for the load bus or PCC to be immune to the fault, when the voltage dip magnitude is less than 0.5 pu at the sending side, the current limit setting of the VSC-HVDC converters has to be at least 1.7 times the total load current. It should be mentioned that the current limit is also dependent on the capacitor size of the AC filter. With an increase of the capacitor size, the required current limit of the converter will decrease.

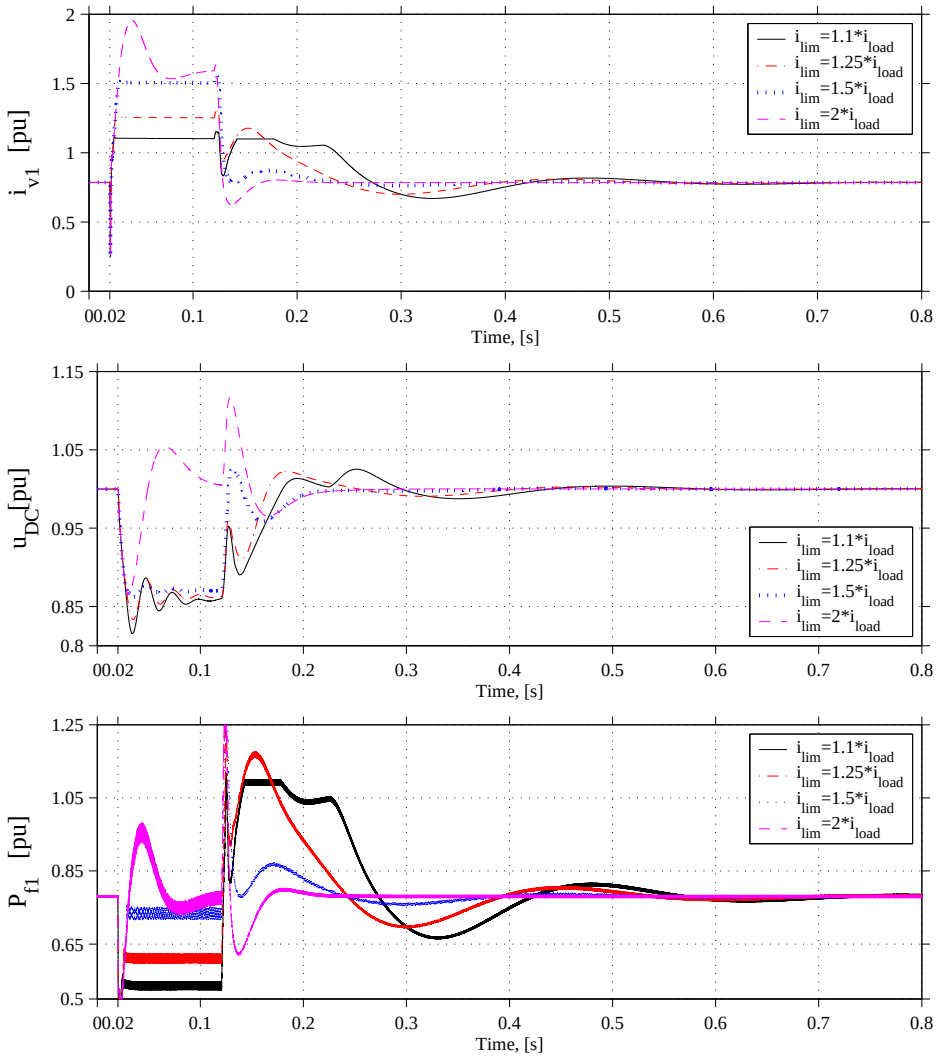

Fig. 5.5 Current amplitude, DC voltage and active power at sending side during a three-phase grid fault.

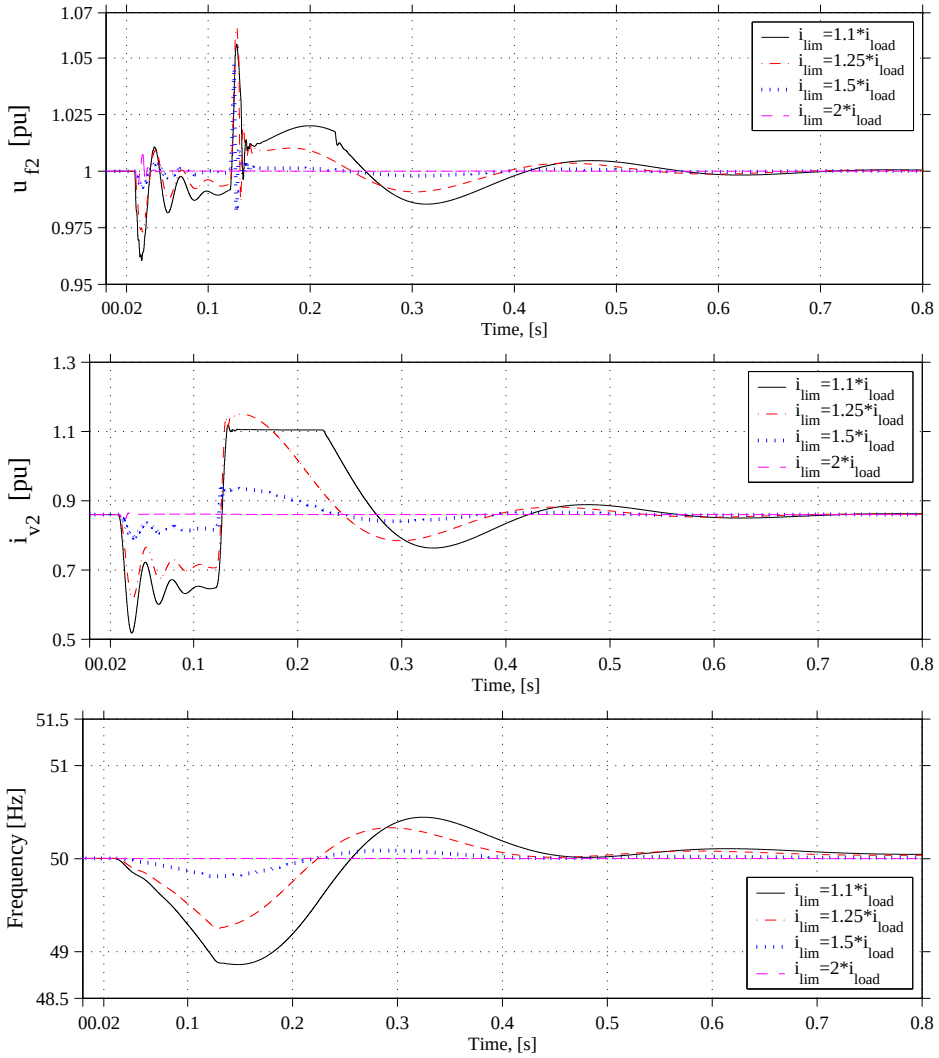

Fig. 5.6 Voltage amplitude, current amplitude and frequency at PCC during a three-phase grid fault.

From the simulation results it can be seen that the current limit significantly affects the dynamics of the system during and after a grid fault. For a sufficiently high current limit the controller is able to maintain the voltage and frequency at the PCC at their pre-event values. In that case the load does not experience any disturbance. When the current limit is lower, the load experiences a drop in frequency and a drop in voltage. Note, however, that even for the lowest current limit (10% above the load current) the voltage does not drop below 0.95 pu. Instead the motor load consumes significantly less active power. The consequence is a drop in the motor speed which causes a higher active and reactive power demand after the dip. This, however, is not perceived as a problem, neither for the motors, nor for other loads. The drop in the estimated frequency, to slightly below 49 Hz, is more severe than normal in large interconnected systems. However, the industrial equipment is rarely sensitive to frequency variations. The drop in speed of the

induction motor is up to 3%, which is sufficient as speed-sensitive processes normally are not powered directly by induction motors.

In order to show the capability of the VSC-HVDC, to enhance the quality of power supply to an industrial system, a comparison of the responses of both induction motors IM_1 and IM_2 after a voltage dip of 50% is shown in Table 5.1. The comparison is made between a conventional AC supply and a VSC-HVDC supply. As can be seen in Table 5.1, the highest current of the induction motor IM_2 is 4.523 pu and the lowest speed is 0.9 pu during the fault when supplied purely by an AC system. However, when supplied by a VSC-HVDC system, the highest current of IM_2 is only 1.086 pu and the speed only slows down to 0.941 pu during the fault. This comparison clearly illustrates that the VSC-HVDC significantly improves the quality of power supply to industrial loads.

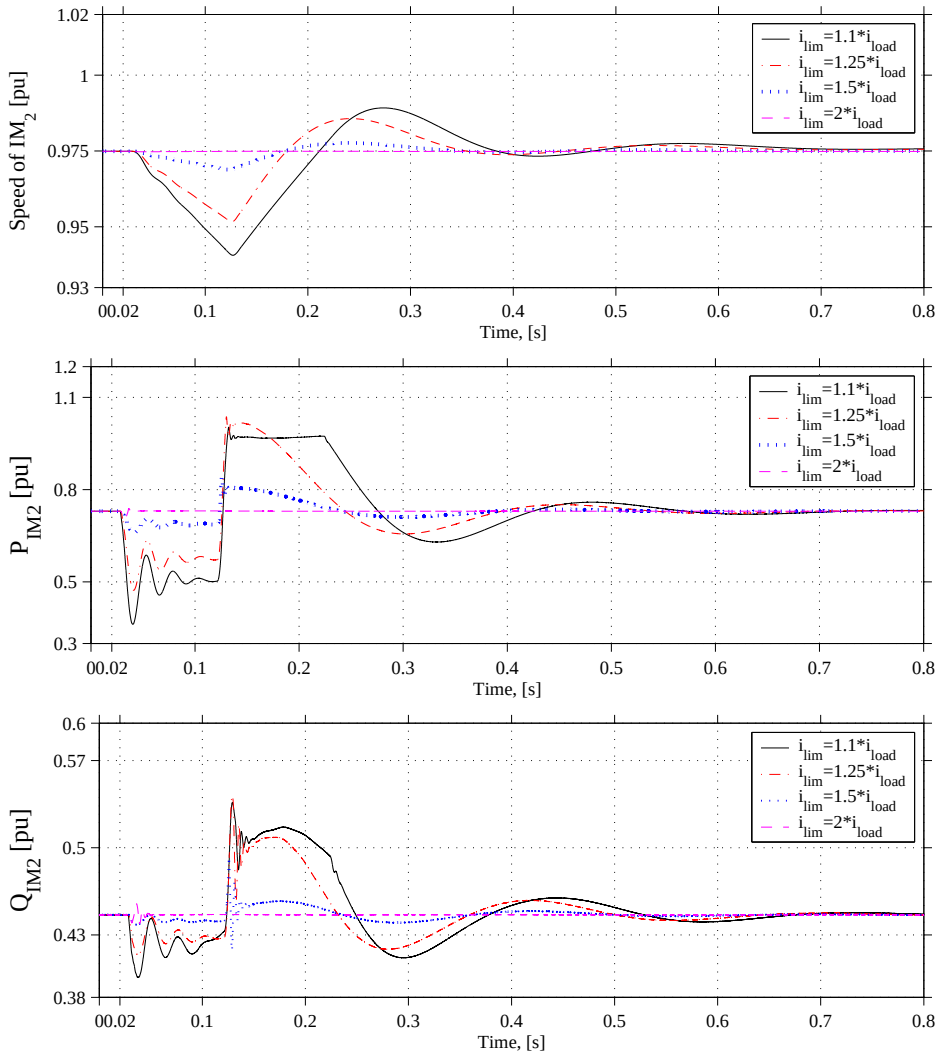

Fig. 5.7 Speed, active and reactive power of IM_2 during a three-phase grid fault.

Table 5.1: Comparison of induction motors in both systems during a three-phase grid fault.

	AC supply	VSC-HVDC supply with $i_{\text{lim}}/i_{\text{load}} = 1.1$
i_{max} of IM_1	0.239 pu	0.035 pu
ω_{min} of IM_1	0.986 pu	0.968 pu
i_{max} of IM_2	4.523 pu	1.086 pu
ω_{min} of IM_2	0.9 pu	0.941 pu
Minimum AC voltage at PCC	0.473 pu	0.961 pu
Minimum frequency at PCC	50 Hz	48.86 Hz

Motor starting

During a motor start the start current can be several times (normally 5-7) as large as the machine rated current. Hence, when a VSC-HVDC supplies an AC system with induction motors, it has to increase the reactive power delivered to the AC system to keep up the voltage during the motor start. However, as previously mentioned, the rating of a VSC is normally close to the load rating and therefore the reactive power capability is limited. Due to this fact it is necessary to perform an analysis of a system with the current limit of the VSC-HVDC converter included.

The comparison is also made in Table 5.2 between a pure AC supplied industrial plant and a VSC-HVDC supplied industrial plant. As shown in Table 5.2, for the IM_1, it takes a longer time to start with the VSC-HVDC supply as compared to the pure AC supply. Moreover, the AC voltage dip at the PCC is deeper and the frequency drops with the

Table 5.2: Comparison of induction motors in both systems during a motor start.

	AC supply	VSC-HVDC supply with $i_{\text{lim}} = 1.1 * i_{\text{load}}$
i_{max} of IM_1	0.448 pu	0.425 pu
Start time of IM_1	0.79s	0.94s
i_{max} of IM_2	0.895 pu	0.747 pu
$\omega_{\text{r,min}}$ of IM_2	0.974 pu	0.966 pu
Minimum AC voltage at PCC	0.963 pu	0.933 pu
Minimum frequency at PCC	50 Hz	49.62 Hz

VSC-HVDC supply. This is because the transformer in the AC supply can be overloaded for a short time whereas the VSC-HVDC does not have any overload capability. With an increase of the VSC-HVDC current limit, the power quality at the PCC will be improved.

System behavior during different voltages dip magnitudes and durations due to three-phase grid faults

Some simulation results and analysis have been presented in **[Paper E]**.

In order to obtain the response of power electronics for the proposed VSC-HVDC control system, a three-phase diode rectifier is included in the industrial plant as shown in Fig. 5.4. Here two groups of simulations are carried out. In the first group of simulations, the applied voltage dips have the same duration (0.1s) and the magnitude is changed from 0.1 pu to 1.0 pu. In the second group of simulations, the magnitude of the voltage dip is fixed to 0.5 pu and the dip duration is varied between 0.1s to 0.3s.

Figs. 5.8, 5.9 and 5.10 show the results of the first group of simulations, where several system variables are plotted as functions of voltage dip magnitude under different current limits of the VSC-HVDC converters. These system variables are: minimum DC voltage of the VSC-HVDC (Fig. 5.8), minimum AC voltage at the PCC (Fig. 5.9), minimum estimated frequency at the PCC (Fig. 5.9), minimum DC voltage of the diode rectifier (Fig. 5.10) and minimum speed of the induction motor IM_2 (Fig. 5.10). Apparently, they increase as the magnitude of the voltage dip becomes higher (i.e. the dip becomes less severe), they also increase when larger values are chosen for the converter current limit.

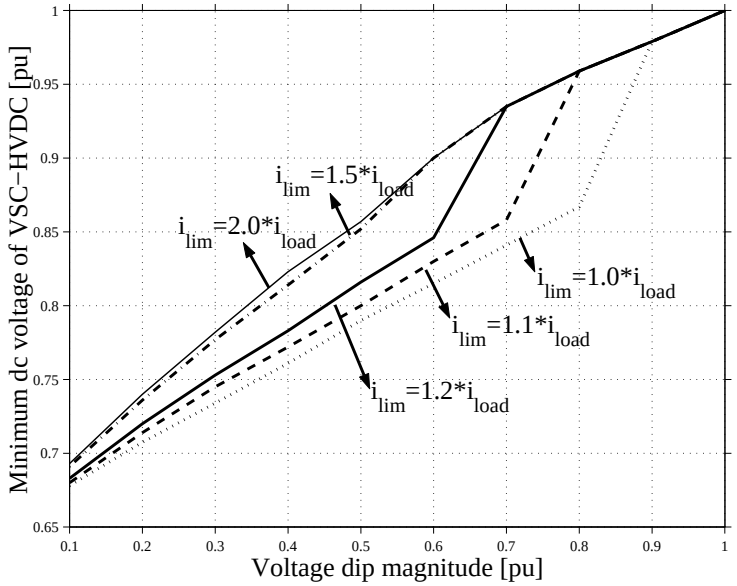

Fig. 5.8 Minimum DC voltage of the VSC-HVDC system as functions of voltage dip magnitude with different current limits of the VSC-HVDC converter. The voltage dip duration is fixed to 0.1s.

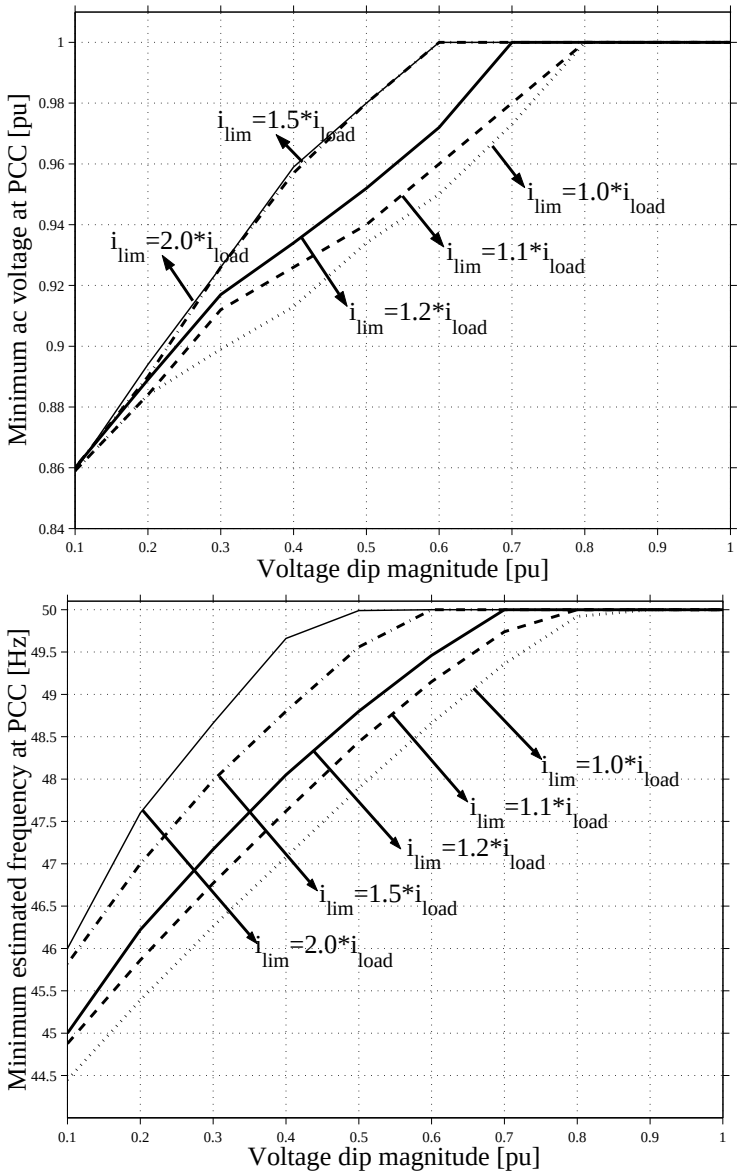

Fig. 5.9 Minimum AC voltage (top) and minimum estimated frequency (bottom) at the PCC as functions of voltage dip magnitude with different current limits of the VSC-HVDC converter. The voltage dip duration is fixed to 0.1s.

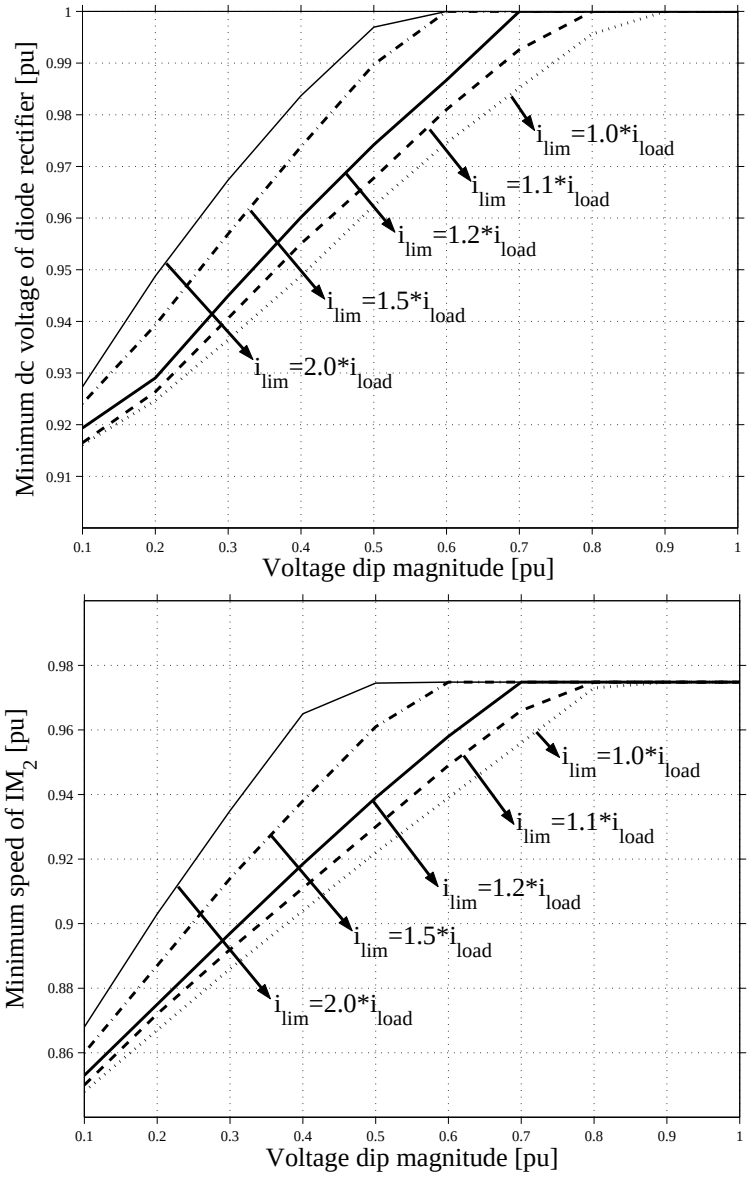

Fig. 5.10 Minimum DC voltage of diode rectifier (top) and minimum speed of induction motor IM_2 (bottom) as functions of voltage dip magnitude with different current limits of the VSC-HVDC converter. The voltage dip duration is fixed to 0.1s.

The results of the second group of simulations are shown in Fig. 5.11, where the minimum estimated frequency at the PCC and minimum speed of the induction motor IM_2 are plotted as functions of the voltage dip duration. It can be seen that the estimated frequency decreases as the voltage dip has longer duration. Consequently, the speeds of the induction motors IM_1 and IM_2 have similar responses as the estimated frequency at the PCC (here, only the speed of IM_2 is shown). In addition the minimum AC voltage at the PCC, the minimum DC voltages of the VSC-HVDC and the diode rectifier are not affected by the voltage dip duration.

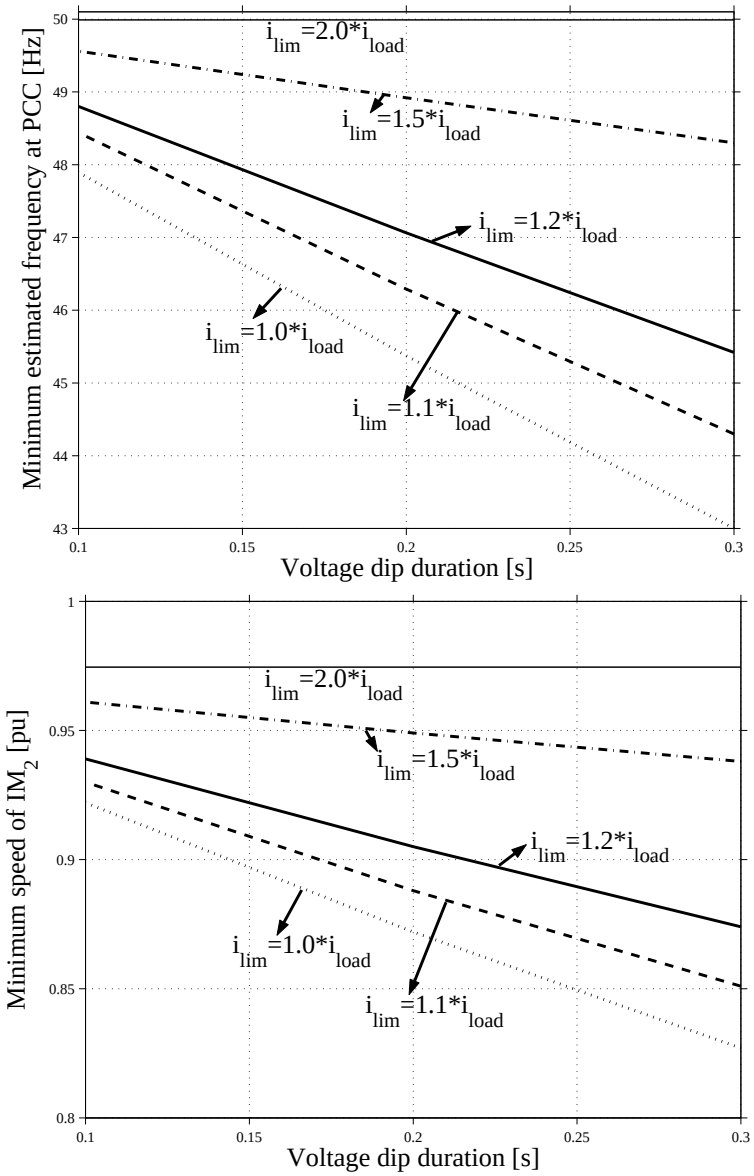

Fig. 5.11 Minimum estimated frequency at the PCC (top) and minimum IM_2 speed (bottom) as functions of voltage dip duration with different current limits of the VSC-HVDC converter. The magnitude of the voltage dip is fixed to 0.5 pu.

Therefore, it can also be obtained that the current limit significantly affects the dynamics of the system during a fault at the grid side.

Comparison of different frequency controllers for a VSC-HVDC supplied system

Some of the simulation results and analysis have been presented in **[Paper G]**.

The aim of this section is to distinguish and compare the effects of different frequency controllers, described in Chapter 3, for preventing voltage instability. Again the

most severe fault, a three-phase fault, is applied at the grid side. Also common small disturbances such as motor starts are considered to test the dynamics and ride-through capability of the system. As can be seen from Table 5.3, when the current limits of the converter are set to be 1.0 and 1.1 times the total load, the system collapses during a motor start if the inverter uses frequency controller I or II. However, the system can ride through these small disturbances when the inverter utilizes frequency controller III. For a balanced voltage dip with a retained voltage of 0.5 pu and a duration of 0.3s, it can be seen from Table 5.4 that when frequency controller I is applied the system will not recover after a fault until the current limit has been increased to 1.5 times the total load. However, the system can ride through the voltage dip when the inverter uses frequency controller II and the current limit is higher than 1.2 times the total load. Furthermore, with frequency controller III the system can avoid a voltage collapse without overrating the converter. This shows that it is possible for the system to increase the ride-through capability without overrating the converter when a suitable frequency control strategy, such as frequency controller III, is adopted.

Table 5.3: System responses with different frequency controllers and current limits during a motor start ($\times$:voltage collapse, O: stable operation).

$i_{\mathrm{lim}}/i_{\mathrm{load}}$	1.0	1.1	1.2
Frequency controller I	$\times$	$\times$	O
Frequency controller II	$\times$	$\times$	O
Frequency controller III	O	O	O

Table 5.4: System responses with different frequency controllers and current limits during a three-phase grid fault ($\times$:voltage collapse, O: stable operation).

$i_{\mathrm{lim}}/i_{\mathrm{load}}$	1.0	1.1	1.2	1.3	1.4	1.5
Frequency controller I	$\times$	$\times$	$\times$	$\times$	$\times$	O
Frequency controller II	$\times$	$\times$	O	O	O	O
Frequency controller III	O	O	O	O	O	O

5.3 VSC-HVDC system for industrial plants with on-site generation

In Section 5.2 and in [47] the VSC-HVDC feeding an industrial system without on-site generation has been studied and the system shows a high control flexibility. In this section, a VSC-HVDC supplied industrial plant with on-site generation is studied. The control

strategy, i.e. the rectifier station controls the AC and DC voltage whereas the inverter station controls the frequency and AC voltage, is adopted in the VSC-HVDC system. Some issues have been addressed in **[Paper H]** and **[Paper I]**.

In most industrial plants having on-site generation facilities the speed control of the on-site generation is normally not activated when synchronized to the main grid. The speed controller becomes active only in island operation [94]. Therefore, this section analyzes the performance of a VSC-HVDC supplied industrial plant with on-site generation, shown in Fig. 5.12 when the turbine operates in constant active power production mode and in speed control mode, respectively.

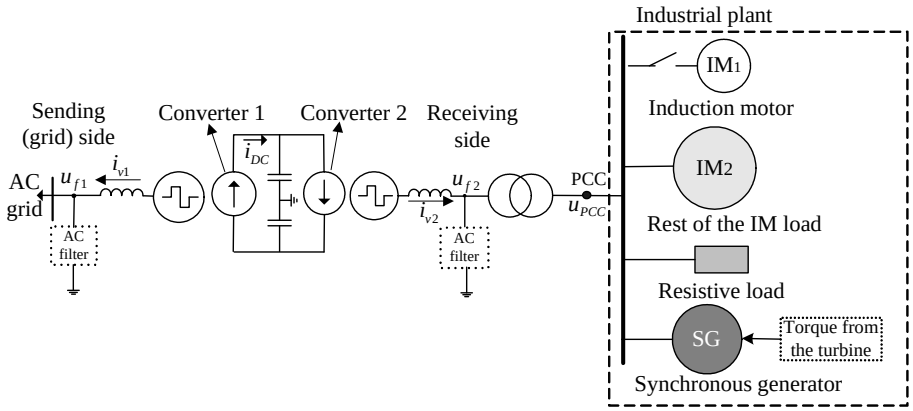

Fig. 5.12 Model for a VSC-HVDC system with different loads and on-site generation.

5.3.1 On-site generation with constant power production

For industrial customers using on-site generation the production is based on back-pressure and condensing turbines. Normally the turbines produce as much as possible. Therefore, this subsection focuses on the investigation of a VSC-HVDC supplied industrial plant with on-site generation when the turbine produces constant active power. Impacts of different conditions, such as the generator field voltage, the generator inertia constant, the generator output and the generator excitation system, have been studied in **[Paper H]**. Here, results with different generator outputs and different generator sizes during the grid faults will be highlighted.

Three-phase grid fault with different torques

Figs. 5.13 - 5.14 show the dynamic responses of the system during a three-phase grid fault when the mechanical torque of the generator $T_{\mathrm{M,SG}}$ is set to 0.1 pu and 0.4 pu respectively. It can be seen that different power production levels affect the dynamic behavior of the system significantly. When $T_{\mathrm{M,SG}}$ is 0.1 pu, the DC voltage decreases during the fault, which implies that the transferred active power from the grid is reduced. Consequently

this affects the decay of the frequency (i.e. speed of synchronous generator) and the dynamics of the AC voltage at the PCC. However, if $T_{\mathrm{M,SG}}$ is set to 0.4 pu or higher, the AC voltage and frequency at the PCC can be kept constant. Fig. 5.14 shows the reaction

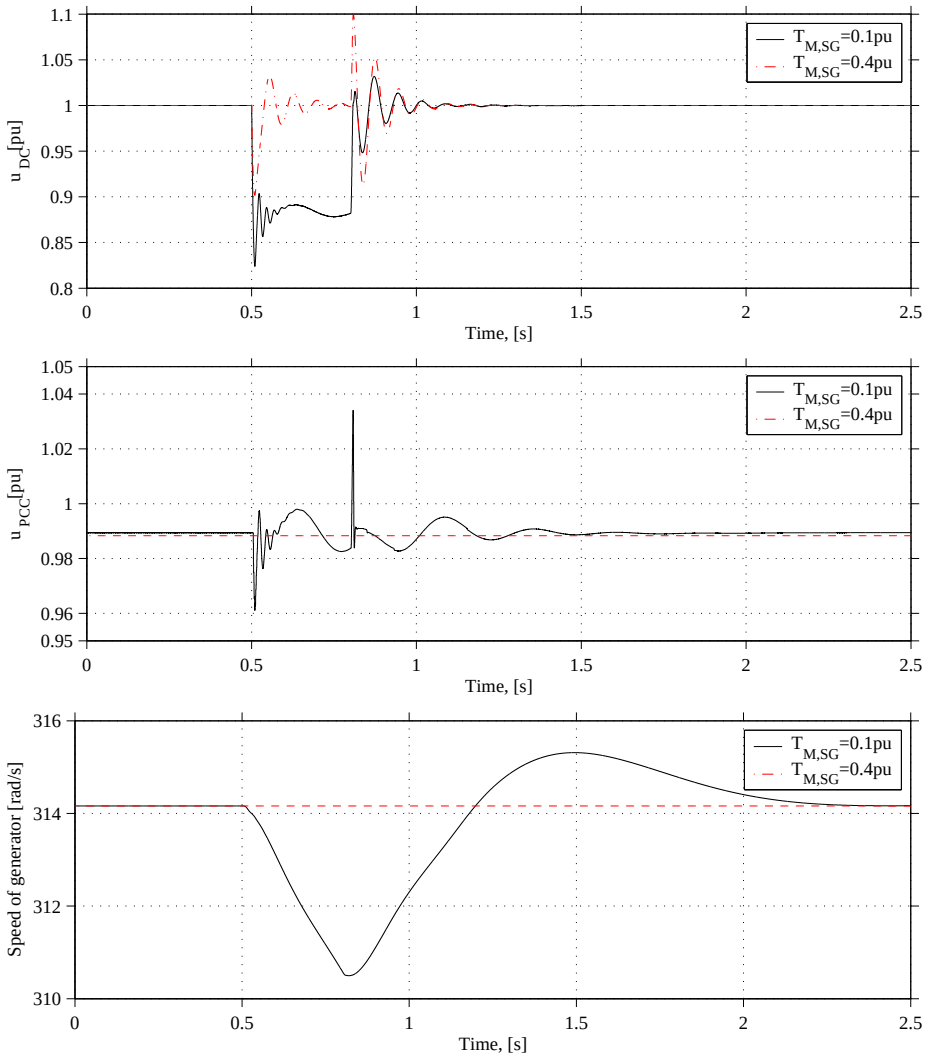

Fig. 5.13 DC voltage, voltage amplitude at PCC and speed of the synchronous generator during a three-phase grid fault with varying mechanical torque $T_{\mathrm{M,SG}}$.

of the generator - both the steady-state and the transient active power characteristics - as a function of the load angle. During the fault the VSC-HVDC system can not supply enough active power to the load due to the current limit of the VSC when $T_{\mathrm{M,SG}}$ is 0.1 pu. Therefore, the power balance between the supplied mechanical power on the turbine and the produced electrical power in the generator is disturbed. During the fault the load angle of the generator increases from 5 to 15 degrees. The generator supplies an active power of about 0.35 pu which implies that the power balance will not be disturbed during the same fault as long as $T_{\mathrm{M,SG}}$ is set to be higher than 0.35 pu. This has been verified from the simulation shown in the Figs. 5.13 - 5.14. It is noted that the voltage at the PCC, i.e. the

terminal voltage of the generator, is generally limited to 105% of its rated voltage during the fault.

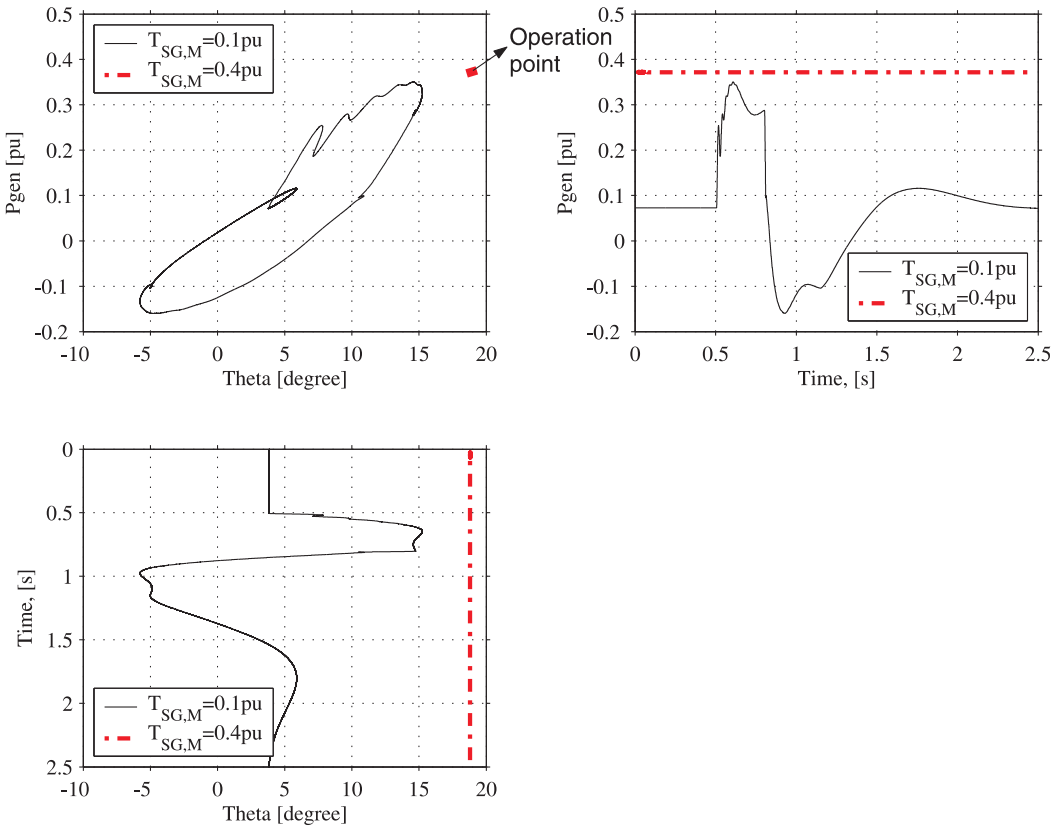

Fig. 5.14 Active power and load angle of the synchronous generator during a three-phase grid fault with varying mechanical torque $T_{\mathrm{M,SG}}$.

A comparison has also been made with industrial plants having two different supplies, i.e. a VSC-HVDC supply and an AC supply. This aim is to demonstrate the power supply improvement capability of the VSC-HVDC to an industrial plant with an on-site generator. Table 5.5 shows the comparison of the responses of both systems. As can be seen the minimum AC voltage and frequency at the PCC are 0.5 pu and 50 Hz, the highest current and the lowest speed of IM_2 are 4.83 pu and 0.857 pu during the fault when the industry is supplied purely by an AC system. However, when supplied by a VSC-HVDC system with $T_{\mathrm{M,SG}} = 0.1\mathrm{pu}$, the minimum AC voltage and frequency at the PCC are 0.96 pu and 49.42 Hz respectively, while the highest current of IM_2 is only 1.068 pu. Moreover, the speed of IM_2 only slows down to 0.964 pu during the fault. Furthermore, when supplied by a VSC-HVDC system with $T_{\mathrm{M,SG}} = 0.7\mathrm{pu}$, the minimum AC voltage and frequency at the PCC are 1.0 pu and 50 Hz. This shows that the industrial plant is immune to this voltage dip due to a three-phase grid fault, and all loads are working in normal operation. Therefore, this comparison clearly illustrates that the VSC-HVDC significantly mitigates voltage dips from the grid and improves the power quality of the

industrial plant.

Table 5.5: Comparison of the system performance including induction motors and synchronous generator in both systems during a three-phase grid fault.

	AC supply & $T_{\mathrm{M,SG}} = 0.7\mathrm{pu}$	VSC-HVDC & $T_{\mathrm{M,SG}} = 0.1\mathrm{pu}$	VSC-HVDC & $T_{\mathrm{M,SG}} = 0.7\mathrm{pu}$
$i_{\mathrm{max,IM_1}}$	0.265pu	0.06pu	0.05pu
$\omega_{\mathrm{min,IM_1}}$	0.907pu	0.965pu	0.975pu
$i_{\mathrm{max,IM_2}}$	4.83pu	1.068pu	0.864pu
$\omega_{\mathrm{min,IM_2}}$	0.857pu	0.964pu	0.974pu
$i_{\mathrm{max,SG}}$	3.528pu	0.353pu	0.685pu
$\omega_{\mathrm{min,SG}}$	0.994pu	0.988pu	1.0pu
$u_{\mathrm{min,PCC}}$	0.5pu	0.96pu	0.99pu
$f_{\mathrm{min,PCC}}$	50Hz	49.42Hz	50Hz

Three-phase grid fault with different generator sizes

From Fig. 5.13 it can be concluded that different mechanical torques $T_{\mathrm{M,SG}}$ have a significant influence on the system when the size of the synchronous generator is equal to the total load. In this section the influence of the synchronous generator size on the system behavior is investigated when the mechanical torque is fixed.

Figs. 5.15 - 5.16 show the response of the system during a three-phase grid fault when varying the size of the synchronous generator S_{SG}. $T_{\mathrm{M,SG}}$ is 0.7 pu of the generator power. It can be seen that when the synchronous generator size increases, the corresponding active power production increases. This results in a reduction of the VSC-HVDC's active power transfer. Consequently the minimum DC voltage increases during a three-phase grid fault. However, a change of the apparent power of the generator hardly affects the reactive power productions of the VSC-HVDC or the generator. When the generator size is less than 0.5 times the total load the minimum AC voltage at the PCC and the minimum speed of the generator decrease with the reduced size of the generator whereas the maximum load angle of the generator rapidly increases with a size reduction. Nevertheless, the minimum AC voltage at the PCC and the minimum speed of the generator are kept constant when the generator is larger than 0.5 pu.

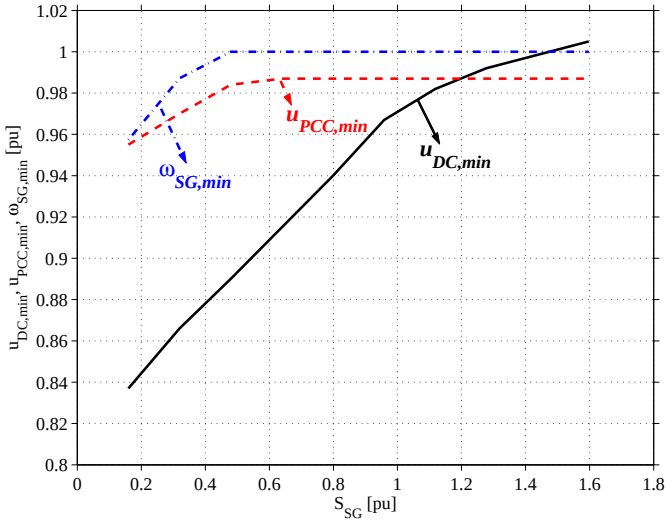

Fig. 5.15 DC voltage and AC voltage amplitude at PCC together with the generator speed during a three-phase grid fault with varying S_{SG}.

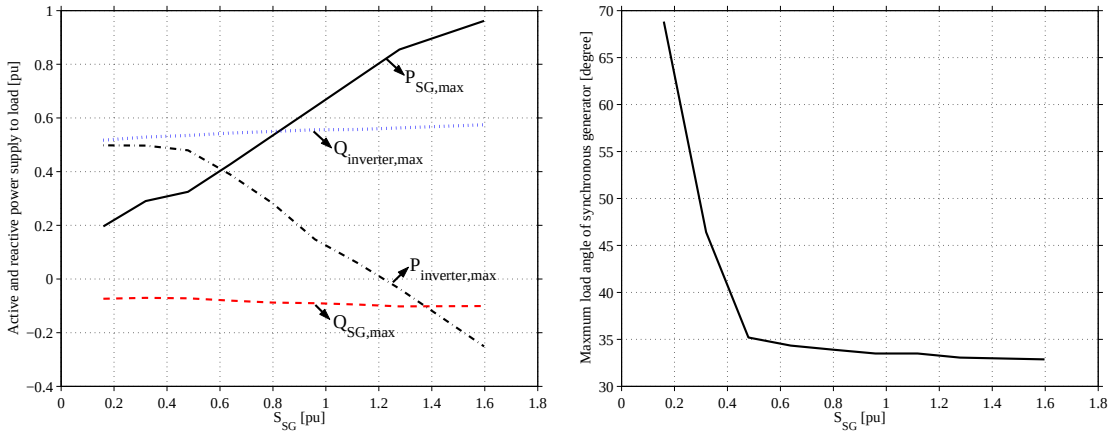

(a) (b)

Fig. 5.16 Active and reactive power from inverter and synchronous generator (a) and load angle of the synchronous generator (b) during a three-phase grid fault with varying S_{SG}.

5.3.2 On-site generation using frequency control

As mentioned in the previous subsection the back-pressure turbines normally produce as much as possible. However, the electricity production is dependent on the production process (pulp, paper etc). In this subsection the VSC-HVDC system for industrial plants with on-site generation will be investigated during load changes and grid faults. During the studies both the inverter and the on-site generation are equipped with frequency and AC voltage controllers. Some of the results included in **[Paper I]** are presented in this subsection. The action of both frequency controllers is analyzed. After that two comparisons, based on the performed simulations, are made:

- a comparison on the system response will be done during load changes when the VSC-HVDC uses two different frequency controllers, i.e. a PI controller and a droop controller.
- a VSC supplied industrial plant will be compared with the same industrial plant supplied by a conventional AC supply.

Frequency control of the VSC and the turbine

As previously mentioned the synchronous generator is equipped with an excitation system and the turbine with a frequency controller. Since the VSC is also equipped with a frequency controller it is important to analyze the effect of both frequency controllers on the system. Therefore, this section will analyze the frequency controllers of the VSC and the turbine [83, 86].

Fig. 5.17 shows the block diagram of the system for small frequency deviations. The frequency controllers of the VSC and the turbine are denoted $F_{\mathrm{VSC}}(s)$ and $F_{\mathrm{GT}}(s)$ respectively. From Fig. 5.17 it can be derived that the frequency deviation $\Delta\omega$ is:

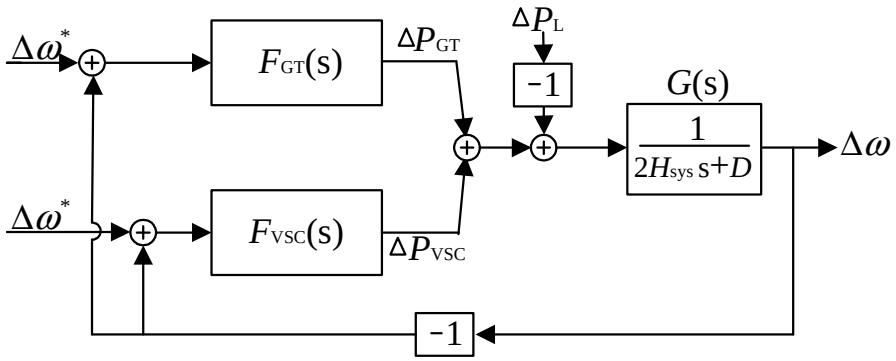

Fig. 5.17 Simplified block diagram of the system with two frequency controllers.

$$\begin{aligned} \Delta\omega &= G(s)(\Delta P_{\mathrm{GT}} + \Delta P_{\mathrm{VSC}} - \Delta P_{\mathrm{L}}) \\ &= \frac{\Delta P_{\mathrm{GT}} + \Delta P_{\mathrm{VSC}} - \Delta P_L}{2H_{\mathrm{sys}}s + D} \end{aligned} \tag{5.1}$$

where $\Delta\omega^* = 0$.

By imposing $\Delta P_{\mathrm{GT}} = -F_{\mathrm{GT}}(s)\Delta\omega$ and $\Delta P_{\mathrm{VSC}} = -F_{\mathrm{VSC}}(s)\Delta\omega$, it can be derived that:

$$\Delta\omega = \frac{-\Delta P_{\mathrm{L}}}{2H_{\mathrm{sys}}s + D + F_{\mathrm{GT}}(s) + F_{\mathrm{VSC}}(s)} \tag{5.2}$$

The turbine is assumed to use a droop frequency controller and the VSC frequency controller is assumed to be:

- a PI controller $F_{\mathrm{VSC,PI}}(s)$ i.e. the frequency droop is zero.

- a droop controller $F_{\mathrm{VSC,droop}}(s)$.

The transfer functions of $F_{\mathrm{GT}}(s)$, $F_{\mathrm{VSC,PI}}(s)$ and $F_{\mathrm{VSC,droop}}(s)$ are described as follow:

$$F_{\mathrm{GT}}(s) = k_{\mathrm{GT}}\frac{1+s\alpha T_{\mathrm{GT}}}{1+sT_{\mathrm{GT}}} \tag{5.3}$$

$$F_{\mathrm{VSC,PI}}(s) = k_{\mathrm{p,fre}} + \frac{k_{\mathrm{I,fre}}}{s} \tag{5.4}$$

$$F_{\mathrm{VSC,droop}}(s) = k_{\mathrm{VSC}}\frac{1+s\gamma T_{\mathrm{cut}}}{1+sT_{\mathrm{cut}}} \tag{5.5}$$

where $\alpha < 1$ and $\gamma < 1$.

By substituting (5.3) and (5.4) or (5.5) into (5.2) and taking account of the "active damping, B_a" adopted in the PI controller, it can be derived that:

$$\begin{aligned}\Delta\omega_{\mathrm{PI}} &= \frac{-\Delta P_{\mathrm{L}}}{2H_{\mathrm{sys}}s + D + B_{\mathrm{a}} + k_{\mathrm{GT}}\frac{1+s\alpha T_{\mathrm{GT}}}{1+sT_{\mathrm{GT}}} + k_{\mathrm{p,fre}} + \frac{k_{\mathrm{I,fre}}}{s}} \\ &\approx \frac{-\Delta P_{\mathrm{L}}}{2H_{\mathrm{sys}}s + B_{\mathrm{a}} + k_{\mathrm{GT}}\frac{1+s\alpha T_{\mathrm{GT}}}{1+sT_{\mathrm{GT}}} + k_{\mathrm{p,fre}} + \frac{k_{\mathrm{I,fre}}}{s}}\end{aligned} \tag{5.6}$$

$$\Delta\omega_{\mathrm{droop}} = \frac{-\Delta P_{\mathrm{L}}}{2H_{\mathrm{sys}}s + D + k_{\mathrm{GT}}\frac{1+s\alpha T_{\mathrm{GT}}}{1+sT_{\mathrm{GT}}} + k_{\mathrm{VSC}}\frac{1+s\gamma T_{\mathrm{cut}}}{1+sT_{\mathrm{cut}}}} \tag{5.7}$$

From (5.6) and (5.7) it can be concluded that at the steady state conditions:

$$\Delta\omega_{\mathrm{PI,ss}} \approx \frac{-\Delta P_{\mathrm{L}}}{B_{\mathrm{a}} + k_{\mathrm{GT}} + k_{\mathrm{p,fre}} + k_{\mathrm{I,fre}}\cdot\infty} \tag{5.8}$$

$$\begin{aligned}\Delta\omega_{\mathrm{droop,ss}} &= \frac{-\Delta P_{\mathrm{L}}}{D + k_{\mathrm{GT}} + k_{\mathrm{VSC}}} \\ &\approx \frac{-\Delta P_{\mathrm{L}}}{k_{\mathrm{GT}} + k_{\mathrm{VSC}}}\end{aligned} \tag{5.9}$$

which means that

- when the VSC uses a PI frequency controller, the integral part of the frequency controller of the VSC-HVDC will regulate $\Delta\omega$ to zero. Fig. 5.18 shows the frequency droop characteristics of the VSC and the turbine.

- when the VSC uses a droop frequency controller, the frequency error of the system is not regulated to zero. The steady state error of the frequency, approximated to $\frac{-\Delta P_{\mathrm{L}}}{k_{\mathrm{GT}}+k_{\mathrm{VSC}}}$ when D can be negligible, depends on the combined effect of the droops of the VSC and the turbine. The total static gain will be $k_{\mathrm{GT}} + k_{\mathrm{VSC}}$. This is the same as for the frequency control strategy of conventional power systems. Fig. 5.19 shows the load sharing of both the VSC and the turbine. As can be seen the initial

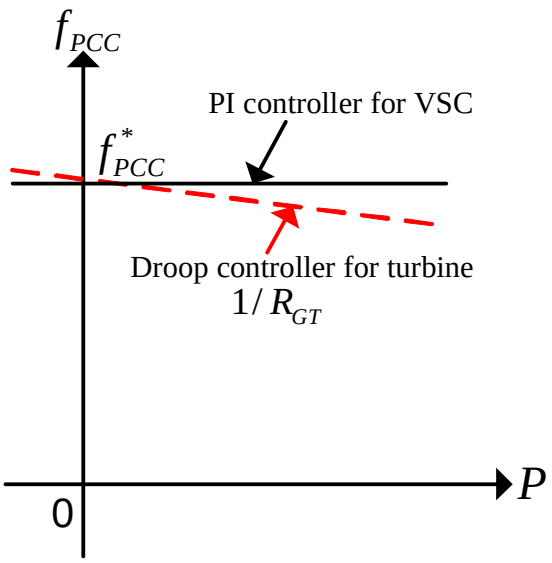

Fig. 5.18 Frequency static characteristics of the VSC and the turbine.

frequency is f_{PCC1} at steady state. The VSC and the turbine supply P_{VSC1} and P_{GT1} respectively. After the load change, the VSC and the turbine supply P_{VSC2} and P_{GT2}. The frequency at steady state is f_{PCC2}. The load sharing between the VSC and the turbine depend on the static droops R_{VSC} and R_{GT} respectively.

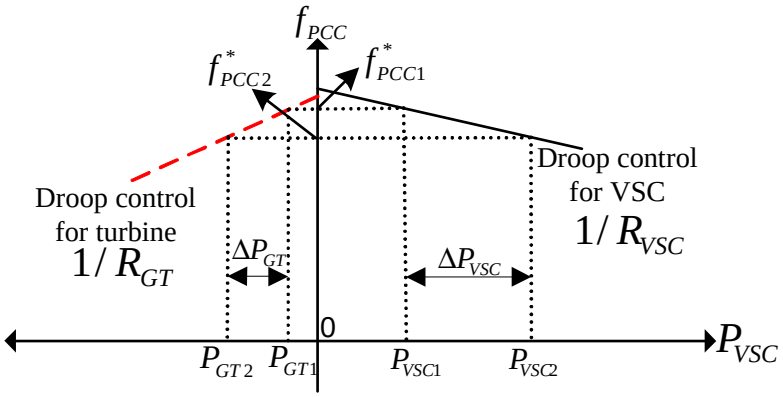

Fig. 5.19 Sharing of a load change between the VSC and the turbine.

Comparison of PI and droop frequency controllers of the VSC in case of load changes

Fig. 5.20 shows the responses due to an IM_2 torque step change which is applied at 0.5s. As can be seen different frequency control strategies have a negligible impact on the DC voltage and AC voltage at the PCC. However, they have an obvious effect on the minimum frequency that varies from 49.15 Hz to 49.4 Hz, and the steady state frequency that varies from 49.5 Hz to 50 Hz. The transferred active powers for the VSC-HVDC and

the generator are shown in Fig. 5.21. The VSC takes care of the torque step change when the frequency controller of the VSC is realized with a PI controller. This implies that the VSC may be insufficient to cover the total load variations. This may have an influence on stability of the system when the size of the VSC is not sufficiently big as compared to the load. However, the VSC and the generator share the load change according to their droops when the VSC and the turbine use droop frequency controllers.

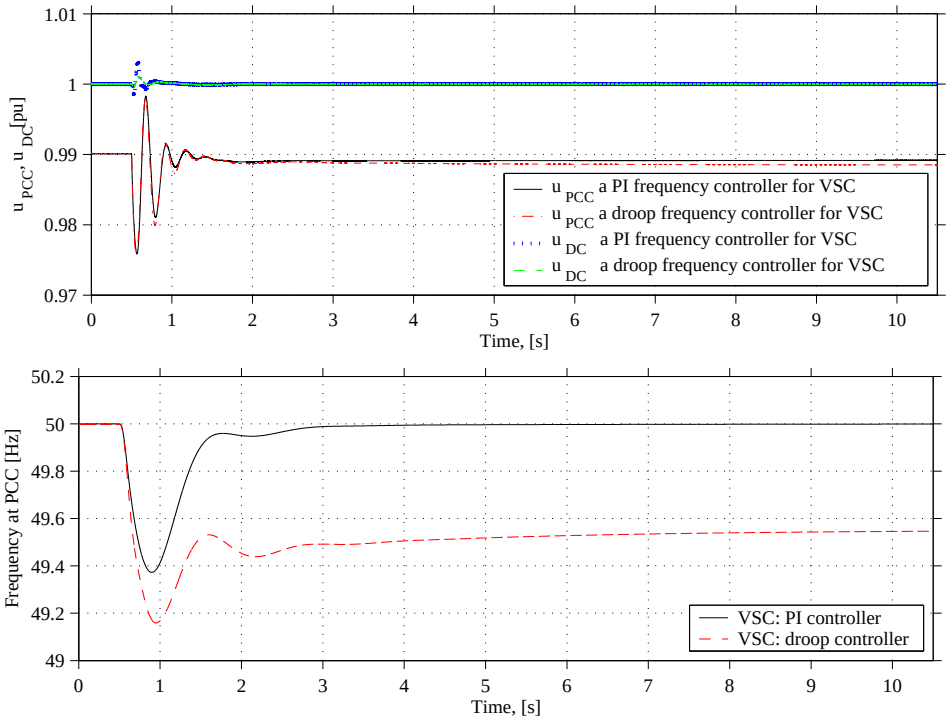

Fig. 5.20 DC voltage, AC voltage and frequency at PCC during a torque step change of IM_2. The turbine and the VSC use droop frequency controllers.

Three-phase grid fault

In Table 5.6 a comparison is made between a pure AC supplied industrial plant and the same VSC-HVDC supplied industrial plant during a 0.3s three-phase grid fault with a 0.5 pu retained voltage. As shown in Table 5.6, when a conventional AC supply is used to the industrial plant with on-site generation, the minimum AC voltage and frequency at the PCC are 0.513 pu and 50 Hz respectively. The highest current and the lowest speed of IM_2 are about 4.87 pu and 0.863 pu during the fault. However, when supplied by a VSC-HVDC system and a generator together with a constant load torque on the turbine, the minimum AC voltage and frequency at the PCC are 0.96 pu and 49.42 Hz respectively. The highest current of IM_2 is 1.068 pu and the speed slows down to 0.964 pu during the fault. Therefore, it can be concluded that the power quality of an industrial plant using on-site generation is significantly improved with a VSC-HVDC supply as compared to a

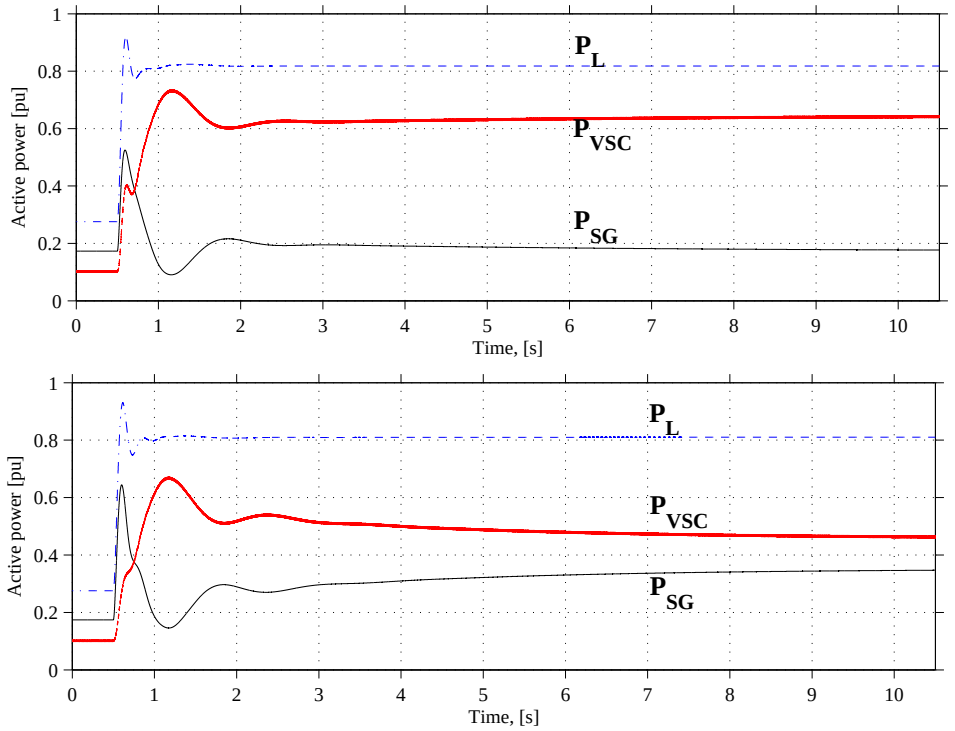

Fig. 5.21 Power responses of the VSC and the generator during a torque step change of IM_2. The turbine uses a droop frequency controller and the VSC uses a PI frequency controller (top) or a droop frequency controller (bottom).

pure AC supply. From Table 5.6 it can also be observed that the transient maximum and minimum values of the loads in the plant show no major differences, when the two cases, i.e. the turbine with and without a frequency controller, are compared. This is due to the slow response of the turbine frequency controller.

Table 5.6: Comparison of the induction motors and the synchronous generator behavior during a three-phase grid fault when having an AC supply or a VSC-HVDC supply.

	AC supply & $T_{\mathrm{M,SG}} = 0.1\mathrm{pu}$	VSC-HVDC &No FC $T_{\mathrm{M,SG}} = 0.1\mathrm{pu}$	VSC-HVDC &FC $P_{\mathrm{SG0}} = 0.1\mathrm{pu}$
$i_{\mathrm{max,IM_1}}$	0.269pu	0.06pu	0.06pu
$\omega_{\mathrm{min,IM_1}}$	0.91pu	0.965pu	0.966pu
$i_{\mathrm{max,IM_2}}$	4.87pu	1.068pu	1.067pu
$\omega_{\mathrm{min,IM_2}}$	0.863pu	0.964pu	0.964pu
$i_{\mathrm{max,SG}}$	3.497pu	0.353pu	0.353pu
$\omega_{\mathrm{min,SG}}$	0.998pu	0.988pu	0.989pu
$u_{\mathrm{min,PCC}}$	0.513pu	0.96pu	0.96pu
$f_{\mathrm{min,PCC}}$	50Hz	49.42Hz	49.45Hz

5.4 Summary

This chapter has presented the performance of a VSC-HVDC supplied industrial plant with and without on-site generation during various disturbances. It focuses on how the use of frequency controllers in the VSC-HVDC control system to increase the ride-through capability of the industrial plant in case of voltage disturbances. The impact of the converter current limit on the dynamics of a VSC-HVDC supplied industrial plant during load changes and grid faults such as three-phase faults and single-phase faults is also investigated. It can be concluded from simulation results that with the use of the frequency controller in the VSC-HVDC control system the power quality of the industrial plant is significantly improved. The extent of improvement depends on the current limit of the VSC-HVDC system, the generator power production levels and the generator ratings when the industrial plant has on-site generation.

Chapter 6

Conclusions and Future Work

This chapter draws conclusions and presents some suggestions for further work.

6.1 Conclusions

After the world's first HVDC Light transmission installation into Gotland, Sweden, 1997, there has been growing interest in the research on this new HVDC technology. The VSC-HVDC uses the IGBTs and PWM, which makes it possible to generate the desired AC output voltage. This high flexibility of control allows for a number of new advantages and applications which have been presented in Chapter 2.

In order to fully exploit the capability of the VSC-HVDC, the control algorithms of the VSC-HVDC are investigated and the performance is tested in different situations in this thesis. Two different control strategies, AC-voltage control and reactive power control, are presented and evaluated when the VSC-HVDC connects two grids. Another control strategy, frequency control, has been implemented in the VSC-HVDC control system to analyze the dynamics of VSC-HVDC supplied industrial systems with and without on-site generation. The investigation focuses on how the frequency of the output voltage of the converters can be controlled in order to increase the ride-through capability for the VSC-HVDC supplied industrial system in case of voltage disturbances. The motivation of choosing this control strategy is to exploit the inertia of the rotating masses by slightly decreasing the frequency of the VSC-HVDC output voltage to ride through the disturbances.

Two control strategies have been implemented when the VSC-HVDC connects two grids. The results show that

- the system response is fast, high quality AC voltages and currents can be obtained, the active and reactive power can be controlled independently and are bi-directional.
- the two different control strategies have different effects on the performance of the VSC-HVDC. For instance, the AC voltage can be kept constant with AC-voltage

control, while the voltage varies with reactive-power control when the reactive power flows change. Therefore, if the system is strong, reactive-power control can be used. Otherwise the AC voltage control is recommendable. The control strategy should be selected depending on the objectives and characteristics of the system.

- during a three-phase grid fault, the DC voltage drops due to the converter current limit. However, the severity of three-phase short circuit currents are reduced as compared with an AC interconnection.

- during an unbalanced grid fault, the DC voltage drops and shows a large oscillation, the unbalance at the faulted side is transferred to the un-faulted side. This unbalance can be reduced either by decreasing the transferred active power or by increasing the converter current limits. Furthermore, the phase currents at the faulted side exceed the current limits. This will stress the valves and may trip the DC link. Therefore, to avoid overcurrents and reduce the oscillations of the DC voltage during the unbalanced fault, modified controllers are introduced into the control system to improve the system dynamics.

- comparisons of the simulation results for both the complete and simplified VSC-HVDC models show good agreements between the two models during transients as well as during steady state.

A new control strategy of the VSC-HVDC system for providing a high-quality supply to industrial plants are proposed. In the proposed control strategy, a frequency controller and an AC voltage controller are implemented in the inverter station of the VSC-HVDC. The motivation of choosing this control strategy is to exploit the inertia of the rotating masses by slightly decreasing the frequency of the VSC-HVDC output voltage when needed. Thus, a momentary surplus of energy is created in the rotating masses of the motors to ride through disturbances such as AC faults and motor starting. In order to validate the proposed control strategy, the dynamic performance of a VSC-HVDC supplied industrial plant is investigated during various disturbances. The simulation results illustrate that

- the VSC-HVDC has the possibility to control the AC voltage and frequency at the PCC to ride through disturbances.

- by comparisons of the performance of the load with a conventional AC supply and a VSC-HVDC supply, it is demonstrated that the use of the VSC-HVDC significantly enhances the quality of power supply to industrial plants during faults at the sending side of the VSC-HVDC.

- during motor starts, it takes a longer time to start, the AC voltage at the PCC drops deeper and the frequency is not constant as compared with a pure AC supply.

- the rating or current limit of the VSC-HVDC converter significantly influences the performance of the system during disturbances. An increase of the rating of the VSCs significantly improves the power quality of the system.

Different frequency controllers, i.e. fixed frequency controller with constant reference frequency, fixed frequency controller with various reference frequency regarding DC voltage dynamics of the DC link, a PI frequency controller, and their effects on the voltage disturbance ride-through capability of a VSC-HVDC supplied industrial system are studied and presented. It shows that

- during small disturbances such as motor starts the system collapses when the inverter station uses the fixed frequency controllers with constant reference frequency and with various reference frequency whereas the system can avoid a voltage collapse with the use of a PI frequency controller without overrating the VSC.

- during three-phase grid faults, the system survives without a voltage collapse or excessive voltage sags after faults without overrating the converter when a PI frequency controllers is used.

- the effect of increasing the capacitor size instead of the converter size on improving the power quality of a VSC-HVDC supplied industrial plant is also investigated. Simulation results show that it is possible to improve the system voltage disturbance tolerance by increasing the DC capacitor on the DC bus. However, an overcurrent of the converter occurs at the end of the fault.

A VSC-HVDC supplying an industrial plant with on-site generation has been investigated when the generator has an exciter and the turbine has a frequency controller. The control strategy utilized in the VSC-HVDC system is that the rectifier controls the DC voltage and the AC voltage at the grid, whereas the inverter controls the AC voltage and frequency at the PCC. A detailed analysis of two frequency control algorithms, i.e. a PI frequency controller and a droop frequency controller in the inverter has been performed. The system dynamics has been investigated under various operation conditions and during grid faults. From the simulation results it can be concluded that

- different frequency controllers in the inverter have different responses on the system. When the inverter uses a PI frequency controller, the frequency at steady state resumes to the nominal value. However, a potential instability problem may occur when the size of the VSC-HVDC is limited. When the inverter uses a droop frequency controller the VSC-HVDC shares the load change with the generator. However, there is a steady state frequency fault if not a secondary frequency control is used.

- by comparing the dynamic behavior of the system when the inverter uses a PI frequency controller and the turbine operates in constant power production mode, frequency control with no reheat turbine mode or frequency control with reheat turbine mode it can be obtained that the system frequency recovers faster when the turbine works with frequency control with no reheat turbine. However, the system transients are more or less the same when the turbine works in the three different modes. Therefore, another comparison has been made when the VSC-HVDC size is reduced to certain percent of the total load, the generator size is varied and the turbine is equipped with or without frequency control. The comparison shows that with the use of the frequency controller at the turbine the frequency drop reduces during both the motor starts and the grid faults.

- a comparison of a VSC-HVDC feeding an industrial plant with a pure AC supply of the same industrial plant shows that the VSC-HVDC can mitigate voltage dips in the grid and the power quality of the industrial customers supply can be significantly improved.

- the converter current limit, different levels of power production and sizes of the synchronous generator have significant impacts on the dynamic response of the system.

In the end, it can be concluded that the VSC-HVDC has a number of advantages as compared with classic HVDC or AC transmission and it is suitable for a wide range of situations when properly designed and operated. We will likely see more VSC-HVDC applications in future power systems.

6.2 Future work

As previously described, VSC transmission and distribution have some disadvantages, which include potentially high losses and costs. However, the technology continues to evolve. To further assess the potential and limitation of VSC transmission and distribution for industrial power systems, a number of possible applications and advancements in the VSC technology are required such as

- faults and protection

  Faults in the DC system remain a serious concern. One of the problems is that the fault currents are limited by the converters. This may make it difficult to apply existing protection strategies. Protection of the DC network is strongly related to the reliability of the network. Fast and reliable DC circuit breakers are a possible solution.

- industrial systems with VSC-HVDC and internal multilevel DC network

  In an industrial system with internal DC distribution, all drive systems are mounted on the same DC-bus, the energy in the rotating masses will then be delivered to the common DC-bus by slightly decreasing the frequency of the VSC output voltage. There is a higher flexibility in this situation, in that the frequency reduction can be applied selectively only to those machines that are not sensitive, while the stored energy through the DC-bus can be used to keep the critical ones on line. Further improvement can be obtained by connecting some additional storage to the common DC-bus. This can result in a more cost-effective solution than increasing the storage (capacitor size) at each DC-bus of the individual drive system, as it is done in the traditional AC solution to increase the ride-through capability of the drive.

- industrial systems with VSC-HVDC and bypass switches

  To prevent industrial system interruptions due to failure of the VSC-HVDC system components, the use of a bypass switch may be considered.

- VSC-HVDC connecting weak AC systems

  When the VSC-HVDC is connected to a weak AC system characterized by a lower short-circuit power, a number of difficulties concerning the operation and design emerge. They are, among others, low resonant frequencies and control strategies for achieving optimal active power flow. More research is required to address those problems.

References

[1] M. M. D. Mueller and M. Samotyj, "Voltage sags in industrial systems," *IEEE Trans. Ind. Applicat.*, vol. 29, no. 2, pp. 397 – 403, March-April 1993.

[2] C. Melhornand, T. Davis, and G. Beam, "Voltage sags: their impact on the utility and industrial customers," *IEEE Trans. Ind. Applicat.*, vol. 34, no. 3, pp. 549 – 558, May-June 1998.

[3] A. Campbell and R. McHattie, "Backfilling the sinewave. a dynamic voltage restorer case study," *Power Engineering Journal*, vol. 13, no. 3, pp. 153 – 158, June 1999.

[4] C. Becker, W. Braun, K. Carrick, T. Diliberti, C. Grigg, J. Groesch, B. Hazen, T. Imel, D. Koval, D. Mueller, T. S. John, and L. Conrad, "Proposed chapter 9 for predicting voltage sags (dips) in revision to IEEE Std 493, the Gold Book," *IEEE Trans. Ind. Applicat.*, vol. 30, no. 3, pp. 805 – 821, May-June 1994.

[5] C. DeWinkel and J. Lamoree, "Storing power for critical loads," *IEEE Spectrum*, vol. 30, no. 6, pp. 38 – 42, June 1993.

[6] A. Sannino, M. Miller, and M. Bollen, "Overview of voltage sag mitigation," in *IEEE Power Engineering Society Winter Meeting, 2000.*, vol. 4.

[7] N. G. Hingorani, "Introducing custom power," *IEEE Spectrum*, vol. 32, no. 6, pp. 41–48, June 1995.

[8] N. G. Hingorani and L. Gyugyi, *Understanding FACTS : Concepts and Technology of Flexible AC Transmission Systems*. New York: Wiley-IEEE Press, December 1999.

[9] R. Arnold, "Solutions to the power quality problem," *Power Engineering Journal*, vol. 15, no. 2, pp. 65–73, 2001.

[10] Å. Ekström, "High power electronics HVDC and SVC," Electric Power Research Center, Royal Institute of Technology, Stockholm, Sweden, 1990.

[11] J. Arrillaga, *High Voltage Direct Current Transmission*. London: The Institution of Electrical Engineers, 1998.

[12] R. Rudervall, J. P. Charpentier, and R. Sharma, "High voltage direct current (HVDC) transmission systems technology review paper," in *Energy Week 2000*, Washington, D.C, USA, March 2000.

[13] D. F. Menzies, J. Graham, and F. U. Ribeiro, "Garabi the Argentina-Brazil 1000MW interconnection commissioning and early operating experience," in *ERLAC Conference*, Foz do Iguacu, Brazil, May-June 2001.

[14] T. Larsson, A. Edris, D. Kidd, and F. Aboytes, "Eagle pass back-to-back tie: a dual purpose application of voltage source converter technology," in *Proc. of IEEE Power Engineering Society Summer Meeting*, vol. 3, July 2001, pp. 1686 – 1691.

[15] U. Axelsson, A. Holm, C. Liljegren, and K. Eriksson, "Gotland HVDC Light transmission-world's first commercial small scale DC transmission," in *CIRED Conference*, Nice, France, May 1999.

[16] B. D. Railing, J. J. Miller, G. Moreau, J. Wasborg, Y. Jiang-Häfner, and D. Stanley, "The DirectLink VSC-based HVDC project and its commissioning," in *CIGRÉ conference*, Paris, France, August 2002.

[17] B. D. Railing, J. J. Miller, P. Steckley, G. Moreau, P. Bard, L. Ronström, and J. Lindberg, "Cross Sound Cable project second generation VSC technology for HVDC," in *CIGRÉ conference*, Paris, France, August 2004.

[18] A. Lindberg, "PWM and control of two and three level high power voltage source converters," Royal Institute of Technology, Stockholm, Sweden, Licentiate Thesis, 1995.

[19] B. Andersen, L. Xu, P. Horton, and P. Cartwright, "Topologies for VSC transmission," *Power Engineering Journal*, vol. 16, no. 3, pp. 142–150, June 2002.

[20] R. Portillo, M. Prats, J. Leon, J. Sanchez, J. Carrasco, E. Galvan, and L. Franquelo, "Modeling strategy for back-to-back three-level converters applied to high-power wind turbines," *IEEE Trans. Ind. Electron.*, vol. 53, no. 5, pp. 1483 – 1491, October 2006.

[21] L. Xu and V. Agelidis, "VSC transmission system using flying capacitor multilevel converters and hybrid PWM control," *IEEE Trans. Power Delivery*, vol. 22, no. 1, pp. 693 – 702, January 2007.

[22] M. Noroozian, A.-A. Edris, D. Kidd, and A. Keri, "The potential use of voltage-sourced converter-based back-to-back tie in load restorations," *IEEE Trans. Power Delivery*, vol. 18, no. 4, pp. 1416 – 1421, October 2003.

[23] P. F. de Toledo, “Feasibility of HVDC for city infeed,” Royal Institute of Technology, Stockholm, Sweden, Licentiate Thesis, 2003.

[24] J. Svensson, “Grid-connected voltage source converter-control principles and wind enertgy applications,” Ph.D. dissertation, Chalmers University of Technology, Göteborg, Sweden, 1998.

[25] L. Lamont and D. Jovcic, “Multivariable interaction indicators for VSC transmission controller design,” in *IEEE Power Engineering Society General Meeting, 2006.*, June 2006.

[26] M. Durrant, H. Werner, and K. Abbott, “Model of a VSC HVDC terminal attached to a weak AC system,” in *Proc. of 2003 IEEE Conference on Control Applications, CCA 2003*, vol. 1, Istanbul, Turkey, June 2003, pp. 178–182.

[27] G. Zhang, Z. Xu, and Y. Cai, “An equivalent model for simulating VSC based HVDC,” in *Transmission and Distribution Conference and Exposition, 2001 IEEE/PES*, vol. 1, Atlanta, GA USA, October-November 2001, pp. 20 – 24.

[28] J. Ottosson and M. Rudberg, “Simplified models for two and three-level voltage source converters,” Master’s thesis, Chalmers University of Technology, Göteborg, Sweden, 2003.

[29] Y. J. Häfner, M. Hyttinen, and B. Pääjärvi, “On the short circuit current contribution of HVDC Light,” in *IEEE/PES T&D 2002 Asia Pacific*, Yokohama, Japan, October 2002.

[30] W. Lu and B. Ooi, “Simultaneous inter-area decoupling and local area damping by voltage source HVDC,” in *IEEE Power Engineering Society Winter Meeting, 2001.*, vol. 3, January - February 2001, pp. 1079 – 1084.

[31] F. Jowder and B. Ooi, “VSC-HVDC station with SSSC characteristics,” *IEEE Trans. Power Electron.*, vol. 19, no. 4, pp. 1053 – 1059, July 2004.

[32] R. Grünbaum, P. Halvarsson, D. Larsson, and P. R. Jones, “Conditioning of power grids serving offshore wind farms based on asynchronous generators,” in *Second IEE International Conference on Power Electronics, Machines and Drives, 2004*, vol. 1, Edinburgh, UK, March-April 2004, pp. 34 – 39.

[33] P. Bresesti, W. Kling, R. Hendriks, and R. Vailati, “HVDC connection of offshore wind farms to the transmission system,” *IEEE Trans. Energy Conversion*, vol. 22, no. 1, pp. 37 – 43, March 2007.

[34] X. Koutiva, T. Vrionis, N. Vovos, and G. Giannakopoulos, "Optimal integration of an offshore wind farm to a weak AC grid," *IEEE Trans. Power Delivery*, vol. 21, no. 2, pp. 987 – 994, April 2006.

[35] A.-K. Skytt, P. Holmberg, and L. E. Juhlin, "HVDC Light for connection of wind farms," in *Second International Workshop on Transmission Networks for Off Shore Wind Farms*, Royal Institute of Technology, Stockholm, Sweden, March 2001.

[36] L. Stendius and P. Jones, "The challenges of offshore power system construction-bringing power successfully to Troll A, one of the worlds largest oil and gas platform," in *The 8th IEE International Conference on AC and DC Power Transmission, 2006. ACDC 2006.*, London, UK, March 2006, pp. 75–78.

[37] H. Jiang and Å. Ekström, "Multiterminal HVDC systems in urban areas of large cities," *IEEE Trans. Power Delivery*, vol. 13, no. 4, pp. 1278 – 1284, October 1998.

[38] R. Billinton, M. Fotuhi-Firuzabad, and S. Faried, "Reliability evaluation of hybrid multiterminal HVDC subtransmission systems," *IEE Proceedings-Generation, Transmission and Distribution*, vol. 149, no. 5, pp. 571 – 577, September 2002.

[39] P. Karlsson, "DC distributed power systems - analysis, design and control for a renewable energy system," Ph.D. dissertation, Lund University, 2002.

[40] W. Lu and B. Ooi, "DC overvoltage control during loss of converter in multiterminal voltage-source converter-based HVDC (M-VSC-HVDC)," *IEEE Trans. Power Delivery*, vol. 18, no. 3, pp. 915 – 920, July 2003.

[41] W. Lu and B.-T. Ooi, "Optimal acquisition and aggregation of offshore wind power by multiterminal voltage-source HVDC," *IEEE Trans. Power Delivery*, vol. 18, no. 1, pp. 201–206, January 2003.

[42] X.-P. Zhang, "Multiterminal voltage-sourced converter-based HVDC models for power flow analysis," *IEEE Trans. Power Syst.*, vol. 19, no. 4, pp. 1877–1884, November 2004.

[43] W. Lu and B. Ooi, "Premium quality power park based on multi-terminal HVDC," *IEEE Trans. Power Delivery*, vol. 20, no. 2, pp. 978 – 983, April 2005.

[44] L. Tang and B. Ooi, "Protection of VSC-multi-terminal HVDC against DC faults," in *IEEE 33rd Annual Power Electronics Specialists Conference, 2002. pesc 02. 2002*, vol. 2, June 2002, pp. 719 – 724.

[45] Y. Jiang-Häfner, H. Duchén, K. Lindén, M. Hyttinen, P. F. de Toledo, T. Tulkiewicz, A. K. Skytt, and H. Björklund, "Improvement of subsynchronous torsional damping

using VSC HVDC," in *Proc. of 2002 International Conference on Power System Technology*, vol. 2, Kunming, China, October 2002, pp. 998–1003.

[46] M. Baran and N. Mahajan, "DC distribution for industrial systems: opportunities and challenges," *IEEE Trans. Ind. Applicat.*, vol. 39, no. 6, pp. 1596 – 1601, November - December 2003.

[47] C. Du, "The control of VSC-HVDC and its use for large industrial power systems," Chalmers University of Technology, Göteborg, Sweden, Licentiate Thesis, 2003.

[48] http://www.abb.com/hvdc, accessed at 2007.

[49] M. A. Laughton and D. J. Warne, *Electrical Engineer's Reference Book*, 16th ed. Oxford [England] ; Boston, MA : Newnes: Newnes, 2003.

[50] E. W. Kimbark, *Direct Current Transmission*. New York: John. Wiley, 1971, vol. I.

[51] K. Eriksson, "Operational experience of HVDC Light," in *Seventh International Conference on AC-DC Power Transmission*, London, U.K., November 2001.

[52] F. Schettler, H. Huang, and N. Christl, "HVDC transmission systems using voltage sourced converters-design and applications," in *Proc. of IEEE Power Engineering Society Summer Meeting*, vol. 2, July 2000, pp. 715–720.

[53] L. Stendius and K. Eriksson, "HVDC Light - an excellent tool for city center infeed," in *PowerGen Conference*, Singapore, September 1999.

[54] "Other ABB HVDC Light systems in operation," http://www.abb.com, accessed at January 2007, Tech. Rep.

[55] B. Jacobson, Y. Jiang-Häfner, P. Rey, G. Asplund, M. Jeroense, A. Gustafsson, and M. Bergkvist, "HVDC with voltage source converters and extruded cables for up to ±300kV and 1000MW," in *CIGRÉ conference*, Paris, France, August 2006.

[56] D. A. Woodford, "HVDC transmission," Manitoba HVDC Research Centre, Tech. Rep., 1998.

[57] V. K. Sood, *HVDC and FACTS Controllers: Applications of Static Converters in Power Systems*. Norwell, Massachusetts USA: Kluwer Academic Publishers, 2004.

[58] J. G. D. Menzies and F. Biledt, "Electrical system considerations for the Argentina-Brazil 1000MW interconnection," in *CIGRÉ conference*, Paris, France, August-September 2000.

[59] M. Häusler, "Multiterminal HVDC for high power transmission in Europe," in *CEPEX99 conference*, Poznan, Poland, March 1999.

[60] G. Morin, L. X. Bui, S. Casoria, and J. Reeve, "Modeling of the Hydro-Quebec - New England HVDC system and digital controls with EMTP," *IEEE Trans. Power Delivery*, vol. 8, no. 2, pp. 559–566, April 1993.

[61] N. Mohan, T. M. Undeland, and W. P. Robbins, *Power Electronics: Converters, Applications and Design, 2nd ed.* New York, NY: John Wiley & Sons, 1995.

[62] D. A. Paice, *Power Electronic Converter Harmonics (Multipulse Methods for Clean Power)*. New York, NY: IEEE Press, 1996.

[63] "Active filters in HVDC applications," CIGRÉ WG 14-28, Technical Brochure No. 223, April 2003.

[64] G. Asplund, K. Eriksson, H. Jiang, J. Lindberg, R. Pålsson, and K. Svensson, "DC transmission based on voltage source converters," in *International Conference on Large High Voltage Electric Systems. CIGRÉ 98*, vol. 4, Paris, France, 1998.

[65] L. Weimers, "New markets need new technology," in *Proc. of 2000 International Conference on Power System Technology*, vol. 2, Perth, Australia, December 2000, pp. 873–877.

[66] B. K. Bose, *Power Electronics and AC Drives*. New Jersey : Prentice-Hall USA, 1986.

[67] Y. Jiang, "Active and reactive power control of transmission systems with voltage source converter," Ph.D. dissertation, Royal Institute of Technology, Stockholm, Sweden, 1997.

[68] M. M. de Oliveira, "Power electronics for mitigation of voltage sags and improved control of AC power systems," Ph.D. dissertation, Royal Institute of Technology, Stockholm, Sweden, 2000.

[69] G. Asplund, K. Eriksson, and O. Tollerz, "HVDC Light, a tool for electric power transmission to distant loads," in *VI Sepope Conference*, Salvador, Brazil, May 1998.

[70] S. G. Johansson, G. Asplund, E. Jansson, and R. Rudervall, "Power system stability benefits with VSC DC-transmission systems," in *CIGRÉ 2004*, Paris, France, August 2004.

[71] R. Grünbaum, B. Halvarsson, and A. Wilk-Wilczynski, "Facts and HVDC Light for power system interconnections," in *PowerDelivery Conference*, Madrid, Spain, September 1999.

[72] M. H. J. Bollen, *Understanding Power Quality Problems: Voltage Sags and Interruptions*. New York: IEEE Press, 2000.

[73] J. Svensson, "Inclusion of dead-time and parameter variation in VSC modelling for predicting responses of grid voltage harmonics," in *Proc. of 7th European Conference on Power Electronics and Applications (EPE'97)*, vol. 3, September 1997, pp. 216–221.

[74] A. Sannino, "Applications of power-electronic devices for improving power quality in industrial systems," Ph.D. dissertation, University of Palermo, December 2000.

[75] M. Bojrup, "Advanced control of active filters in a battery charger application," Lund Institute of Technology, Lund, Sweden, Licentiate Thesis, 1999.

[76] A. Sannino and J. Svensson, "Power Electronics 2," Dept. of Electric Power Engineering, Chalmers University of Technology, Göteborg, Sweden, 2004.

[77] M. Alakula, "Power electronic control," Lund University, Lund, Sweden, Tech. Rep., 2002.

[78] Z. Palmor, *The Control Handbook*. USA: CRC Press and IEEE. Press, 1996.

[79] R. Ottersten and J. Svensson, "Vector current controlled voltage source converter-deadbeat control and saturation strategies," *IEEE Trans. Power Electron.*, vol. 17, no. 2, pp. 279 – 285, March 2002.

[80] L. Harnefors and H. P. Nee., "Control of variable-speed drives," Electrical Machines and Power Electronics, Dept. of Electrical Engineering, Royal Institute of Technology, Stockholm, Sweden, 2000.

[81] K. J. Åström and T. Hägglund, *PID Controllers, 2nd edition*. United States of America: Instrument Society of America, 1994.

[82] B. M. Weedy and B. J. Cory, *Electric Power Systems, 4th Edition*. Baffins Lane, Chichester, West Sussex, England: John Wiley & Sons Ltd., 1998.

[83] P. Kundur, *Power System Stability and Control*. New York: McGraw-Hill, 1994.

[84] A. Engler, "Applicability of droops in low voltage grids," *DER Journal*, no. 1, January 2005.

[85] K. D. Brabandere, B. Bolsens, J. V. den Keybus, A. Woyte, J. Driesen, R. Belmans, and K. Leuven, "A voltage and frequency droop control method for parallel inverters," in *IEEE 35th Annual Power Electronics Specialists Conference*, vol. 4, Aachen, Germany, June 2004, pp. 2501–2507.

[86] F. Saccomanno, *Electric Power Systems : Analysis and Control*. New York: Wiley-IEEE Press, 2003.

[87] J. Machowski, J. W. Bialek, and J. R. Bumby, *Power System Dynamics and Stability*. Chichester, England: John Wiley & Sons Ltd., 1998.

[88] D. Zmood, D.N.; Holmes, "Stationary frame current regulation of PWM inverters with zero steady-state error," *IEEE Trans. Power Electron.*, vol. 18, no. 3, pp. 814 – 822, 2003.

[89] P. Karlsson, J. Bjornstedt, and M. Strom, "Stability of voltage and frequency control in distributed generation based on parallel-connected converters feeding constant power loads," in *2005 European Conference on Power Electronics and Applications*, Lund, Sweden, September 2005.

[90] C. Du, M. Bollen, E. Agneholm, and A. Sannino, "A new control strategy of a VSC-HVDC system for high-quality supply of industrial plants," December 2006, Accepted by *IEEE Transactions on Power Delivery*.

[91] T. N. Le, "Kompensation schnell veränderlicher blindströme eines drehstromverbrauchers (in German)," *etzArchiv, Bd. 11*, vol. H. 8, pp. 249 – 253, 1989.

[92] H.-S. Song and K. Nam, "Dual current control scheme for PWM converter under unbalanced input voltage conditions," *IEEE Trans. Ind. Electron.*, vol. 46, no. 5, pp. 953 – 959, October 1999.

[93] P. F. de Toledo, G. Asplund, and E. Jansson, "Aspects on infeed of multiple HVDC into one ac network," in *CEPSI 2004*, Shanghai, China, October 2004.

[94] J. Lopes, "Integration of dispersed generation on distribution networks-impact studies," in *IEEE Power Engineering Society Winter Meeting*, vol. 1, January 2002, pp. 323 – 328.

Appendix A

Selected Publications

Paper A

C. Du, A. Sannino, and M. Bollen, ”Analysis of the Control Algorithms of Voltage-Source Converter HVDC”, in *Proc. IEEE-PES Power Tech 2005,* St. Petersburg, June 2005.

Paper B

C. Du, A. Sannino, and M. Bollen, ”Analysis of Response of VSC-Based HVDC to Unbalanced Faults with Different Control Systems”, in *Proc. IEEE/PES Transmission and Distribution Conference and Exhibition: Asia Pacific, 2005*, Dalian, August 2005.

Paper C

C. Du and E. Agneholm, ”Investigation of Frequency/AC Voltage Control of Inverter Station of VSC-HVDC”, in *Proc. 32nd Annual Conference on IEEE Industrial Electronics, IECON 2006*, Paris, November 2006, pp. 1810 - 1815.

Paper D

C. Du, M. Bollen, E. Agneholm, and A. Sannino, ”A New Control Strategy of a VSC-HVDC System for High-Quality Supply of Industrial Plants”, accepted by IEEE Transactions on Power Delivery.

Paper E

C. Du and M. Bollen, ”Power-Frequency Control for VSC-HVDC during Island Operation”, in *Proc. The 8th IEE International Conference on AC and DC Power Transmission, 2006. ACDC 2006*, London, March 2006, pp. 177 - 181.

Paper F

C. Du and E. Agneholm, ”A Novel Control of VSC-HVDC for Improving Power Quality of an Industrial Plant”, in *Proc. 32nd Annual Conference on IEEE Industrial Electronics, IECON 2006*, Paris, November 2006, pp. 1962 - 1967.

Paper G

C. Du, E. Agneholm, and G. Olsson, ”Comparison of different frequency controls for VSC-HVDC”, submitted to IEEE Transactions on Power Delivery.

Paper H

C. Du, E. Agneholm, and G. Olsson, ”VSC-HVDC System for Industrial Plants with On-Site Generators”, submitted to IEE generation, transmission and distribution.

Paper I

C. Du, E. Agneholm, and G. Olsson, ”Use of VSC-HVDC for Industrial Systems with On-Site Generation with Frequency Control”, submitted to IEEE Transactions on Power Delivery.